DUPLEX CRYSTALS AND TWO-PHASE BICRYSTALS OF ALPHA-BETA BRASS--GROWTH AND MECHANICAL PROPERTIES

Thesis for the Degree of Ph. D.
MICHIGAN STATE UNIVERSITY
ANIL KRISHNAJI HINGWE
1973

This is to certify that the

thesis entitled

DUPLEX CRYSTALS AND TWO-PHASE BICRYSTALS OF
ALPHA-BETA BRASS -- GROWTH AND MECHANICAL PROPERTIES

presented by

ANIL KRISHNAJI HINGWE

has been accepted towards fulfillment
of the requirements for

__, Ph. D. degree in METALLURGY

L. N. Subramanian

Major professor

Date June 15, 1973

O-7639

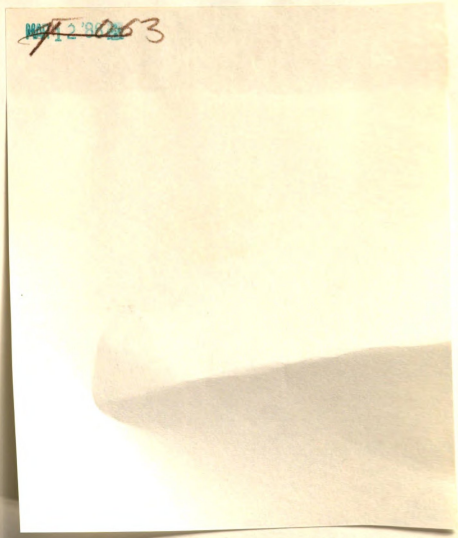
063

ABSTRACT

DUPLEX CRYSTALS AND TWO-PHASE BICRYSTALS OF
ALPHA-BETA BRASS - GROWTH AND DEFORMATION BEHAVIOR

by

Ideal models for studying the properties of two-phase polycrystals are duplex crystals and two-phase bicrystals. A technique for growing duplex crystals and two-phase bicrystals of alpha-beta brass has been developed. A two-stage growth technique usually occurs when alpha and beta phases are joined. Upon heat treatment schedules, such as lowering through a temperature gradient, and cyclic liquid annealing under a steep temperature gradient, have been devised to alleviate this transition zone and to produce a sharp phase boundary between the alpha and beta crystals. The effect of the heat treatments on the transition zone can be explained on the basis of diffusion and solid-state transformations. The observed morphological changes in the structure can be explained by mechanisms based on grain growth and phase transformations.

Mechanical tests on duplex and two-phase bicrystals of alpha-beta brass were carried out in uniaxial tension. Initiation and propagation of the plastic flow were studied by optical and electron microscope techniques. In both types of specimens, the phase boundary initially poses a resistance to the approaching slip in alpha. In specimens with certain specific crystallographic relationships between alpha and beta phases, the phase boundary does not act as an effective barrier for slip propagation. When such crystallographic relationships are not satisfied, the boundary can resist slip effectively up to higher stress levels.

ABSTRACT

DUPLEX CRYSTALS AND TWO-PHASE BICRYSTALS OF
ALPHA-BETA BRASS -- GROWTH AND MECHANICAL BEHAVIOR

by

Anil Krishnaji Hingwe

Ideal models for studying the properties of two-phase materials are duplex crystals and two-phase bicrystals. A technique for growing duplex crystals and two-phase bicrystals of alpha-beta brass has been developed. A two-phase transition region normally occurs when these two phases are joined. Special heat-treatment schedules, such as lowering through a temperature gradient, and cyclic local annealing under a sharp temperature gradient, have been devised to eliminate this transition zone and to produce a sharp phase boundary between the alpha and beta crystals. The effect of the heat treatments on the transition zone can be explained on the basis of diffusion and solid-state transformations. The observed morphological changes in the structure can be explained by mechanisms based on grain growth and phase transformations.

Mechanical tests on duplex and two-phase bicrystals of alpha-beta brass were carried out in uniaxial tension. Initiation and propagation of the plastic flow were studied by optical and electron microscope techniques. In both types of specimens, the phase boundary initially poses a resistance to the approaching slip in alpha. In specimens with certain specific crystallographic relationships between alpha and beta phases, the phase boundary does not act as an effective barrier for slip propagation. When such crystallographic relationships are not satisfied, the boundary can resist slip effectively up to higher stress levels.

The repulsive stresses at the phase boundary and the Lomer-Cottrell barriers within the alpha phase cause dislocation pile-ups. The resultant stress concentration is high enough for unpinning the dislocation sources present either inside the beta regions or at the phase boundary. This stress concentration, however, cannot cause the dislocations to penetrate through the phase boundary.

Irrespective of the kind of boundary present--coherent or incoherent--no void formation was observed during the plastic deformation of alpha-beta brass at the boundary.

DUPLEX CRYSTALS AND TWO-PHASE BICRYSTALS OF ALPHA-BETA BRASS--GROWTH AND MECHANICAL PROPERTIES

by

ANIL KRISHNAJI HINGWE

A THESIS

Submitted to
Michigan State University
in partial fulfillment of the requirements
for the degree of

DOCTOR OF PHILOSOPHY

Department of Metallurgy, Mechanics, and Materials Science

1973

To

My Parents

ACKNOWLEDGMENTS

I can only inadequately express my deepest gratitude to Dr. K. N. Subramanian for his counsel, interest, guidance and encouragement.

Thanks are also due to all the members of my guidance committee, especially Dr. S. M. Adams and Dr. A. J. Smith, for their valuable suggestions. My appreciation is extended to Dr. D. J. Montgomery for his constant encouragement.

I sincerely thank all the members of the Materials Research Group, particularly Mr. Chris Nilsen, for their help during the course of this work.

Thanks are also extended to Dr. R. Summitt, Chairman, Department of Metallurgy, Mechanics, and Materials Science, and Mr. J. W. Hoffman, Director, Division of Engineering Research, for financial assistance.

Thanks are also due to Mrs. Thelma Liszewski for her excellent typing.

Finally, I wish to extend my gratitude to my wife Anuradha and daughter Suchitra for their patience and sacrifice.

TABLE OF CONTENTS

LIST OF TABLES

LIST OF FIGURES

I. INTRODUCTION

Two-phase and poly-phase aggregates play important roles in engineering materials. The mechanical properties of such materials depend on the properties of the constituent phases, and on the interactions that take place at the phase boundary. The latter, in turn, depend on the size, shape, distribution and crystallographic orientation of the phases.

Among two-phase metallic systems, those containing either a finely-dispersed or a fiber-strengthening phase have been widely investigated. In other systems, the second phase may also exist as a distributed aggregate. Common examples are normalized steels, duplex stainless steels, and two-phase alloys of titanium-aluminum, copper-zinc, copper-tin, and copper-aluminum. A clear understanding of the mechanical behavior of such alloys is far from complete.

To aid in understanding the basic mechanisms involved in the deformation of such two-phase alloys, the number of variables that affect the mechanical behavior must be reduced. In the case of single-phase materials, single crystals are used as basic units. This procedure eliminates the variables such as grain size, shape, and interactions at the grain boundaries. Bicrystals and multicrystals provide a means of extending the understanding to polycrystalline materials. Just as single crystals constitute an ideal unit for single-phase materials, duplex crystals and two-phase bicrystals are ideal units for two-phase

materials. C. S. Smith[1] has defined a duplex crystal as "an oriented crystallographic unit consisting of two phases with a definite relationship to each other." A two-phase bicrystal may be defined as a macroscopic unit consisting of a single crystal of one phase joined to a single crystal of another phase. A specimen in which a single crystal of one phase is joined with a large-grained polycrystal of another phase may be termed as a two-phase multicrystal. Such units correspond to bicrystals or multicrystals of single phase materials.

The purpose of this investigation is to grow macroscopic duplex crystals and two-phase multicrystals of alpha-beta brass and to study their mechanical properties under uniaxial tension. Ideas pertinent to growth of single crystals and bicrystals, to phase transformations, and to mechanical properties as affected by the presence of boundaries and phases are considered in the following review.

1.1 Crystal Growth

1.1.1 Growth of Metallic Single Crystals

Single crystals of pure metals and single phase alloys can be grown by solid, liquid, or vapor phase techniques. Growth from the melt by the Bridgman technique is the most widely utilized method for growing metal single crystals. Here the melt is contained in a sharp-tipped crucible, and the crucible is moved through a temperature gradient. Owing to the presence of the sharp tip at the base, only a few nuclei are formed. As the solidification proceeds, a faster growing grain outstrips the others and a single crystal is produced. The Bridgman technique is the simplest method for producing large single crystals. With care, crystals of high purity and crystalline perfection can be produced.

In growing alloy single crystals, maintaining the uniformity of composition is the main problem. A volatile constituent may be lost during melting. Segregation is another major cause for the nonuniformity of composition. The regions solidifying first contain less solute than those solidifying last. Thus the liquid is always in contact with solids of different composition. If the freezing rate is low, diffusion in the solid phase and the liquid phase will eliminate all concentration gradients and no segregation will occur. Diffusion rates in the solid are low, however, and equilibrium freezing rarely takes place.

For alloy systems in which the solute addition decreases the melting point, the liquid layer immediately ahead of the moving solid-liquid interface becomes enriched in solute. Each point in the liquid ahead of the interface has a liquidus temperature increasing with the distance from the interface. The liquid is also subject to an applied temperature gradient. If this gradient is not large enough, the liquid ahead of the interface will be supersaturated as shown in Figure 1. This phenomenon is called 'constitutional supercooling'[2]. When constitutional supercooling takes place, the solid-liquid interface transforms from a smooth interface into a cellular interface. The probability of stray nucleation also increases with constitutional supercooling. Slower growth rates and higher temperature gradients tend to reduce the constitutional supercooling and to prevent resultant defects[3,4].

Although such problems present themselves during the growth of single crystals of alpha brass, they may be avoided by following the detailed conditions for growing good single crystals as described in the literature. Savitskii and Novokhatskaya[5] have grown single crystals of alpha brass with diameters between 10 and 30 mm. To minimize the

Temp. gradient
in liquid
Equilibrium
liquidus temp.
Temperature
Distance from the interface

FIG. 1

Fig. 1. Consitutional supercooling ahead of the moving solid/liquid interface for an alloy system in which the addition of solute lowers the melting point (J. W. Rutter and B. Chalmers[2]).

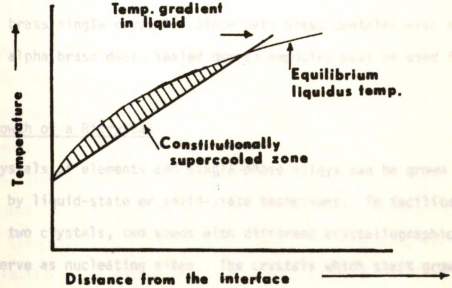
Temp. gradient
in liquid
Equilibrium
liquidus temp.
Constitutionally
supercooled zone
Temperature
Distance from the interface

FIG. 1

problem of zinc loss, the crystals were grown in sealed quartz ampoules. A steep temperature gradient was created with a non-uniform winding on the heater tube of the furnace. If microsegregation occurs, it can be removed by a homogenization treatment at 800°C for 16 hours, according to Maddin.[6]

Whereas the liquidus and the solidus temperatures for alpha brass (containing 30 w/o zinc) differ by 30°C, beta brass (containing 48 w/o zinc) melts at a constant temperature. Hence a steep temperature gradient and a slow growth rate are not needed for the successful growth of a beta brass single crystal. Since beta brass contains even more zinc than alpha brass does, sealed quartz ampoules must be used for the melt.

1.1.2 Growth of a Bicrystal

Bicrystals of elements and single-phase alloys can be grown successfully by liquid-state or solid-state techniques. To facilitate the growth of two crystals, two seeds with different crystallographic orientations serve as nucleating sites. The crystals which start growing at these two seeds grow in competition with each other. The grain boundary runs along the direction of growth. This technique has been used successfully for growing bicrystals of various elements and single-phase alloys[7].

1.1.3 Two-Phase Alloys: Growth of a Basic Unit

The two basic units for the study of the properties of two-phase alloys are "duplex crystals" and "two-phase bicrystals." Livingston[8] has recently reviewed the methods for growing duplex crystals of various materials. Duplex crystals can be grown by carrying out solidification

or solid-state phase transformation in a unidirectional manner by providing very sharp temperature gradients. Most of the studies in this field are concerned with unidirectional solidification of eutectic alloys.

A two-phase bicrystal consists of a single crystal of one phase joined to a single crystal of another phase. Only a few investigations have been attempted to produce such bicrystals by growth from the liquid of large single crystals of one phase using a single-crystal seed of another phase[9,10,11]. Sang and Miller[9] have grown large (∿5 cm long, ∿1 cm diam.) single crystals of lead on various crystallographic planes of copper single crystals. Chstyakov et al.[10] have grown molybdenum on tungsten single crystals, and Lemercier and Thuillier[11] have grown selenium on tellurium. Both of these systems show extensive solubility. Nevertheless, a very thin two-phase transition layer was present between the single crystals of the different phases. The thinness of the layer can be attributed to the large difference between the melting points of the components. On the other hand, in copper-lead system, the mutual solubilities of copper and lead in each other are low, and the transition layer produced is once again extremely small.

Owing to the existence of extensive solubility in the copper-zinc system and the closeness of liquidus temperatures for alpha and beta phases, a two-phase region of alpha and beta will develop when a single crystal of alpha brass is joined with a single crystal of beta brass. A number of studies have been carried out on the diffusion couples of copper-zinc and copper-nickel-zinc alloys. For example, Sisson and Dayananda[12] have investigated diffusion in multiphase copper-nickel-zinc couples. In this system, the size and the microstructure of the transition zone was found to be dependent on the migration of the

interfaces. Hence diffusion affected both the size and morphologies within the transition region.

1.1.4 Phase Transformations in the Copper-Zinc System

The copper-zinc phase diagram is shown in Figure 2. Alloys containing 40-45 w/o zinc are of importance because of the transformations that occur on cooling from the high-temperature beta phase. The transformation product depends on the zinc concentration and the cooling rates.

Shewmon[13] has given a concise review of the phase transformations that occur in the copper-zinc system. He has pointed out that the precipitation of alpha during cooling from beta state is similar to that of ferrite precipitating from austenite. He has described the cooling of copper-zinc alloys containing 39 and 44 w/o zinc. When an alloy containing 39 w/o zinc is cooled below 800°C, alpha can nucleate and grow. The alpha precipitates appear primarily as Widmanstätten plates. The higher the rate of cooling, the finer is the structure. An alloy containing 44 w/o zinc cannot transform unless it is cooled below 575°C. The diffusion rate is slow since the transformation temperature is low, and zinc atoms can travel only through short distances during the transformation. In the absence of long-range diffusion, the Widmanstätten-precipitate plates of alpha in the alloy containing 44 w/o zinc are finer than in the alloy containing 39 w/o zinc.

The precipitation of alpha from the metastable beta on cooling from high temperature can be suppressed by increasing the rate of cooling. Flewitt and Towner[15] water-quenched various alloys from a high-temperature beta state to metastable beta-prime structure. An isothermal decomposition of this beta-prime structure was carried out by reheating between

FIG. 2

Fig. 2. Copper-zinc phase diagram (M. Hansen and K. Anderko[14]).

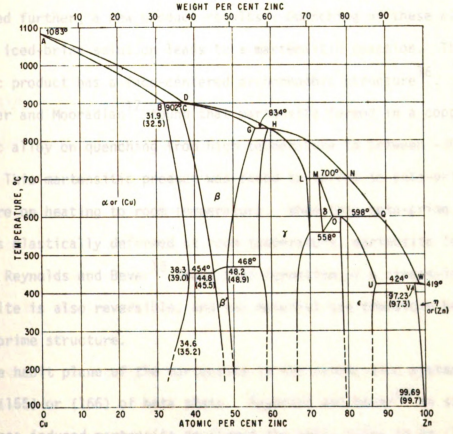
WEIGHT PER CENT ZINC
10
20
30
40
50
60
70
80
90
1100
1000
900
800
700
600
500
400
300
200
100
TEMPERATURE, °C
1083°
A
D
B
902°C
31.9
(32.5)
834°
G
H
M
700°
N
L
α or (Cu)
β
P
598°
Q
R
O
558°
γ
38.3
(39.0)
454°
44.8
(45.5)
468°
48.2
(48.9)
β'
424°
W
V
419°
U
ε
97.23
(97.3)
η
(or Zn)
34.6
(35.2)
99.69
(99.7)
0
Cu
10
20
30
40
50
60
70
80
90
100
Zn
ATOMIC PER CENT ZINC

FIG. 2

170 and 470°C. Below 350°C, a plate-like product appeared, whereas above 350°C a rod-like product formed. The plate-like precipitate was bainitic in nature and had a faulted f.c.c. structure. The rod-like precipitate had equilibrium alpha structure. The rods were found to grow lengthwise along <111> direction of beta phase.

When the rate of cooling of the alloys with 40 to 45 w/o zinc is increased further, a new product results. Quenching of these alloys into an iced-brine solution leads to a martensitic reaction. The martensitic product has a face-centered orthorhombic structure[16]. Greninger and Mooradian[17] found that martensite formed in a copper-39.2 w/o zinc alloy on quenching from high temperature to between -30° and -40°C. This martensitic product was found to revert to beta-prime structure on heating to room temperature. When this beta-prime structure was plastically deformed at room temperature, martensite formed in it. Reynolds and Bever[18] found that formation of a stress-induced martensite is also reversible, and the material can transform back to a beta-prime structure.

The habit plane of the martensite in the copper-zinc system is either {155} or {166} of beta phase. Reynolds and Bever[18] in studying the stress-induced martensite confirmed the habit plane to be $\{155\}_{\beta}$. Hull and Garwood[19] have determined an intermediate habit plane of {2 11 12} type.

Alloys with about 38 w/o zinc can undergo massive transformation when cooled at a rate intermediate between that for the martensitic reaction and that for the Widmanstätten reaction[19]. The transformation product is blunt or massive in nature. It involves a change in the crystal structure without a compositional change. An advancing planar interface

transforms a grain of the stable beta into stable alpha of a different crystal structure.

The beta phase always undergoes an ordering reaction, and changes to beta prime irrespective of the rate of cooling and the product of the transformation. The beta prime has a cubic lattice with the copper and zinc atoms ordered so that the copper atoms have only zinc nearest neighbors and vice versa. It has been found that the ordering reaction in beta cannot be suppressed by any means.

1.2 Grain-Boundary and Phase-Boundary Effects

1.2.1 Grain-Boundary Effects

The influence of grain boundaries on mechanical properties has received a great deal of attention. The most recent of the several reviews on this subject is by Hirth[20]. The grain boundaries are known to have a strengthening effect, but the exact mechanism is not yet pinpointed. The subject has been examined by theoretical analysis of interactions of slip dislocations with the boundaries, and by experimental studies on bicrystals and on polycrystals. These approaches are now presented.

1.2.1.1 Dislocations and Grain Boundaries

Grain boundaries can be considered to be made up of dislocations. Low-angle boundaries of tilt type and of twist type can be considered to be made up of arrays of edge dislocations and of screw dislocations respectively. High-angle boundaries are forests of dislocations of edge, screw and mixed character. The grain-boundary dislocations have a Burgers vector different from that of the lattice-slip dislocations.

However, the grain-boundary dislocations exist in such forms that a lattice dislocation can dissociate itself as it enters a boundary to form grain-boundary dislocations. On the other hand, a grain-boundary dislocation can dissociate itself to form a lattice dislocation and leave a residue at the grain boundary. Alternatively, two grain-boundary dislocations can react to form a lattice dislocation. Thus the grain boundary can act both as a source and as a sink for dislocations[21].

1.2.1.2 Studies Conducted with Bicrystal Specimens

Chalmers and his group[22-24], Hirth and Hook[25], and many others have done extensive research on the behavior of cubic bicrystals. Investigators have explored deformation behavior of various cases of bicrystals such as symmetric, iso-axial and noniso-axial bicrystals. In a symmetric bicrystal the grain boundary is a structural mirror plane. An iso-axial bicrystal is the one in which the two crystals have the same crystallographic direction along the axis of tension. A symmetric bicrystal is a special case of iso-axial bicrystal.

Under any general state of stress, the macroscopic and microscopic compatibility conditions should be satisfied at a grain boundary. For the case of the bicrystal consisting of crystal A and crystal B shown in Figure 3, with the planar boundary normal to the y axis, the macroscopic compatibility conditions that must be satisfied at the boundary are

$$\epsilon_{xx}^{A} = \epsilon_{xx}^{B} \qquad \epsilon_{zz}^{A} = \epsilon_{zz}^{B} \qquad \epsilon_{xz}^{A} = \epsilon_{xz}^{B}$$

In addition, the strain of the entire specimen ϵ_{zz} should be the strain ϵ_{zz} in crystal A and in crystal B.

FIG.3

Fig. 3. A model for a bicrystal consisting of crystals A and B.

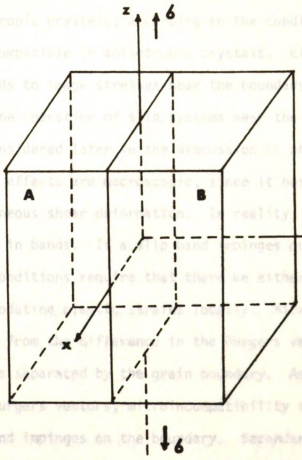

FIG. 3

Thus, in the general bicrystal, four independent relations must be satisfied for deformation, requiring four independent slip systems or sources of plastic strain[22,24]. In the specially symmetric bicrystals, a single slip system in each crystal suffices to fulfill the equations and the external constraints. On the other hand, the strains which would be compatible in isotropic crystals, according to the conditions listed above, can become incompatible in anisotropic crystals. Elastic incompatibility, which leads to image stresses near the boundary, is also an important factor in the operation of slip systems near the boundaries. Image stresses are considered later in the discussion on phase boundaries.

All of the above effects are macroscopic, since it has been assumed that slip is a homogeneous shear deformation. In reality, slip is discontinuous and occurs in bands. If a slip band impinges on a grain boundary, compatibility conditions require that there be either accommodating slip or accommodating elastic strains locally. Micro-incompatibility can arise also from the difference in the Burgers vectors of slip dislocations in grains separated by the grain boundary. As a result of the mismatch of the Burgers vectors, microincompatibility stresses are realized if a slip band impinges on the boundary. Secondary slip dislocations have been shown to arise as a result of such stresses[25].

The compatibility conditions are more complicated in a polycrystalline aggregate as shown next.

1.2.1.3 Behavior of Polycrystalline Aggregates

With several crystals, it is more difficult to satisfy the compatibility conditions. Kocks[26] has considered the extreme case of an aluminum inclusion in a steel matrix. The inclusion has to conform with

the deformation of the hole that it occupies. In an aggregate, strain is imposed upon the crystal by its surroundings. The six independent components of the imposed strain tensor are restricted only by the condition that volume remains constant during plastic deformation. In order to conform with the entire deformation, five independent glide systems are therefore required. As Kocks points out, however, in the actual case this requirement need not be followed rigorously, because the crystal also contributes to the mutual interaction of the grains. Hence the number of actually operating glide systems would probably vary from crystal to crystal. But the average at any spot is expected to be closer to five than to one. The operation of several slip systems to satisfy the compatibility conditions is called "polyslip."

As a consequence of polyslip, dislocation forests can be barriers to primary slip, and can cause latent hardening of sources active in primary slip plane[25]. This effect is sensitive to whether slip is coplanar. If the slip is noncoplanar--in other words if the cross slip is easy--the barriers mentioned above cannot be very effective, and the primary sources can keep on operating.

The microincompatibility can arise owing to a change of Burgers vector[25]. When a set of dislocations initially propagates through the boundary, the change in the Burgers vector causes a grain-boundary dislocation to be left behind for each penetrating dislocation. Unless the grain-boundary dislocations propagate away, they will generate a back stress and prevent further slip.

1.2.2 Phase-Boundary Effects

A phase boundary may be considered as a special case of a grain boundary. Structurally, it is also made up of dislocations. However,

these dislocations have to account for the lattice discontinuity across the phase boundary and are termed as "interface dislocations." The effect on strengthening due to phase boundaries is similar to that due to grain boundaries. On the level of dislocation interactions, the presence of image dislocations and geometrically-necessary dislocations has been taken into account. Extensive studies have been carried out on the mechanical properties of polycrystalline aggregates containing two phases. Fundamental units such as macroscopic two-phase bicrystals, however, have not been used to understand the role of phase boundaries in the mechanical properties of two-phase materials.

1.2.2.1 Interface Dislocations

Van der Merwe[27] originally put forward the idea of an interface dislocation. He considered the case of interfacial misfit and bonding between oriented single-crystal films and their substrates. At the interface between the substrate and the oriented overgrowth, a discontinuity exists in the periodic crystalline structure. Hence a misfit or disregistry will exist between the atoms on either side of the interface. Over large interfacial areas, the disregistry is reduced by forming interfacial strips of good fit, separated by relatively narrow strips of bad fit. These strips of bad fit are interfacial dislocations. They are illustrated schematically in Figure 4. The network of these interfacial dislocations can hinder the passage of dislocations through the interface.

1.2.2.2 Image Dislocations

The concept of image dislocations was first presented by Eshelby[28]. A dislocation approaching a free surface experiences a force. Such a

Fig. 4. Schematic diagram showing an interphase boundary between alpha and beta with interface dislocations. Lattice parameters of alpha and beta are a_1 and a_2 respectively.

Fig. 4. Schematic diagram showing an interphase boundary between alpha and beta, with interface dislocations. Lattice parameters of alpha and beta are a_1 and a_2 respectively.

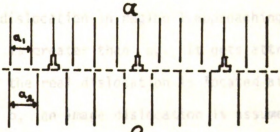

FIG. 4

force can be obtained from a stress field that is the sum of the real dislocation and its image across the surface. The stress function is devised to satisfy the boundary conditions at the surface by canceling the normal forces at the free surfaces.

Head[29] has considered the case of screw dislocations near an interface between two phases. The simple geometry under consideration is shown in Figure 5. Near an interface between two media of shear moduli μ_1 and μ_2, a screw dislocation in region 1 approaching the interface gets repelled if μ_2 is greater than μ_1. It gets attracted if μ_2 is less than μ_1. If the real dislocation is located at $x = +r$ and has a Burgers vector $Б$, an image dislocation is assumed to be present at $x = -r$. The Burgers vector of the image dislocation is $[(\mu_2 - \mu_1)/(\mu_2 + \mu_1)]Б$.

The force acting on the real dislocation due to the presence of an interface is then given by

$$F_x = \frac{(\mu_2 - \mu_1)}{(\mu_2 + \mu_1)} \mu_1 \frac{b^2}{4\pi r} \quad . \tag{1}$$

This expression cannot hold true for $r \leq 2b$, since the material in the dislocation core would then be strained beyond elastic limit. Consider a substrate of modulus μ_1 with a coating of modulus μ_2 and thickness t. When μ_2 is less than μ_1, the dislocation is attracted to the surface but when μ_2 is greater than μ_1, there will be an equilibrium position for a dislocation. Thus, a repulsive force is experienced by dislocations. The equilibrium position depends on μ_1, μ_2, and t. Head[29] has also considered the case of an interface and its interaction with an array of screw dislocations. He has calculated the dependence of the distribution of n dislocations for n up to 20

FIG 5

Fig. 5. Schematic of a real dislocation located at +r and an image dislocation at -r, near a phase boundary.....

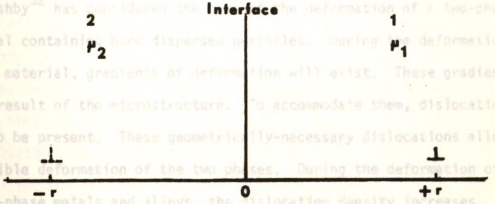

FIG 5

on the strength of the boundary. Conners[30] has carried out similar stress-field calculations for a straight edge dislocation. Yoffe[31] has studied the case of a straight dislocation inclined to a free surface at an arbitrary angle. Although these models consider various possible dislocation geometries, the conclusions obtained are similar to those reached by Head[29].

1.2.2.3 Geometrically-Necessary Dislocations

Ashby[32] has considered the case of the deformation of a two-phase material containing hard dispersed particles. During the deformation of such a material, gradients of deformation will exist. These gradients are a result of the microstructure. To accommodate them, dislocations have to be present. These geometrically-necessary dislocations allow compatible deformation of the two phases. During the deformation of single-phase metals and alloys, the dislocation density increases. These dislocations are statistically-necessary dislocations and are required to explain the usual three-stage hardening observed in single crystals. When the density of geometrically-necessary dislocations exceeds that of the statistically-necessary ones, the former control the work hardening. This is because the geometrically-necessary dislocations act as individual obstacles or create long-range back stresses.

1.2.3 Effect of the Presence of Different Phases

One of the first systematic investigations of the deformation of two-phase materials was made by Unckel[33]. Alloys like copper-6%-iron, leaded brass, alpha-beta brass, complex brass, alpha-delta bronze, aluminum-8%-copper and aluminum-12%-silicon were deformed by cold rolling. The particle sizes were measured before and after rolling.

When the second-phase particles were harder than the matrix, they deformed less than the matrix. Unckel[33] also reported that additional plastic flow must take place in the vicinity of inclusions or second-phase particles owing to the different deformations of inclusion and matrix.

Microscopic and x-ray analyses of the deformation and recrystallization of 60:40 brass were reported by Honeycombe and Boas[34]. Slip was first observed in f.c.c. alpha. Alpha phase was heavily deformed before slip occurred in ordered beta phase. Slip traces were observed to cross the alpha-beta phase boundary occasionally. In beta phase more deformation seemed to occur near an alpha-beta phase boundary than in the interior of the grains.

Clareborough[35], and Clareborough and Perger[36] studied the deformation of two-phase alloys of silver-magnesium, copper-zinc, and copper-iron. They have considered the effect of volume fractions of the two phases on the flow of these alloys. In specimens that contained small volume fractions of the harder phase, most of the deformation was restricted to the softer phase, and an additional flow of the matrix was found around the hard particles. On heavier deformations, both deformed uniformly. When the volume fraction of the harder phase exceeded 0.3, deformation of both phases was nearly uniform from the beginning.

Baldwin and Edelson[37] have stated that all second-phase particles cause embrittlement in composites such as copper-chromium, copper-iron, copper-molybdenum. According to them, this embrittlement depends only on the volume fraction of the second phase and not on the particle size, shape or composition. Palmer et al.[38], in their studies on copper-silicon and copper-zinc systems, assert that the size, shape, composition,

and distribution of the second phase, and its interfacial energy with the matrix, are the important variables which can affect the failure mechanism.

Recently, x-ray investigations have been carried out to study the internal stresses in two-phase materials after elastic and plastic deformations. Honda and Arima[39] and Arima et al.[40] have done such work on copper-zinc alloys, aluminum-silicon alloys, and steels. Bolenrath et al.[41] have studied the stress patterns during the deformation of sintered copper-iron specimens. The residual stresses arise from the difference in the yield stresses of the two phases. In two-phase copper-zinc alloys after small extensions, the alpha phase remained in compression and the beta phase in tension.

Mogford[42] has provided an excellent review on the deformation and fracture of two-phase materials.

1.3 Deformation Behavior of Alpha and Beta Brass

1.3.1 Deformation Behavior of Alpha-Brass Single Crystals

Alpha brass is the f.c.c. terminal solid solution of zinc in copper. Since alpha brass has a face-centered cubic crystal structure, slip in alpha brass occurs along {111} planes in $\langle 1\bar{1}0 \rangle$ directions. Although the slip system is the same as in the case of copper, alpha brass is stronger than copper. This increase in strength may be attributed to the solid-solution hardening caused by the addition of zinc atoms, whose presence affects both the stress necessary to initiate the plastic deformation and the subsequent work-hardening.

1.3.1.1 Critical Shear Stress

VonGöler and Sachs[43] studied the deformation of copper-zinc alloy crystals of increasing zinc content. They found that for dilute alloys the critical shear stress increased linearly with concentration.

The increase in critical shear stress may be explained by various mechanisms such as order hardening[44], the segregation of solute atoms around a dislocation by elastic interaction[45], or the chemical interaction of solute atoms with the stacking fault[46].

Order hardening or Fisher hardening[44] occurs in alloys which are partly ordered on a local scale. If, in equilibrium, an alloy has some short-range order, then the passage of a dislocation must reduce the degree of order. This reduction in order increases the energy and results in a higher yield stress. The increased yield stress produced by the order-hardening mechanism is $\tau = \gamma/b$, where γ is the disordering energy per unit area of the slip plane, and b is the Burgers vector. For 70:30 brass, the value of 10 ergs/cm^2 has been used for γ; then τ is 4 kg/mm^2. At room temperature, the yield stress of 70:30 brass single crystals is 1.5 kg/mm^2. It is claimed that a significant fraction of the yield strength of brass is caused by short-range order.

Cottrell[45] first pointed out that a substitutional solute atom with different atomic radius, or an interstitial solute atom, interacts with the dilatational stress field around a dislocation. Hence the solute atoms form an atmosphere. The binding energy, γ_B, of a solute atom situated at a point having cylindrical coordinates r, θ from a positive edge dislocation is given by

$$\gamma_B = \frac{4}{3} \mu \varepsilon r_a^3 b \frac{1 + \nu}{1 - \nu} \frac{\sin \theta}{r} \qquad (2)$$

where μ is the shear modulus, ν is Poisson's ratio, b is the Burgers vector, and r_a and $r_a(1+\varepsilon)$ are the respective atomic radii of the solvent and the solute atoms. An important feature of Cottrell effect is the strong dependence of the locking force on the angle between Burgers vector and the dislocation line. As compared with carbon in alpha iron, very large amounts of zinc in copper are needed to obtain a yield point. This large amount is necessary partly because a zinc atom in copper has a smaller degree of misfit, 'ε', and partly because it distorts the lattice with spherical symmetry. Thus it can interact strongly only with the hydrostatic component of the stress field of an edge dislocation.

Chemical interaction of solute atoms with the stacking fault and its relation to the critical shear stress have been proposed by Suzuki[46]. In an f.c.c. crystal, partial dislocations of type $\frac{a}{6}$ <112> are more stable than the ordinary dislocations of type $\frac{a}{2}$ <110>, where a is the lattice parameter. The region separating the two partials is called a stacking fault. It has a hexagonal-close-packed crystal structure (h.c.p.). Since the cohesive energy between atoms in the h.c.p. stacking fault differs from that in the f.c.c. material, the concentration of the solute atoms also differs. This heterogeneous distribution of solute atoms is suggested to act in the same way as the Cottrell atmosphere. The locking force caused by such chemical interaction is independent of the angle between the Burgers vector and the dislocation line. This locking force is considerably weaker, however, than that due to Cottrell atmosphere. The locking force obtained by chemical interaction varies only slightly with temperature.

Meakin and Wilsdorf[47] have examined all the theories of increased critical shear stress by solid-solution hardening. For the case of alpha brass, they conclude that the Cottrell effect is the most important mechanism for solid-solution strengthening.

1.3.1.2 Lüders Band Formation

Sudden large deformation at the yield stress is known as Lüders strain. In the system copper-zinc, a sudden yield and large deformations are ascribed to the unlocking of dislocations pinned by the impurities present. A sudden yield drop and a yield elongation associated with a Lüders band occur whenever the initiation of slip is more difficult than its continuation. During loading, as the upper yield stress is approached, a small plastic strain results. When the yielding occurs suddenly, deformation propagates across the length of the specimen in the form of Lüders band. This propagation cannot be stopped by unloading. Lüders bands are observed to start at more places than one and spread until they meet each other. When every portion of the crystal is strained to the extent of Lüders strain, normal work-hardening begins.

1.3.1.3 Work-Hardening Behavior of Alpha Brass

As the concentration of zinc is increased in a copper-zinc alloy, the easy-glide range becomes longer, the stage-II linear-hardening range increases, and the stage III starts at a higher stress.

At the end of the easy-glide region, a delay has been observed in the change of the slip system from primary to conjugate as a function of strain[48,49]. Since a very high stress is required to initiate the slip on the secondary system, slip does not start in this system even if it

is favorably oriented. This phenomenon is called 'overshooting.' Overshooting may be measured in terms of the ratio of the applied shear stresses $\rho = \tau_{secondary}/\tau_{primary}$ at the beginning of secondary slip. $\rho = 1$ indicates no overshoot, and $\rho > 1$ indicates overshooting. For Cu-30%zn, $\rho = 1.28$, independent of the temperature and the initial orientation[50].

It has been found that the macroscopic resolved shear stress on the operative secondary-slip planes is very small[51]. Hence the shear stress on the primary system must be the controlling factor in initiating secondary slip. It is assumed that the easy glide ends when the stress concentration around clusters of dislocations on the primary slip plane is sufficiently large to initiate slip on another plane. In the case of alpha brass, higher stress concentration is required to initiate the secondary slip. This means that bigger clusters of dislocations are required on the primary planes, which is achieved by long easy glide.

Alternative explanation for the phenomenon of 'overshooting' has been proposed in terms of the low stacking-fault energy of alpha brass. Measurements of dislocation nodes in solid-solution alloys indicate that γ_{SFE}, the stacking-fault energies of solid solutions, are lower on corresponding pure metals. Stacking-fault energy of copper is lowered from 73 ergs/cm^2 [52] to 12-16 ergs/cm^2 [53] in 70:30 brass. Consequently, as the solute concentration in a solid solution is increased, the dislocations become more widely separated. It has been proposed that the widely extended dislocations cannot move easily from the primary slip system to the secondary slip system. This results in overshooting.

Stacking-fault energy is responsible for the ease or difficulty of cross-slip which begins at the onset of the third stage of hardening.

As mentioned above, the lower the stacking-fault energy, the wider is the separation between the partial dislocations. The wide separation of partial dislocations makes cross-slip difficult. However, an exception to this rule is the activity of dislocations in the cross-slip plane observed in alpha brass. Fourie[54] has proposed that the pile-ups of dislocations in the primary slip plane lead to the activation of nearby sources on cross-slip planes. In this process, dislocations do not have to constrict and then move from primary slip plane to cross-slip plane. Hence the cross-slip process can take place in spite of the low stacking-fault energy.

The phenomenon of dynamic strain ageing has also been observed in the deformation of alpha brass.

1.3.1.4 Nature of Slip Lines and Etch Pits in Alpha Brass

Kuhlmann Wilsdort and H. Wilsdorf[55] have shown that the slip lines in alpha brass do not assemble to form slip bands as in other metals. The slip lines are arranged at random and are of greatly varying depth. They are more widely spaced and are stronger than on pure metals. In between the strong lines, no fine slip is observed. Cross slip is observed in abundance. It may interconnect the slip lines until sometimes, especially at high deformations, more or less all lines on one system are linked with each other.

Kuhlmann Wilsdorf and H. Wilsdorf[55] have further stated that in the case of alpha brass it is easy to etch the repolished surface of a deformed specimen and make the slip traces reappear. Burke and Barrett[56], and McLean[57] have called these etched lines as striations or strain markings.

Wilsdorf and Fourie[58], and Meakin and H. Wilsdorf[47] have carried out extensive etch-pit studies on alpha brass. The slip observed in alpha brass has been termed inhomogeneous, since it occurs primarily on single atomic planes.

1.3.2 Deformation Behavior of Beta-Brass Single Crystals

Beta brass is an intermediate solid solution of zinc in copper. The ordered structure of beta brass is classified as a B2 type superlattice.

1.3.2.1 Dislocations in a B2 Type Superlattice

As shown in Figure 6, the passage of a dislocation whose Burgers vector is the unit vector of the disordered lattice through an ordered lattice would disorder an entire atomic plane. The passage of a second dislocation would reorder the plane. The creation of the large amount of disorder requires a large amount of energy. Thus the average force to move the single dislocation along such a slip plane is large. In order to avoid such a large expenditure of energy, Koehler and Seitz[59] originally put forward the idea of a 'superdislocation.' If two dislocations of the same sign follow one another closely across the slip plane, the disorder will be limited to a relatively small region. A superdislocation or a superlattice dislocation is made up of two such dislocations. The two dislocations are separated by an anti-phase boundary hereafter referred to as APB. Hence Brown[60] has stated that it is a geometric requirement that APB's originate and end on the dislocations.

The necessity of having the superlattice dislocation with a strip of APB is emphasized by Cottrell[61]. The stress to move the dislocation,

Fig. 6. Effect of the passage of a unit dislocation through an ordered lattice. (a) The ordered lattice. (b) Slip plane to the left of the dislocation shows disorder. (c) Disorder across the slip plane over the entire block (J. S. Koehler and F. Seitz[59]). . . . . .

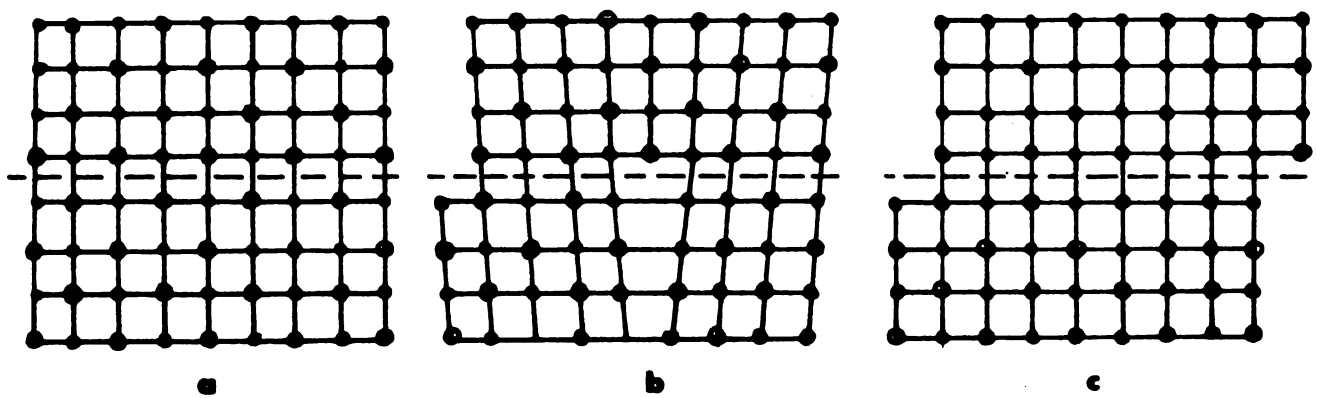

FIG. 6

τ, is given as

$$\tau = \frac{\text{Surface Energy of the fault}}{\text{Burgers vector}} \quad . \tag{3}$$

In the case of beta brass, τ is about 3×10^9 dynes/cm^2. However, the observed critical shear stress is an order of magnitude less than this value. A similar problem in the case of f.c.c. metals is explained with the help of the partial dislocations and the attached stacking fault. By analogy, Cottrell[61] states that the dislocations which cause slip in ordered beta-brass are not single dislocations of the $\frac{a}{2}$ <111> type, but either perfect unit dislocations in the ordered lattice or coupled pairs of $\frac{a}{2}$ <111>, leaving an ordered lattice in their wake during their motion.

Rachinger and Cottrell[62] have discussed the possibilities of having the Burgers vector of the type a <111>, a <110>, and a <100> in a B2 type superlattice. The travel of these perfect dislocations through the lattice does not affect the order. Assuming that they do not dissociate into imperfect dislocations, the following dissociations are possible:

$$\begin{aligned} a[111] &= a[110] + a[001] \\ a[110] &= a[100] + a[010] \quad . \end{aligned} \tag{4}$$

These reactions do not result in reduction of energy.

In order to have slip along [111], the following dissociation must take place:

$$a[111] = \frac{a}{2}[111] + \frac{a}{2}[111] \quad . \tag{5}$$

According to Rachinger and Cottrell[60], if $r >> a$, r being the separation between dislocations and a being the lattice parameter,

dislocation a[111] cannot undergo dissociations given in equation (4) and slip must occur along [111]. But when r = a, the structure at the center of the a[111] dislocations is not altered enough to prevent it from dissociating (according to equation 4) and thus a[100] slip can proceed. This phenomenon is related to the bond strength and the [111] slip is indicative of an exceptionally small atomic binding force, whereas the [100] should be a common mode of slip in alloys of B2 nature. Accordingly Tl(Br,I), LiTl, MgTl, and AuZn glide along [100]. AgMg slips along [111], but it has been considered a borderline case.

Head et al.[63] have, however, shown that a[111], a[100], $\frac{a}{2}$[111] are the types of dislocations that exist in beta brass. Because of the highly anisotropic nature of beta brass, the electron-microscope contrast theory based on the isotropic invisibility criterion fails, except for pure edge or pure screw dislocations. Head et al.[63] computed the theoretical image profiles according to the two-beam dynamical theory, and considering the full anisotropic strain fields of the dislocations. Comparing the character of the theoretical and experimental images, they found that the majority of dislocations in beta brass were screw dislocations of type a<111> gliding on $\{\bar{1}10\}$. Some of these a<111> dislocations were split into two $\frac{a}{2}$ <111> dislocations. Other dislocations were <010> type, which are glissile on {001}. This observation contradicts Rachinger and Cottrell's[62] argument that <001> dislocations will not be observed in beta brass owing to the very small bonding face.

1.3.2.2 Mechanical Strength of Crystals with Superlattice Structure

The strength is dependent both on the degree of long-range order and on the size of a sub-grain structure. The sub-grain structure in the case of ordered materials consists of anti-phase domains. Slip creates additional anti-phase boundaries and, hence, extra energy is required for further slip. Strength has also been observed to increase as a result of decreasing long-range order; and the maximum strength is found at a critical size of the domain[64]. Cottrell[61] has shown that the critical size is due to two conditions -- the smaller the domain size, the more disorder is created at an early stage of deformation, and hence it is harder to initiate slip. On the other hand, the material is more disordered when the domain size is smaller. Hence, the difference between the slipped and the unslipped condition is less energetic and thus the material is weaker. Cottrell[61] has derived an equation which relates the stress τ to the domain size 'ℓ',

$$\tau = \gamma_{DB}\ell^{-1}[1 - \alpha A\ell^{-1}] \qquad (6)$$

where γ_{DB} is the surface energy of the domain boundary, A is the thickness of the domain boundary and α is a shape factor. The basis for the maximum predicted in the equation above is as follows: (a) at $\ell = 0$, there are no domain boundaries because there is complete disorder and (b) at 'ℓ' = the specimen diameter, the specimen is one domain and hence there are no domain boundaries. Thus an intermediate value of 'ℓ' gives the maximum opportunity for creating disorder by dislocations cutting the domain boundaries.

The degree of order and the domain size cannot be controlled independently[65], and hence the strength maxima can occur at different

combinations of these two in various systems. Temperature is a major factor in controlling both the degree of order and the domain size. The relation between the resolved shear stress and the temperature is indicated in Figure 7. The feature observed near Tc is the result of the following two effects: (a) As Tc is approached from the higher temperature there is a rise in the short-range order to give an increase in strength; (b) As Tc is approached from below there is an increasing drag on the motion of superdislocations with decreasing long-range order.

1.3.2.3 Quenching Effects

Irrespective of the rate of quenching, beta brass always remains ordered at room temperature. Both the temperature from which the quenching is done and the rate of cooling affect the strength of beta brass[66,67].

Brown[68] has proposed that the dislocations are affected in two ways as a result of quenching. The spacing between the dislocations can be frozen during quenching. The spacing between the frozen-in superdislocations decreases with the quenching temperature. Thus the dislocations move more coherently. Further, the dislocations can come close together during the quench in order to form the superdislocation which is characteristic of complete order. In this process, the distance which the dislocations have to travel to reach their equilibrium spacing decreases with quenching temperature. Hence the entanglement and the jog production decrease with a resulting decrease in strengthening. Thus, whatever the mechanism, the strength decreases with decreasing temperature of the material prior to quenching.

The rate of quenching affects the strength through the number of vacancies quenched in the material. Brown[68] has suggested the following

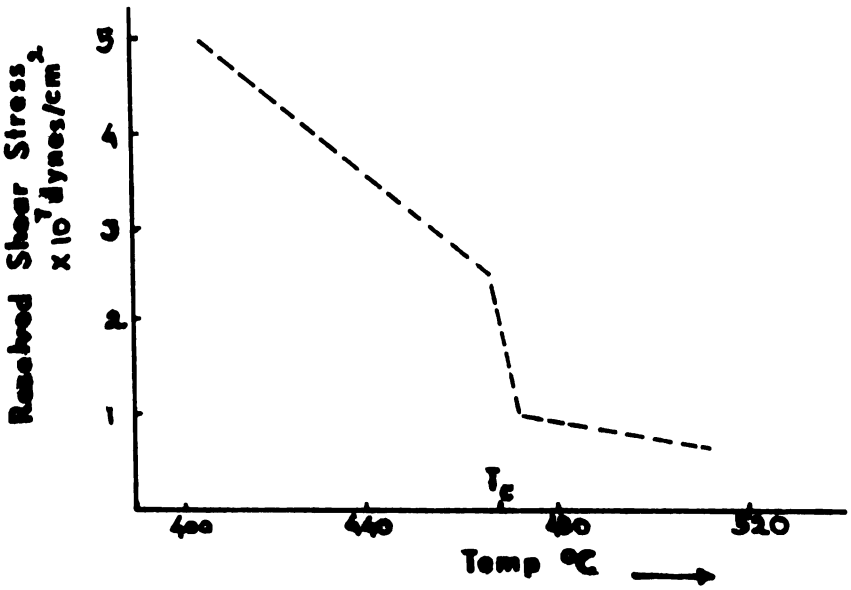
Residual Shear Stress
x 10⁷ dynes/cm²
5
4
3
2
1
T_c
400
440
480
520
Temp °C

FIG. 7

explanation for strengthening of ordered structures. The dislocations try to pair with each other during quenching. During their motion to pair up, they interact and climb. Jogs result due to such interactions and cause the strengthening. The change of the as-quenched properties with time at room temperature[69] has been explained on the following basis. During aging at room temperature, the excess vacancies which are quenched can migrate to the jogs and cause them to collapse. This reduces their strengthening effect.

1.3.2.4 Nature of Slip and Etch Pits in Beta Brass

Two distinct structural characteristics, namely the slip lines and the deformation bands, have been observed in the deformed beta brass[70,71]. Slip lines in beta brass are less prominent than those in f.c.c. metal and alloy crystals. These slip lines are very hard to observe under vertical illumination. Prominent deformation bands are easily visible with the naked eye, but under the microscope, oblique illumination must be used to see them.

Both the temperature and the mode of deformation affect the occurrence and the spacing of deformation bands[70]. Above the critical temperature, band spacing approaches the grain size of the material.

Bassi and Hugo[72] have carried out etch pit studies in beta brass. The density of etch pits was found to be higher inside the deformation band than that outside the band. The bands were not sharply defined, and they were found to originate from the grain boundaries.

1.4 Purpose and Objectives

Properties of materials are influenced by the presence of surfaces and interfaces. Effect of the interfaces on the properties of single-

phase materials has been explored in detail. The basic units for such investigations are bicrystals. In the field of two-phase materials, there is a need for corresponding research. Fundamental studies about the slip propagation using models like duplex crystals or two-phase bicrystals will help to explain the role of a phase boundary on the deformation behavior.

The main purpose of the present work is to develop a technique for obtaining duplex crystals and two-phase bicrystals of alpha-beta brass, and to find the growth mechanisms that will play important roles in preparing such crystals.

Another purpose of this work is to study the mechanical behavior of such fundamental units in uniaxial tension to understand the role of phase boundary during plastic deformation of two-phase materials. The interaction of slip with the phase boundary will be analyzed by dislocation models, with the hope that the results will shed some light on the work-hardening behavior of two-phase materials.

II. EXPERIMENTAL PROCEDURE

2.1 Crystal Growth

2.1.1 Growth of Alpha-Brass Single Crystals

Randomly-oriented single crystals of alpha brass were grown by the Bridgman technique in sharp-tipped graphite crucibles having internal diameters of 6.35 mm and 9 mm. Crucibles holding chemically-cleaned cylindrical pieces of commercial purity 70:30 brass were sealed in quartz tubes, which were placed in alumina crucibles and packed with refractory cement and water. These assemblies were allowed to dry before placing in the furnace. A schematic of an assembly is shown in Figure 8.

The tube furnace for growing single crystals was maintained at 980^{o}C with a constant-temperature zone of about 75 mm. Following two hours soaking in this zone, the assembly was lowered at a rate of 10 mm per hour. A schematic of the furnace is shown in Figure 9. The assembly was lowered for 12 to 14 hours before cooling to room temperature. The quartz seal was then broken to remove the specimen from the crucible.

2.1.2 Preparation of Alpha-Brass Single Crystals

The single crystals of alpha brass obtained as just described were sealed in closely-fitting quartz tubing and were annealed for 16 hours at 800^{o}C. Such annealing of alloy single crystals facilitates the removal of any microsegregation.

The end of the crystal that solidified last was ground off mechanically on an 80-grit continuous belt. The crystal was then

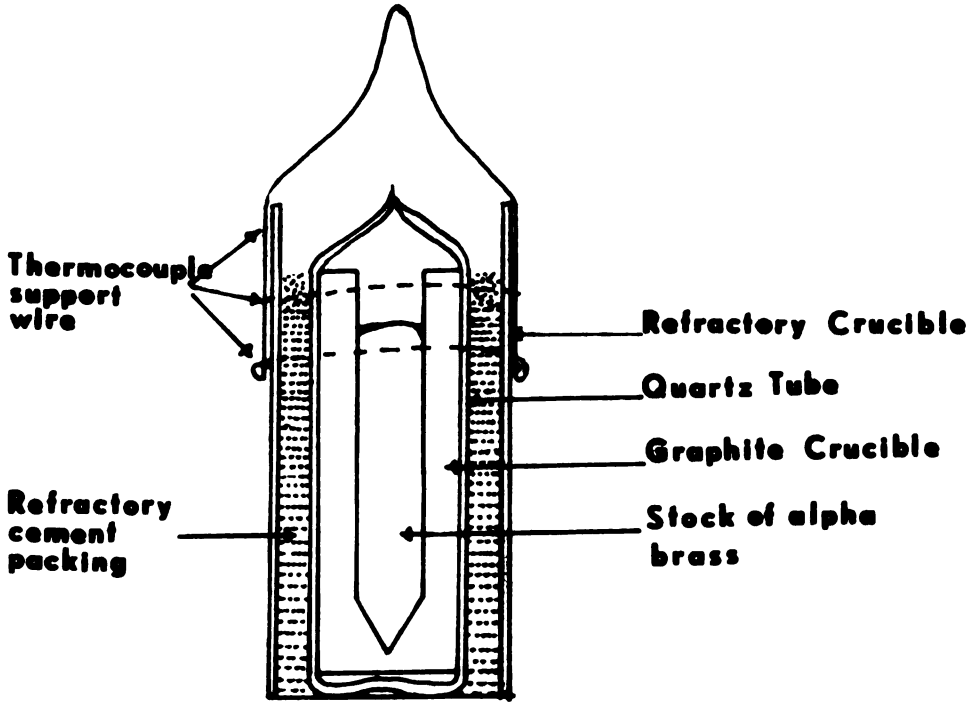
Thermocouple support wire
Refractory Crucible
Quartz Tube
Graphite Crucible
Refractory cement packing
Stock of alpha brass

FIG. 8

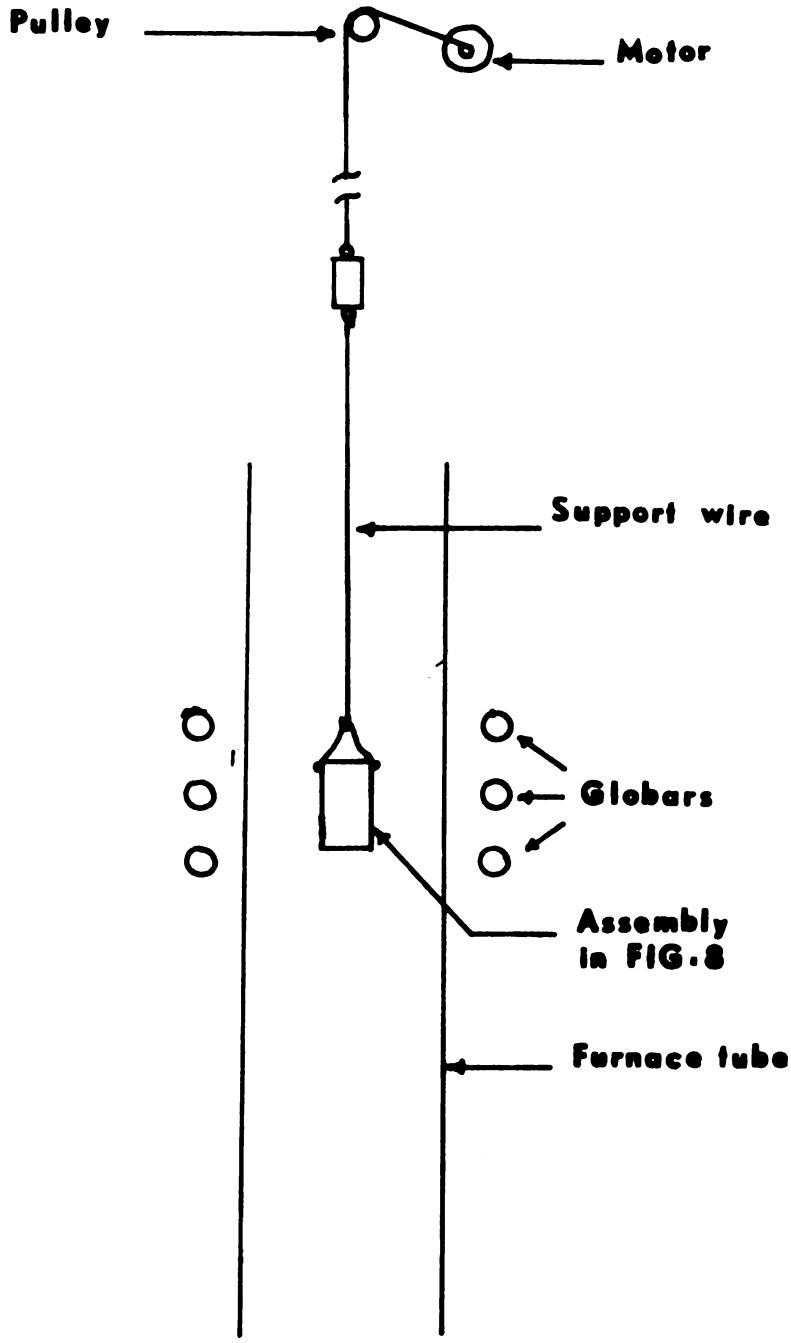
Pulley
Motor
Support wire
Globars
Assembly
in FIG.8
Furnace tube

FIG.9

polished with 240, 320, 400, and 600 grit Carbimet papers and a canvas lap soaked with 600-grit alumina. Large quantities of water were used on belt, papers, and the wheel. The final mechanical polishing was done on a velvet cloth with a 3-micron diamond paste and 'Metadi' fluid.

The mechanical damage introduced during grinding and polishing was removed between consecutive steps by chemical dissolution. Depending on the degree of mechanical damage, two different solutions were used. Deformed layers of the single crystals, caused by grinding and polishing up to 600-grit paper, were removed by a 1:1 solution of nitric acid and water. Damage caused by mechanical polishing beyond the 600-grit stage was small, and the above solution caused pitting. Therefore, a chemical polish of composition 66% acetic acid, 17% nitric acid, and 17% ortho-phosphoric acid was resorted to. The solution worked best in the temperature range of 35-45^{o}C, and specimens were accordingly soaked in hot water and the polishing solution was applied with a swab.

2.1.3 Preparation of Beta Brass and Alpha-Beta Brass Prior to Joining

2.1.3.1 Preparation of the Beta Stock

After melting a stock of 70:30 alpha brass under charcoal cover, weighed amounts of zinc were added to the melt, and the melt was thoroughly mixed by stirring. The crucible containing this melt was again kept in the furnace for about a half hour to achieve homogenization. Rectangular slabs were then cast in steel molds. After mechanical reduction by about 10% with the rolling mill, the slabs were annealed at 750^{o}C for four to six hours. To minimize the loss of zinc during annealing, specimens were packed in cast iron pipes together with charcoal and loose chips of brass.

Annealed stock was then analyzed microscopically and chemically, the latter with a Beckman DK-2A spectrophotometer. The chemical analysis was accurate within $\pm$ 0.5%. Remelting was sometimes necessary to adjust the concentration of zinc. The whole procedure of casting, rolling, annealing, and chemical and microscopic analysis was then repeated until beta brass (47.5-50 w/o zinc) was obtained.

The beta brass prepared as above was then cut and machined to obtain cylindrical pieces about 2.5 cm long and of approximately the same diameter as the alpha single crystal. These pieces were polished flat on one end and cleaned chemically.

2.1.3.2 Preparation of the Alpha-Beta Brass Foil

Alpha-beta brass foil for the joining process was in the form of circular discs having the same diameter as the single crystals of alpha brass. These discs were cut from a rolled sheet of 60:40 alpha-beta brass, and then chemically cleaned and reduced to thickness of 0.125 mm with a 1:1 solution of nitric acid and water.

2.1.4 Joining Beta Brass to Alpha Brass Single Crystals

An open-ended quartz tube containing an alpha brass single crystal, a thin disc of polycrystalline alpha-beta brass, and a cylindrical piece of polycrystalline beta brass was kept on an asbestos sheet supported by a steel block, as shown in Figure 10. A nichrome heating element, in the form of a strip 3.175 mm wide and with a resistance of 0.03 ohm/cm, was wound around the quartz tube in order to melt the beta brass and the foil. One turn of the heating element surrounding the top portion of the alpha-brass single crystal facilitated the wetting of alpha brass by

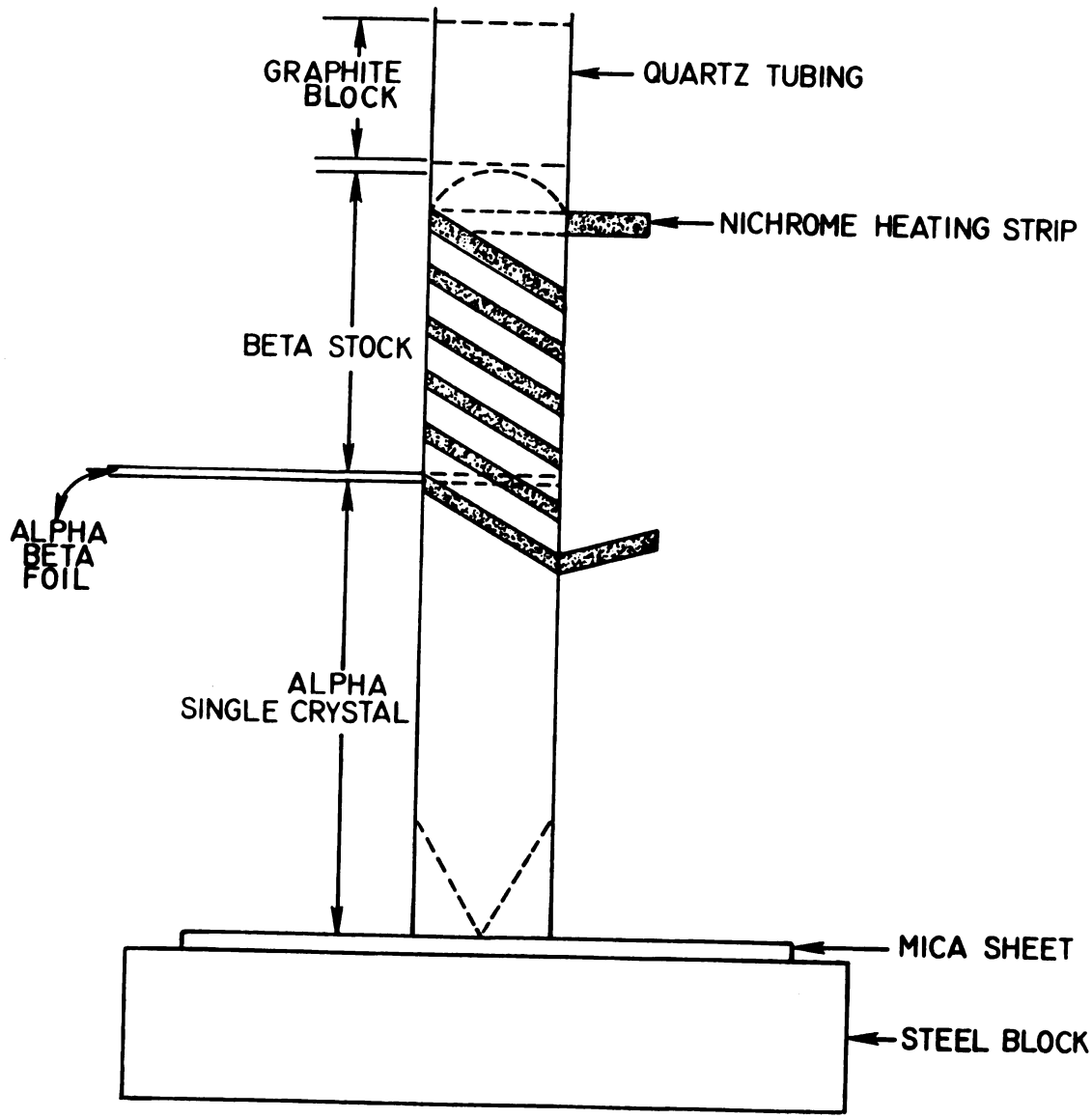
GRAPHITE BLOCK
QUARTZ TUBING
NICHROME HEATING STRIP
BETA STOCK
ALPHA BETA FOIL
ALPHA SINGLE CRYSTAL
MICA SHEET
STEEL BLOCK

FIG. 10

the molten alpha-beta brass foil and beta brass. After allowing the melt to heat in this way for 3 to 5 minutes, the asbestos sheet was removed from the bottom of the tube. The tip of the alpha single crystal then rested on the steel block facilitating unidirectional solidification.

2.1.5 Heat Treatments Following the Joining Operation

The specimens, joined as described in 2.1.4, had a two-phase transition zone consisting of alpha and beta between the single-crystal alpha and the polycrystalline beta. In order to reduce the extent of this transition zone, two heat treatments were scheduled.

In the first heat treatment, a quartz tube containing the as-joined specimen was placed in an alumina crucible, and this assembly was suspended by a chromel support wire in a tube furnace maintained at 800^{o}C. The assembly was placed in a temperature gradient of 32^{o}C/cm in the furnace, with the transition zone at 760^{o}C. After soaking for 15 minutes in this position, the specimens were lowered at a rate of 10 cm/hour. Such soaking and lowering was repeated two or three times. This heat treatment alone was found to be sufficient to obtain duplex crystals.

The second heat treatment employed a single strip nichrome heating element to heat only the transition zone up to 760-780^{o}C. This 'local-annealing' arrangement is illustrated in Figure 11. Following this treatment, which lasted one hour at a time, the specimens were air cooled. A small flat for microscopic examination was then polished along the specimen length. Photomicrographs were taken to cover the entire transition zone. As the transition zone decreased in width, local annealing cycles were occasionally reduced to 15 to 30 minutes. Local

Fig. 11. Schematic diagram of the apparatus for local annealing.

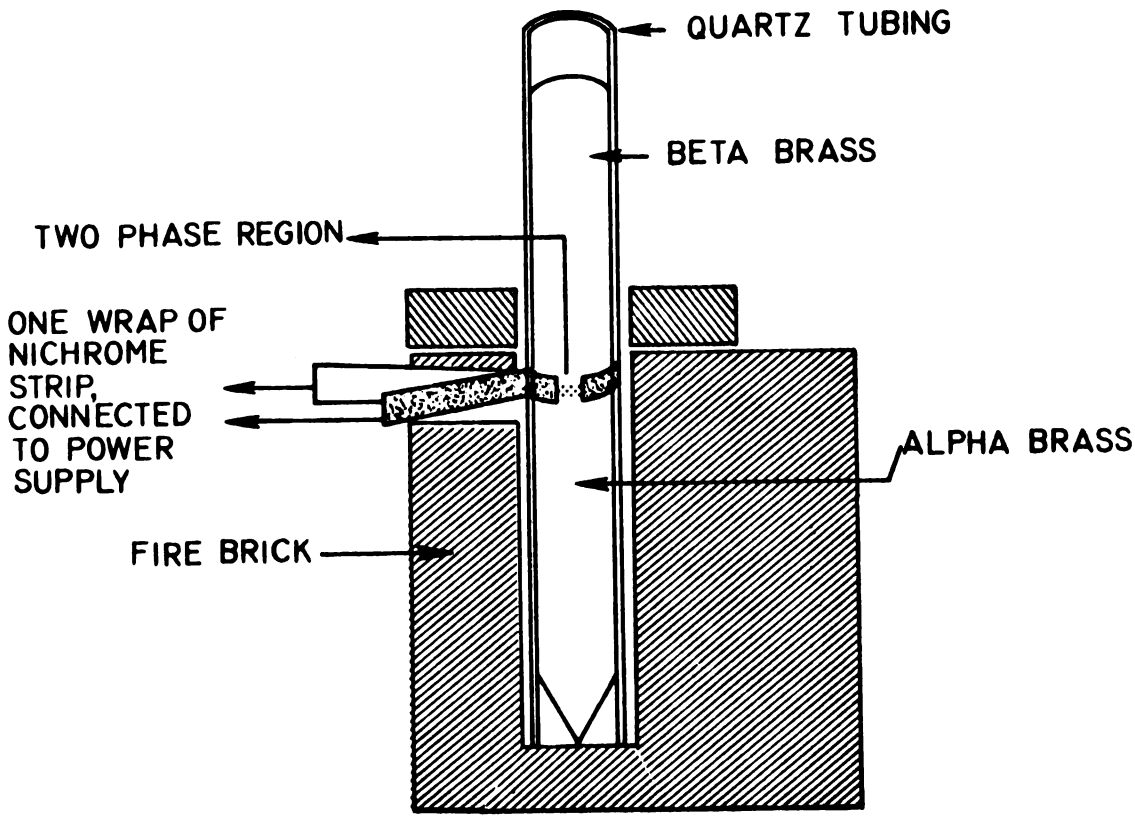
QUARTZ TUBING
BETA BRASS
TWO PHASE REGION
ONE WRAP OF NICHROME STRIP, CONNECTED TO POWER SUPPLY
ALPHA BRASS
FIRE BRICK

FIG. 11

annealing cycles were repeated until the transition zone became small enough to yield a very sharp boundary between the single crystal of alpha and the multi-crystal of beta.

2.2 Specimen Preparation for Mechanical Testing

To get a rectangular cross-section and a reduced gage section of 3.8 cm on the specimens, careful machining was carried out removing only 0.05 mm thick layers during every cut. The final cuts were only 0.025 mm deep. The machined specimen is shown in Figure 12. Following the machining, the specimens were mechanically and chemically polished according to the same procedure as described in 2.1.2. Because of the reduced gage section, polishing on two of the four sides was not possible by usual methods. Therefore, small strips of various grade carbimet papers were attached to thin aluminum plates, which were rubbed back and forth on the specimens.

After polishing, steel nuts were silver soldered to the specimen ends. One end was soaked in water while the other end was being soldered, as suggested by Brindley et al.[73] Mechanical and chemical polishing were repeated after soldering the nuts.

Laue back-reflection x-ray photographs were taken on two adjacent surfaces, in both the alpha and the beta regions, to determine the crystallographic orientations.

2.3 Mechanical Testing and Observations

After light etching, the specimens were tested in uniaxial tension in an Instron testing machine. The rate of displacement of the cross-head was 0.05 cm/min. At various stages during the testing, the specimens were unloaded and removed from the grips in order to study the

Fig. 12. A machined tensile-test specimen.

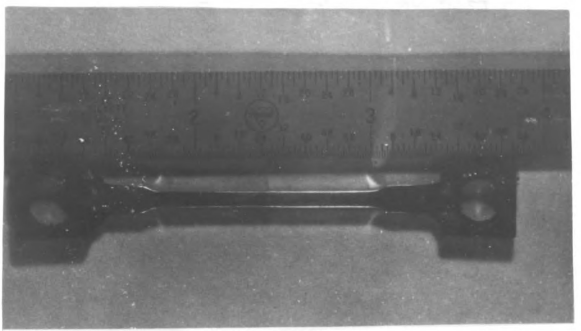

FIG. 12

slip distribution by optical microscopy. Attention was mainly focused on the slip patterns in the vicinity of phase boundaries. All the four surfaces of the specimens were studied to find the orientation of the active slip planes with respect to the tensile axis.

For more detailed observations, single stage Formvar and double stage plastic-carbon replicas of the surfaces were prepared. In the latter method, a replicating tape was softened in acetone and pressed on the specimen surface. This plastic replica was a negative impression of the surface topography. A carbon film a few hundred Angstroms thick was deposited on this plastic replica. The plastic backing was then dissolved by placing the specimen in acetone for 24 hours. A thin layer of petroleum jelly was applied on the carbon film to prevent its disintegration in acetone. After the plastic backing was dissolved, the jelly was dissolved in carbon tetrachloride. Using copper grids, the carbon film was first transferred to a 1:1 solution of alcohol and water, and then dried. Occasionally, the original plastic replica was taken while the specimen was in the testing machine. The replicas were observed with the Hitachi HU-11 A electron microscope operated at 50 kv.

2.4 Electron Microprobe Analysis

A two-phase bicrystal of alpha-beta brass containing a sharp phase boundary and a specimen at an intermediate stage of heat treatment were analyzed for zinc concentration with an 'Advanced Research Laboratories' microprobe. The two-phase bicrystal specimen was traversed in a direction perpendicular to the sharp phase boundary. The other specimen was probed through the transition zone in directions which are parallel and perpendicular to a set of Widmanstätten plates. The accelerating

voltage for this operation was 25 kv and the column current was stabilized to within 1%.

Prior to the use of the microprobe, the specimens were polished, etched, and photographed. The etching effect was then removed by repolishing. Once in the microprobe, the phase boundary in the bicrystal specimen, and the transition zone in the other specimen, were located with the help of fiducial identification marks on the photographs.

2.5 Scanning Electron Microscopy

The surface topological features of the morphologies developed during the heat treatment and slip-line distribution were observed with 'Advanced Metals Research' scanning electron microscope operated at 21 kv. The specimens were cut with a jeweler's saw to minimize any damage introduced by cutting, and were coated with a 200 A^{o} thick gold-palladium film. The specimens were examined in the emissive mode with a tilting of 40 to 50^{o}.

III. RESULTS

During the course of this work, duplex crystals and two-phase bicrystals of alpha-beta brass were prepared by the techniques described in the previous chapter. Mechanical testing under uniaxial tension was carried out after careful machining and polishing. Observations made on these specimens during their growth and mechanical testing are presented in the following sections.

3.1 Growth of Duplex Crystals and Two-Phase Bicrystals

The specimens were obtained by melting the beta brass on the substrates of the single crystals of alpha brass covered with thin foils of alpha-beta brass. A two-phase transition region consisting of both alpha and beta phases occurs between the single-crystal alpha and the polycrystalline beta. In most of the specimens prepared in this work, this transition zone was about one millimeter wide. This zone consisted of alpha precipitates of various morphologies in the beta matrix, and along the beta grain boundaries. Two different kinds of morphologies were observed. In the first kind, the precipitate of alpha present in the transition zone was continuous with the alpha single crystal, as shown in Figure 13. In the second kind, a continuous layer of beta phase separated the precipitate from the alpha single crystal. This feature is illustrated in Figure 14. After undergoing the first heat treatment, the continuous layer of beta broke down and the alpha precipitates grew in continuation with the alpha single crystal. The precipitate

morphology was predominantly in the form of primary Widmanstätten plates. The continuous layer of beta shown in Figure 14 breaks down on heat treatment, as can be observed in Figure 15. The specimens wherein the alpha-precipitate plates are connected to the alpha single crystal were not subjected to the first heat treatment of lowering through the temperature gradient.

During both the heat treatments, grain growth was observed in beta regions that were in contact with the transition zone. To obtain duplex crystals of alpha-beta brass it was sufficient to repeat the first heat treatment two or three times. Cyclic local annealing (the second heat treatment) was not required. Because of the repetitive first heat treatment, the transition zone was minimized, the alpha-beta segments in the transition zone were coarsened, and the alpha segments were crystallographically oriented with respect to each other. Such a duplex region obtained after repetitive treatments is illustrated in Figure 16.

For preparing the two-phase bicrystal specimens, the second heat treatment was very effective. Here the specimens were locally annealed only in the vicinity of the two-phase region. Local annealing cycles of one hour gave the best results. The effect of cyclic local annealing on the two-phase zone is shown in Figures 17 and 18. Two series of pictures from two specimens shown in these figures illustrate the morphological features observed at the various stages during the heat treatment. The reduction of the transition zone did not necessarily progress at the same rate in different specimens. This difference could be attributed to the different response of various plate morphologies to the heat treatment.

The progressive decrease in the size of the two-phase transition zone took place by two distinct modes. In one, the alpha plates dissolve in beta during heating and precipitate as split islands during cooling, as shown in Figure 17. During heat-treatment cycles, the islands shrink in size and eventually dissolve completely in beta. In the other mode, the alpha plates get progressively thinner at the tip and thicker at the base as illustrated in Figure 18. The grain growth of the beta phase during this heat treatment can also be seen in Figure 18. Such grain growth tended to reorient the alpha plates present in the two-phase transition region. The grain boundary 'z' in Figure 18(b) is seen to be moving to the left on prolonged cyclic annealing, as shown in micrographs (c) and (d) of the same figure. As this grain boundary shifted, the platelet orientations have likewise changed to conform with the plates already existing in the growing grain.

The grain boundaries also helped to reorient the platelets by grain boundary diffusion. Regions of low zinc in the consumed grain help to change the platelet orientation; and the latter is guided by crystallographic considerations. These features are illustrated in Figure 19.

Observations under the scanning electron microscope bring out the platelike nature of the precipitates. The tip of an alpha segment ending towards beta is seen at point 'A' in Figure 20. The beta regions pointing towards the alpha single crystal are seen at points 'B' in Figures 21 and 22.

Irrespective of the mode of platelet dissolution, cyclic local annealing was continued until a sharp boundary formed between the alpha single crystal and the beta grains as shown in Figure 23. Often the

grain growth in beta was predominant enough to provide a single grain of beta in contact with the single crystal of alpha.

A two-phase bicrystal having a sharp boundary, and a specimen with the transition zone (as obtained at an intermediate state of annealing), were analyzed with an electron microprobe. The results obtained in this analysis are shown in Figure 24. At the phase boundary in the two-phase bicrystal, the zinc concentration is seen to change abruptly from 37-38% zinc (alpha side) to 48% zinc (beta side). Inside alpha away from the boundary the concentration of zinc dropped further to 30% zinc, which is the composition of single crystals of alpha over a distance of 80 microns. There was no such change in composition inside the beta region.

3.2 Deformation Behavior of Duplex Crystals

Each specimen tested for investigating the deformation behavior consisted of a single-crystal alpha, duplex-crystal alpha and beta, and a large-grained polycrystalline beta in series, as shown in Figure 25. The results of the tensile tests on these specimens are presented in Figure 26 and Table 1. At different stages during the test, the specimens were unloaded and removed from the testing machine in order to study the slip distribution. All the specimens were ultimately loaded to fracture.

Observations made during the uniaxial tensile test can be classified as:

1) deformation behavior of alpha,

2) slip accommodation in the duplex region,

3) deformation behavior of the entire specimen.

These observations are presented in the following subsections.

3.2.1 Deformation Behavior of Alpha

Progress of the slip front in the alpha-brass single crystal during deformation is shown in Figure 27. The plastic deformation started as single slip in the alpha single crystal at a point away from the duplex region as shown in Figure 27(a). With increasing strain, slip progressed towards the duplex region. The travel of the front of the plastic deformation towards the duplex region is illustrated in Figure 27(b), (c) and (d).

Typical slip distributions in the alpha single crystal after 11% total strain at 4.8 mm, 6.4 mm, and 12.8 mm away from the duplex region are shown in Figure 28(a), (b), and (c) respectively. These figures show that different slip planes become active as the deformation progresses towards the duplex region. Away from the interface in alpha, slip was observed mainly as single slip at this point.

At higher strains, extremely heavy slip was observed in alpha. Examples of such slip distribution are seen in Figures 29 and 30.

3.2.2 Slip Accommodation in the Duplex Region

Initial deformation of the duplex region occurs only in the alpha segments as a result of the continuation of slip from the alpha single-crystal regions, as shown in Figure 31. Slip traces observed in these alpha segments are parallel to the primary slip traces in the alpha single crystal. Such a duplex region of alpha-beta segments may be regarded as an oriented composite.

With increasing strain, the slip-line density in each alpha segment increased, and secondary and cross-slip systems became active near every individual alpha-beta phase boundary. At the same time, beta segments

began slipping on a very fine scale. Figures 32 and 33 show these features as seen under an optical microscope. The regions where slip lines have propagated through the phase boundary are indicated by the letter A. Regions marked B and C show multiple slip and cross-slip, respectively, in the alpha segments.

At very large strains, slip in beta segments gets coarse, and at various places slip lines are observed to continue from alpha segments on a one-to-one basis. This feature is illustrated in Figure 34, an electron micrograph of the deformed specimen studied with a two-stage plastic-carbon replica.

3.2.3 Deformation Behavior of the Entire Specimen

On further deformation, slip in beta segments continues over to the beta grain which is in contact with the duplex region, and proceeds into the beta region. As shown in the region between 'x' marks in Figure 35, slip traces in beta grains can be detected by the naked eye at total strains of 70-90%. By the time that slip started in beta, the alpha single crystal was necking and twisting. Necking in alpha traveled back and forth similar to Lüders-band progression in the single crystals of alpha, as observed by Brindley et al.[73] During the necking of alpha, the applied stress remained constant. In beta, however, more and more slip occurred.

3.3 Deformation of Two-Phase Bicrystals

The results of the tensile tests on the two-phase bicrystal specimens are presented in Figure 36 and Table 2. All the specimens were tested at the same deformation rate. The crosshead displacement rate was 0.05 cm/min.

The deformation behavior of the two-phase bicrystals can be divided into three parts, as in the case of the deformation behavior of the duplex crystals. These parts are as follows: (1) deformation of alpha away from the phase-boundary region; (2) deformation of alpha at about 1 to 2 mm from the phase boundary; and (3) deformation of beta.

The deformation initially starts away from the phase boundary and progresses towards it as single slip. These portions of the alpha single crystal show slip lines of nearly uniform depth. As the slip lines approach the phase boundary, however, they are seen to decrease in their depth and intensity. They show a distinct tapering towards the phase boundary, as illustrated in Figure 37.

As the loading continues, the slip lines come closer to the phase boundary. Secondary slip and cross-slip appear. The most important observation at this point is that the tip of the primary-slip system, where the cross-slip originates, need not be at the phase boundary. As can be observed in Figure 38, the intersection of the primary and cross-slip systems may be either at the phase boundary or away from it.

Depending on the relative crystallographic orientation of the alpha and beta regions, slip continued across the phase boundary. The nature of slip lines in beta is distinctly different from that in alpha. Often slip in beta can be observed by naked eye but cannot be located with an optical microscope. Oblique illumination has to be used to observe the slip distribution.

Various features of the slip in beta are shown in Figures 39, 40, 41, and 42. Deformation of beta can take place by fine sliplines (Figure 41), or by surface rumples (Figure 42).

If the crystallographic orientation of the two phases is not suitable for the progress of slip, extremely heavy deformation takes place in alpha without any observable deformation in beta. This feature can be observed in Figure 43.

Fig. 13. A two-phase transition zone with alpha-precipitate plates connected with alpha single crystal. Alpha phase is etched light with ferric-chloride etch . . .

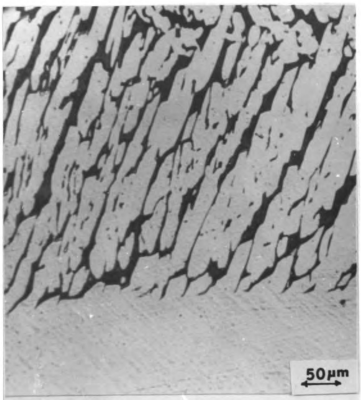

Fig.13

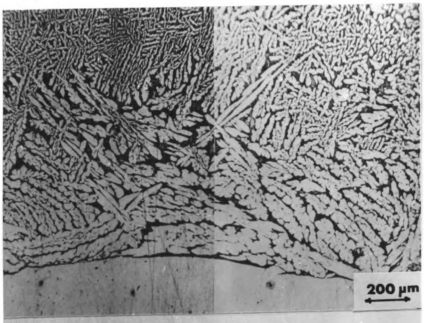

Fig. 14

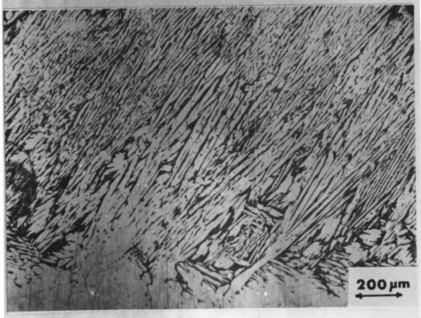

Fig. 15

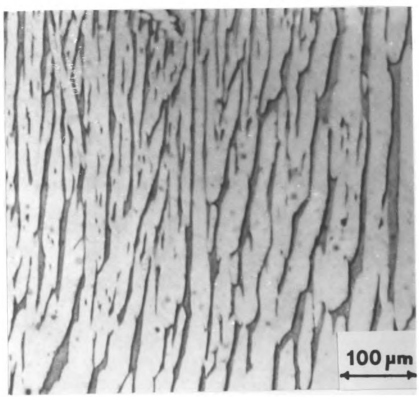

Fig.16

Fig. 17. Dissolution of alpha platelents and alpha island formation as a result of cyclic local annealing for (a) 3 hours, (b) 5 hours, and (c) 7 hours. Ferric chloride etch (60X). Regions marked Y show the alpha islands.

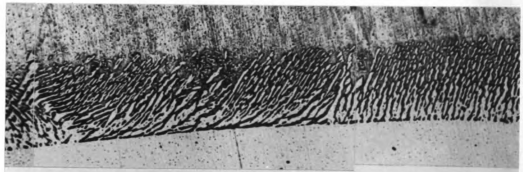

a

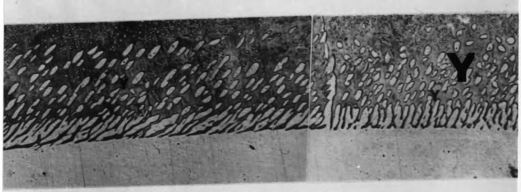

b

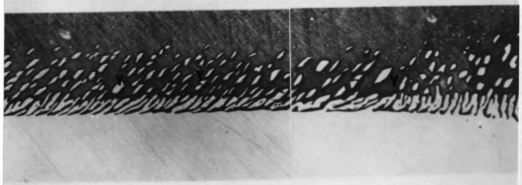

c

FIG. 17

Fig. 18. Grain growth in beta and widening of the base of the alpha plates after cyclic local annealing for (a) 3 hours, (b) 7 hours, (c) 18 hours, and (d) 20 hours. Ferric chloride etch (60X). Regions marked X show the widening of the precipitate plates, and symbol Z indicates the migrating grain boundary . . . . . .

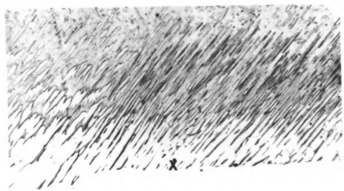

a

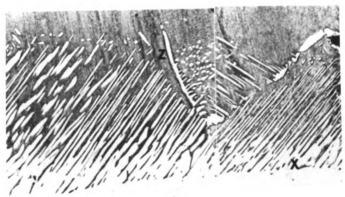

b

FIG. 18

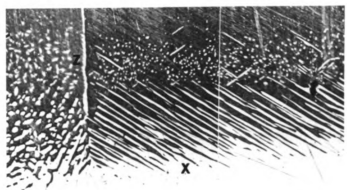

c

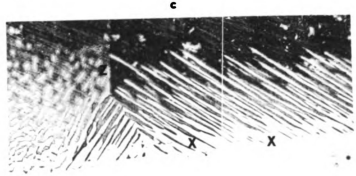

d

Fig. 19. Change in orientation of the platelet. The arrow indicates a typical platelet . . . . . .

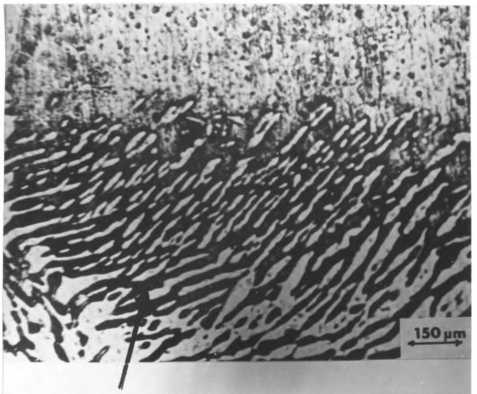

FIG. 19

Fig. 20. Scanning-electron micrograph showing the sharp tip of an alpha platelet. (Note the region A) . . . . . .

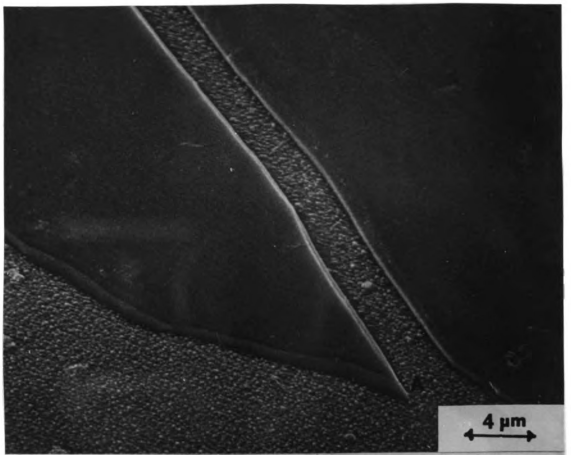

Fig. 20

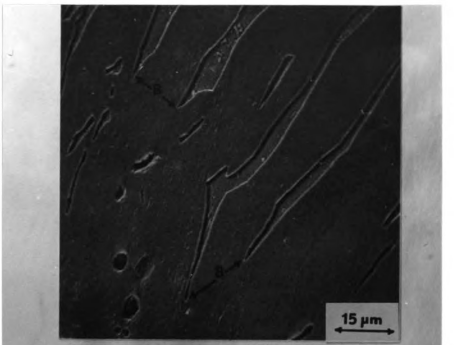

Fig. 21

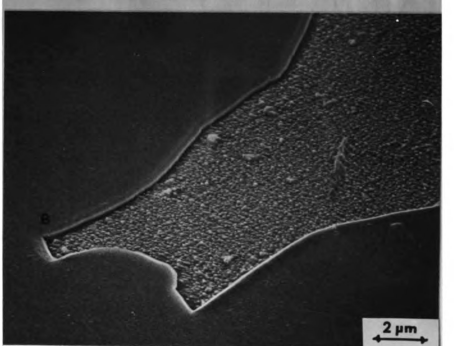

Fig. 22

Fig. 23. (a) A specimen showing a sharp boundary after the completion of all heat treatments. (1.5X)
(b) The sharp alpha-beta phase boundary in a two-phase bicrystal. Ferric chloride etch. (60X) . . . .

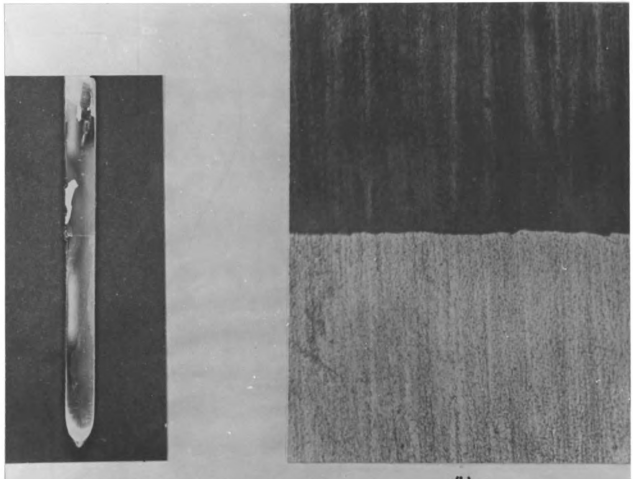

FIG. 23

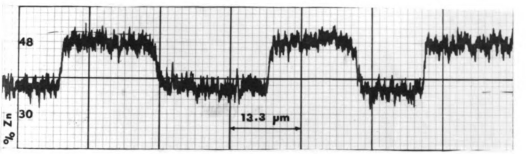

(a)

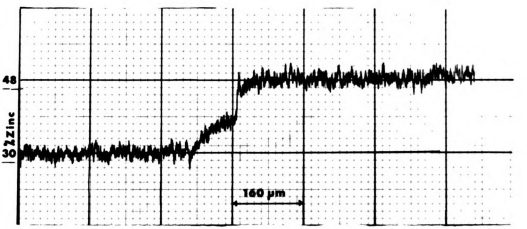

(b)

FIG. 24

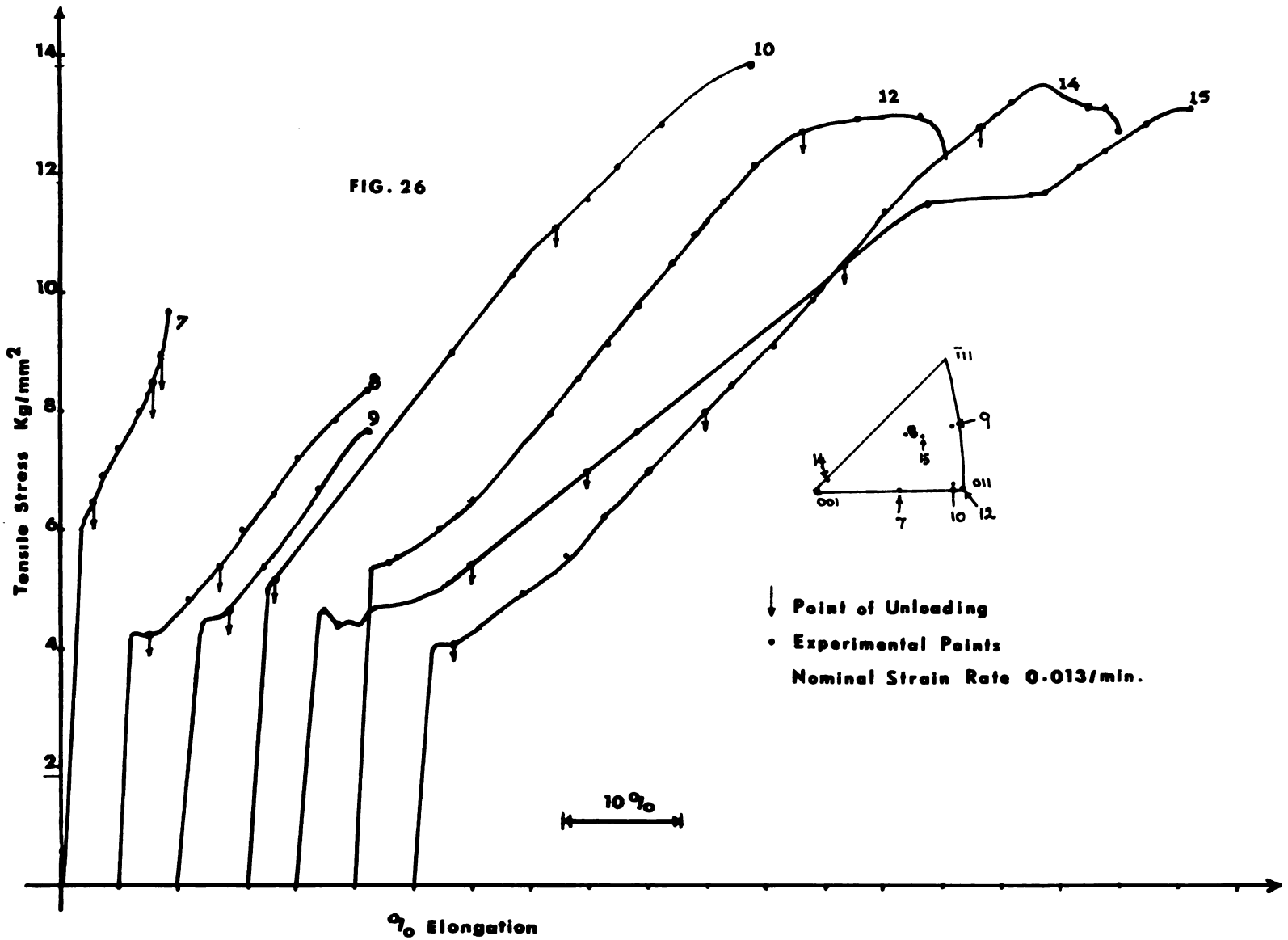
FIG. 26
Tensile Stress Kg/mm²
% Elongation
10 %
Point of Unloading
Experimental Points
Nominal Strain Rate 0.013/min.
7
8
9
10
12
14
15
001
011
111

Table 1. Results of the Tensile Tests on Duplex-Crystal Specimens

Specimen No.	Yield Stress of Alpha kg/mm^2	Ultimate Tensile Stress kg/mm^2	% Elongation	Fractured in
7	6.00	9.70	10	Beta
8	4.2	8.45	23.35	Beta
9	4.57	7.73	18.16	Interface
10	4.89	13.91	42.69	Beta
12	4.65	12.71	74.19	Interface
14	5.37	13.06	50.73	Alpha
15	4.00	13.22	61.51	Alpha

Fig. 27. Slip distribution in the alpha single crystal at various strains, (a) 2.3%, (b) 4.5%, (c) 5.5%, and (d) 6.3%, total strain (X5) . . . . . .

(a)

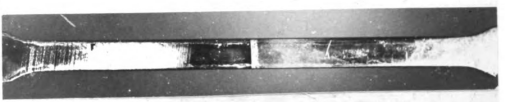

(b)

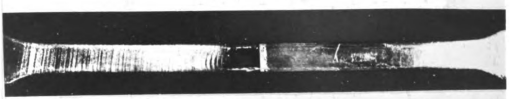

(c)

(d)

FIG 27

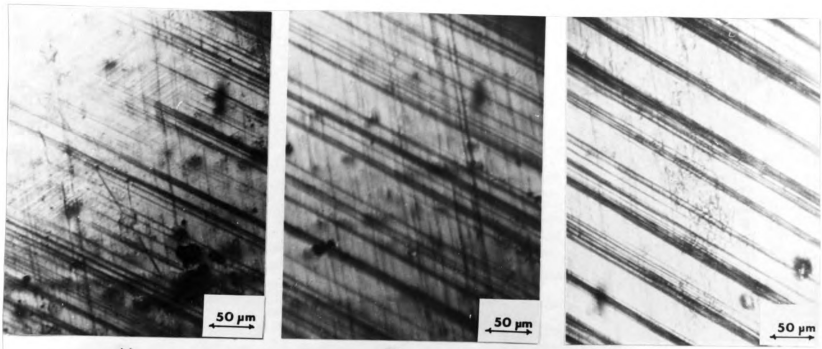

(a) (b) (c)

FIG. 28

Fig. 29. Heavy slip in alpha single crystal at 50% total strain.

Fig. 30. Heavy slip in alpha single crystal at 45% total strain.

FIG. 29

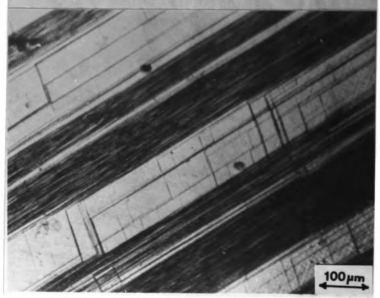

FIG. 30

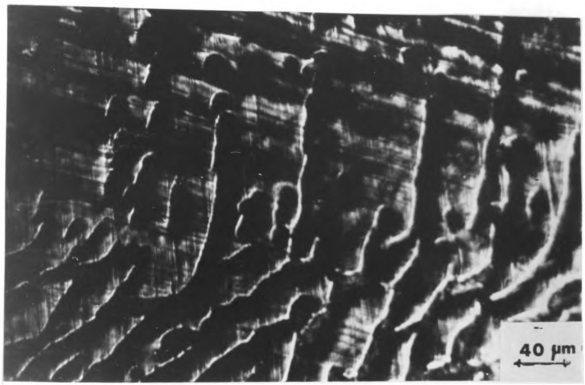

FIG.31

Fig. 32. Slip propagation through the alpha-beta phase boundary in the duplex region. Regions marked A show the propagation of slip through the phase boundary, B and C show secondary slip and cross-slip in alpha respectively . . . . . .

FIG.32

Fig. 33. Slip propagation across the alpha-beta phase boundary in regions containing alpha islands. Regions marked A show the propagation of slip through the phase boundary, B and C show secondary slip and cross-slip in alpha respectively . . . . . .

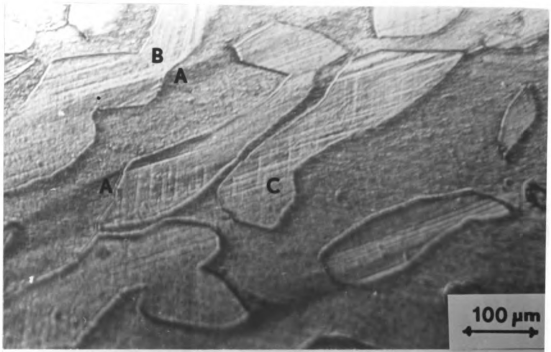

FIG·33

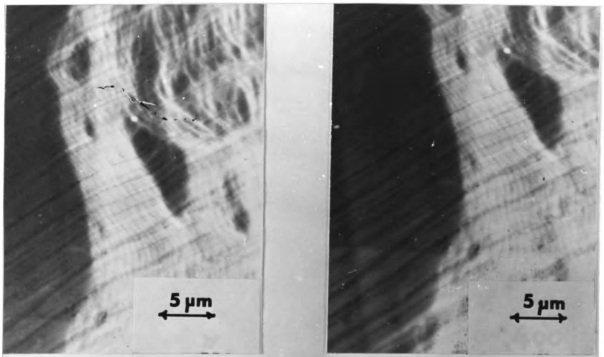

FIG. 34

Fig. 35. Macrograph showing coarse slip in beta, after considerable deformation of the alpha single crystal. (x5) (Note the region between 'X' marks) . . . . . .

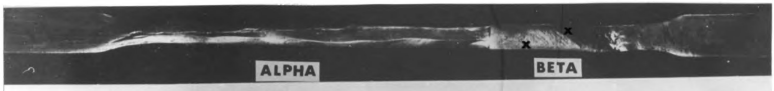

FIG.35

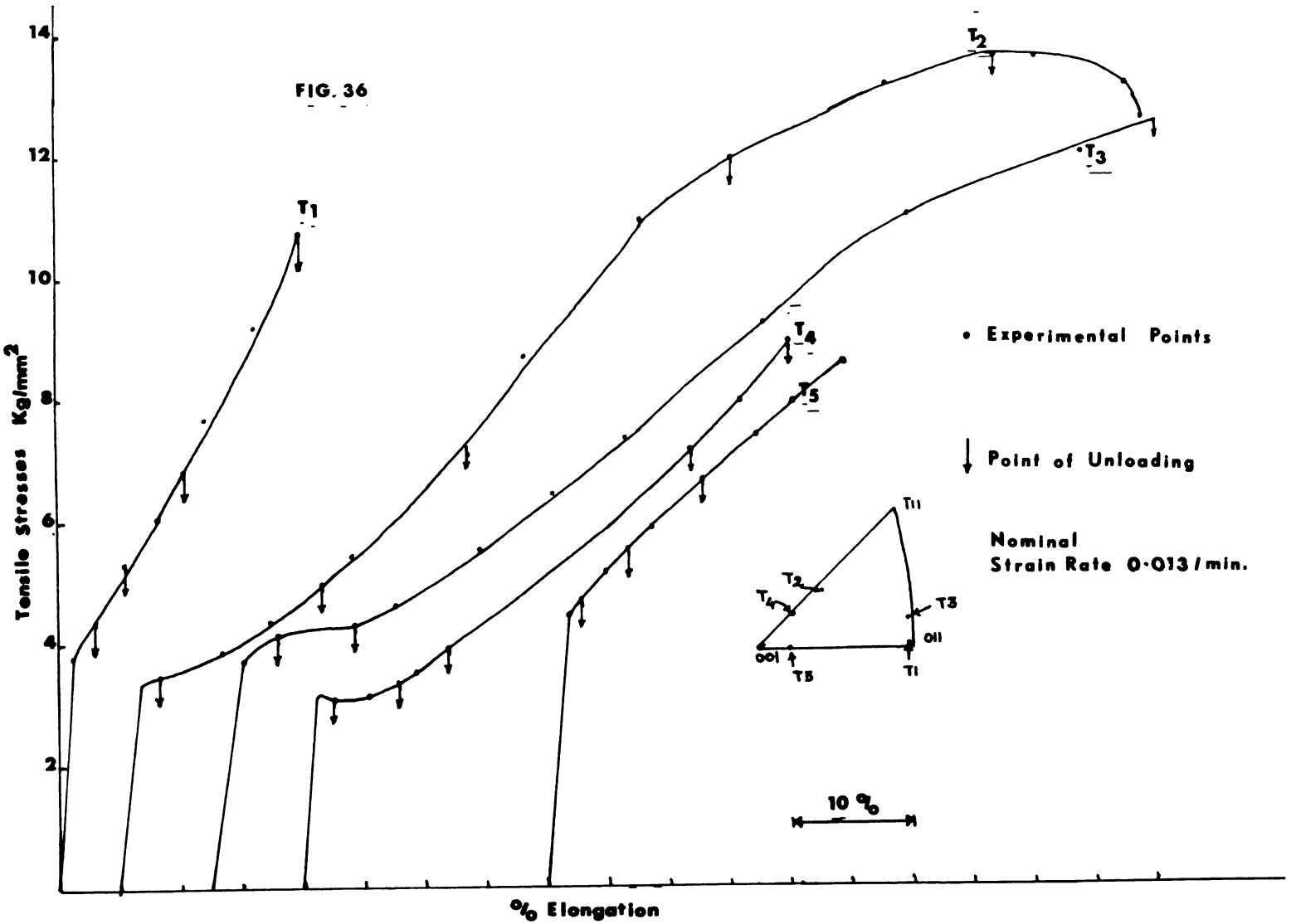
FIG. 36
Tensile stresses Kg/mm²
% Elongation
T1
T2
T3
T4
T5
• Experimental Points
Point of Unloading
Nominal
Strain Rate 0·013/min.
10 %
T11
T2
T4
T3
011
001
T5
T1

Table 2. Results of the Tensile Tests on Two-Phase Bicrystal Specimens

Specimen No.	Yield Stress of Alpha Kg/mm^2	Maximum Stress up to which the specimen was loaded Kg/mm^2	% Elongation at maximum stress	Resolved Shear Stress in alpha at which slip occurred in beta Kg/mm^2
T_1	3.8	10.75	20	2.4
T_2	3.35	13.6	76.5	4.0
T_3	3.7	12.5	75.00	2.56
T_4	3.2	8.95	39.6	3.2
T_5	4.49	8.6	24.5	2.65

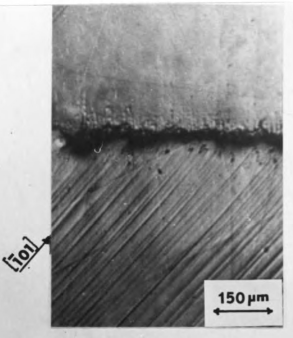

Fig. 37

Fig. 38

Fig. 39. Slip initiation in beta. A diffuse slip band 'D' is present in beta. It is parallel to the slip direction in alpha. (Applied stress 6.94 kg/mm^2, resolved shear stress 2.32 kg/mm^2, total strain 10.62%. Active slip plane in alpha is parallel to the active slip plane in beta) . . . . . .

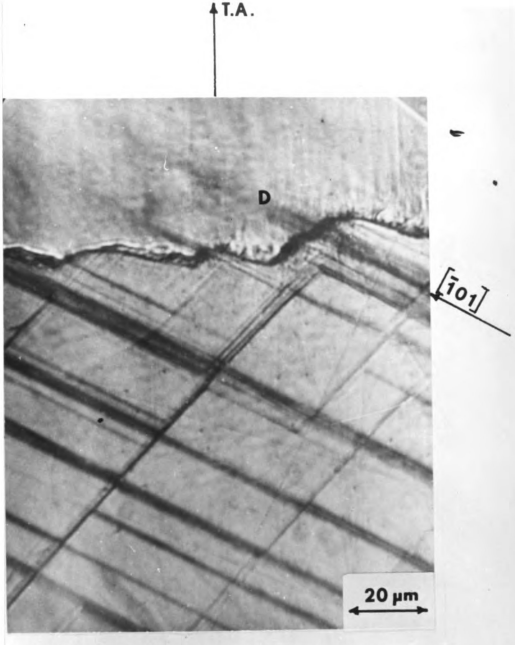

Fig. 39

Fig. 40. Slip in beta after 19.68% elongation. Slip in alpha cannot be observed because of the drastic change in the cross-section at the phase boundary. 'X' is a grain boundary in beta. In this specimen, the active slip plane in alpha is parallel to that in beta . .

Fig. 40

Fig. 41. Fine slip lines observed in beta have joined together to give an appearance of a coarse band (total strain 19.68%). In this specimen, the active slip plane in alpha is parallel to that in beta . . . . . .

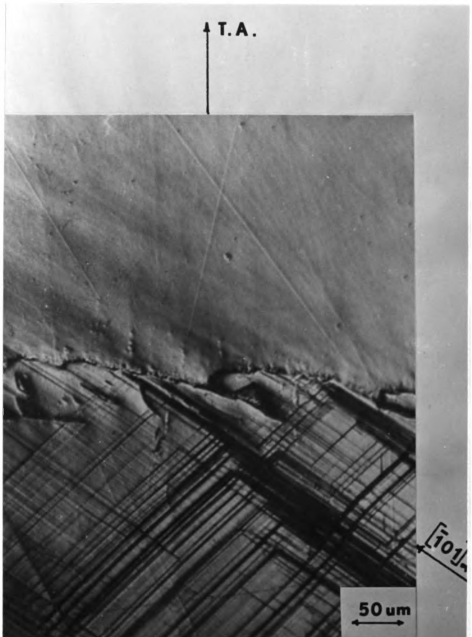

Fig. 41

Fig. 42. Slip propagation in beta. Deformed areas of beta indicate both fine slip lines (S) and rumpling (R). (Resolved shear stress 4.4 kg/mm^2, 20% total strain) Active slip plane in alpha is parallel to that in beta . . . . . .

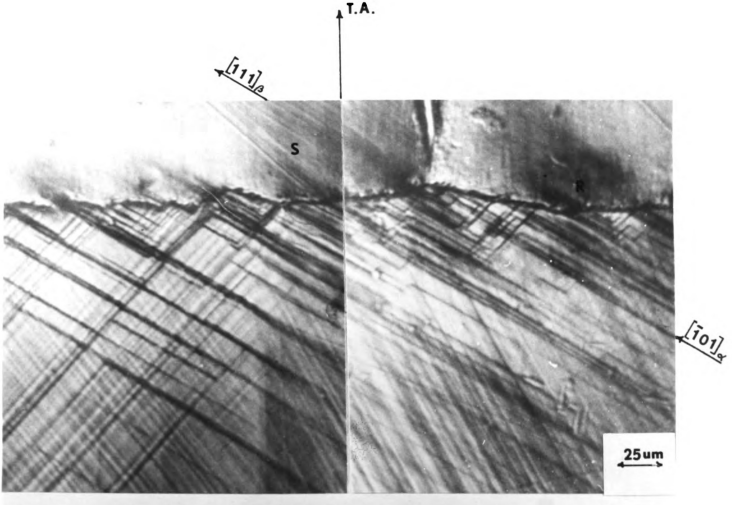

Fig. 42

Fig. 43. Heavy slip in alpha without any indication of slip in beta. (Total strain of 12.72%. Resolved shear stress 3.25 kg/mm^2) Compare with Fig. 39. In this specimen, the active slip plane in alpha is <u>not</u> parallel to that in beta . . . . . .

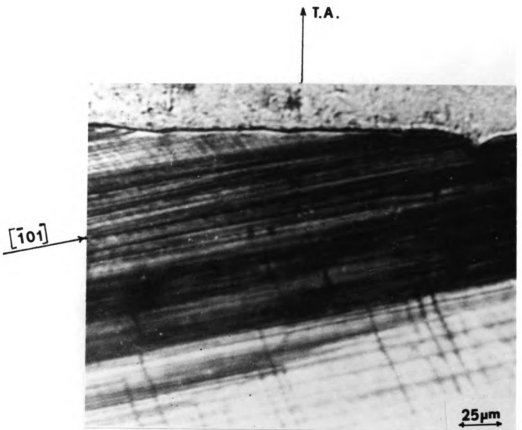

Fig.43

IV. DISCUSSION

4.1 Growth of Duplex and Two-Phase Bicrystals of Alpha-Beta Brass

4.1.1 General

As designated in Section 1.4, the main purpose of this work is to obtain duplex crystals and two-phase bicrystals of alpha-beta brass. These two phases are joined by melting beta brass over a substrate of a single crystal of alpha covered with alpha-beta foil. During this joining process, a two-phase transition zone occurs between the single-crystal alpha and coarse-grained polycrystal beta. For producing a two-phase bicrystal, such a zone must be narrowed in size, and a sharp boundary must be obtained between alpha and beta. The transition zone was narrowed in size by the special heat treatments described in Section 2.1.5.

In the ensuing discussion, the reason for choosing this joining procedure is first stated. Various approaches to the problem at hand are then discussed, and a phenomenological description combining various viewpoints is provided. Finally, individual mechanisms operative during the history of the heat-treatment are analyzed.

4.1.2 The Selection of Joining Procedure

The method of joining beta brass to alpha-brass single crystals as described in 2.1.4 has been selected out of several possibilities. These procedures will now be reviewed in order to justify the method selected for joining.

Since the specimens in this work consisted of two phases, it was considered necessary to begin with a two-phase material. Muntz metal, a commercial alloy containing 60% copper and 40% zinc, consists of both alpha and beta phases in its room-temperature structure. The principles of single-crystal growth by the Bridgman technique and recrystallization annealing were adopted with the hope that modifications might provide the required bicrystal specimens of this alloy.

The Bridgman technique consists of solidifying a melt in a sharp-tipped crucible under a temperature gradient. While cooling from liquid state to room temperature, an alloy like Muntz metal undergoes the following phase transformations:

$$L \xrightarrow[\text{Peritectic}]{902^{\circ}C} \beta \xrightarrow{760^{\circ}C} (\alpha + \beta)$$

where symbols L, α, and β represent liquid, alpha, and beta phases respectively.

It can be seen from the above that immediately on solidification a single crystal of beta containing 40 w/o zinc can be obtained by the Bridgman technique. However, this beta is stable only in the temperature region between $902^{\circ}C$ and $760^{\circ}C$. If a crucible containing the beta single crystal is slowly moved through the $\beta \rightarrow \alpha + \beta$ transformation temperature, alpha will start nucleating at the sharp tip of the crucible. Owing to the precipitation of alpha, the region in the immediate neighborhood of alpha gets richer in zinc, and can exist as beta even after cooling to room temperature. The composition of beta changes discontinuously as the transformation front progresses. An aligned lamellar structure is finally produced. Specimen diameters varying from 3 mm to 19 mm, and lowering rates varying between 12.5 mm/hour to 12.5 mm/day were tried.

The largest grain of alpha which could be obtained by this method was about 1 mm in size -- an order of magnitude smaller than that needed. The rate of lowering for preparing this specimen was 12.5 mm/day, and the entire process took 15 days.

Attempts were made to grow two-phase bicrystals by recrystallization annealing. Several specimens of varying thicknesses and varying amounts of cold work were given recrystallization anneals. The annealing temperatures chosen were between 450 and 750°C. The combination of the highest temperature (750°C) and longest period (14 days) gave grains as large as 0.1 mm. Besides the smallness of the grains, presence of annealing twins was a problem.

Greninger's work[74] on precipitation studies suggested an entirely different approach. His study was concerned with the lattice relationships developed during precipitation of beta as a result of the peritectic reaction in the copper-zinc system. To simplify the orientation studies, only one orientation of alpha was chosen. To facilitate x-ray studies, large grains of beta which had nucleated at high temperature had to be preserved to room temperature. Specimens with these desirable characteristics were prepared by solidifying a beta alloy under a unidirectional temperature gradient, with the crystallization seeded with a copper or alpha-brass single crystal.

Greninger's procedure is as follows: A single crystal of alpha was polished on one end and kept in a graphite crucible. The crucible containing the single crystal of alpha and a stock of beta brass above it was placed in a vertical tube furnace maintained at 1050°C. The crucible was observed through a small opening at the top of the tube. As soon as the beta brass had melted, the crucible was removed from the furnace,

placed on an iron block, and allowed to cool to room temperature. A transition zone consisting of alpha and beta, about 2.5 to 3 mm wide, was observed between the alpha single crystal and large-grained beta polycrystal.

For the purpose of this work, minimizing the transition zone is the most critical step. From this point of view, the temperature of 1050°C selected by Greninger[74] for melting beta is too high. In Greninger's method, the crucible is kept in the tube furnace. As a result, the entire length of the seed crystal is heated and the diffusion process becomes easier. Another major cause of the increased rate of diffusion and the large transition zone is the large difference in composition of the alpha-brass single crystal (30 w/o zinc) and the molten beta brass (48 w/o zinc).

In the modified joining procedure adopted in this work, these difficulties were avoided. The temperature was high enough to melt beta (containing 49 w/o zinc) in a short time without superheating (900-925°C). The entire length of the alpha-brass single crystal (containing 30 w/o zinc) was not heated; and yet epitaxy between the seed single crystal of alpha and the molten stock of beta was facilitated by placing a single turn of the heating element around the top of the single crystal. A foil of intermediate composition (containing 40 w/o zinc was kept between the alpha-brass single crystal and the stock of beta. This foil helped to reduce the drastic concentration variation between alpha and beta. The width of a typical transition zone obtained was 1 mm as against 2.5 to 3 mm obtained by Greninger's procedure.

Before considering the means of eliminating the transition zone, it is necessary to analyze how its structure develops. For this purpose,

consider the region of the copper-zinc diagram sketched in Figure 44. During the joining process, beta brass melts first, and the foil melts at the end. Once molten, the foil loses its identity as a solid and can be considered to be a pool of liquid containing 40 w/o zinc. This pool is in contact with the heated substrate of the alpha-brass single crystal below and the molten beta brass above. Since there was no stirring of the liquid, the compositional adjustments can be considered to be occurring by diffusion alone. Zinc atoms can diffuse from the molten beta into the pool of molten foil, and from this liquid into the alpha-brass single crystal. Diffusion of copper will take place in the opposite direction. As a result, there will be regions varying from 30 to 48 w/o zinc between the top portions of alpha single-crystal brass and beta brass. Of these regions, those containing 35-47 w/o zinc consists of alpha and beta in their room-temperature microstructure. From the Figure 44, it can be seen that the alloys within this range solidify by nucleating (i) alpha up to 38 w/o zinc and (ii) beta beyond 38 w/o zinc. Thus the two-phase transition zone consists of primary crystallized alpha together with beta grains whose nuclei originated by the peritectic reaction.

4.1.3 Phenomenological Description of the Effect of Heat Treatments

4.1.3.1 Approaches to the Problem

The heat treatments for obtaining a sharp phase boundary involve diffusion, phase transformations, and grain growth. It is necessary that these processes complement each other. In terms of distribution of zinc, the procedure involves (i) removal of microinhomogeneities caused by the two-phase structure in the transition zone, and (ii) establishment of a sharp concentration change at the phase boundary. Cycling during heat treatment helps to reach these conditions.

Fig. 44. A region of copper-zinc phase diagram above 600°C for compositional range of 0-50 w/o zinc . . . . . .

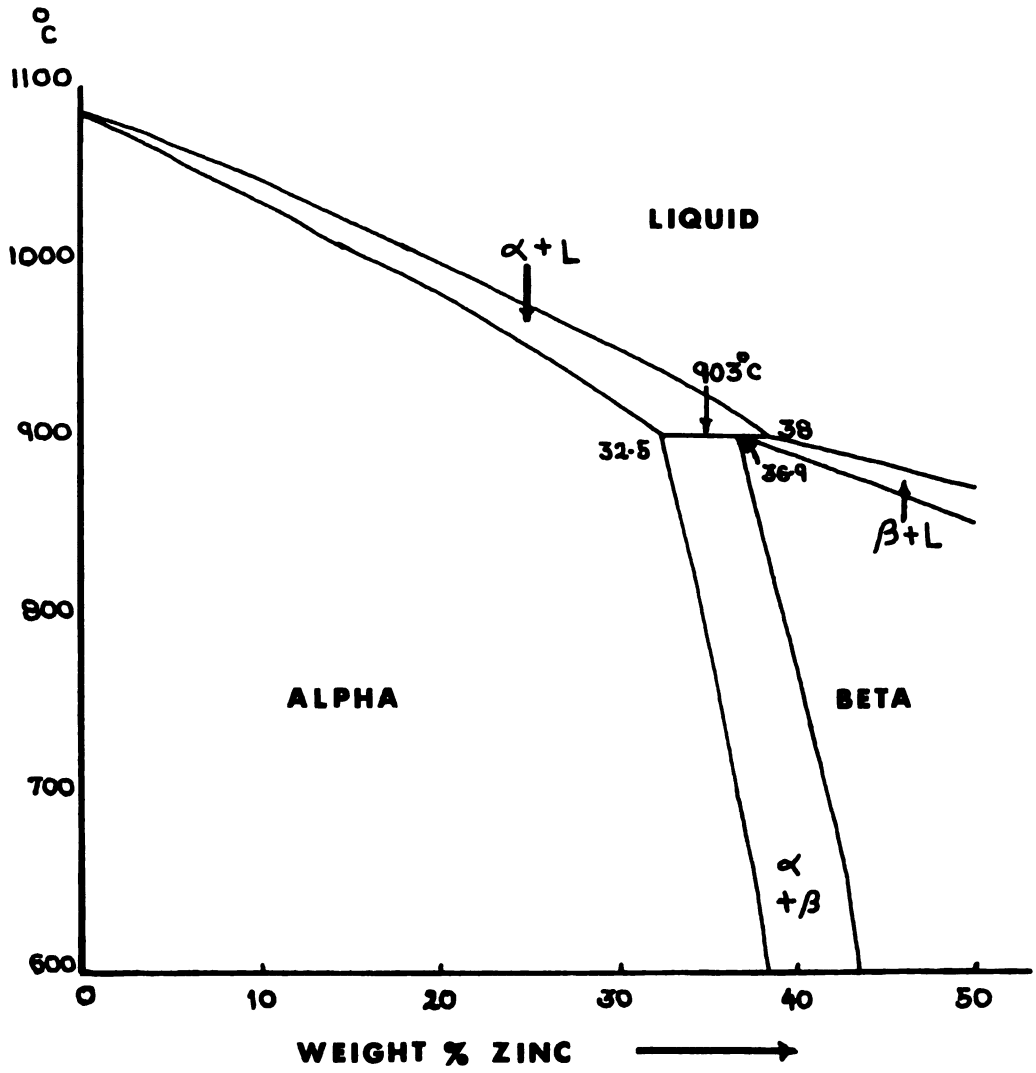
°C
1100
1000
900
800
700
600
LIQUID
α + L
903°C
38
32·5
36·9
β+L
ALPHA
BETA
α
+β
0
10
20
30
40
50
WEIGHT % ZINC

FIG. 44

For the purpose of the following discussion, the two-phase transition zone is assumed to consist of Widmanstätten plates precipitated in a direction parallel to the length of the specimen. In terms of the variations of zinc concentration, the transition zone can be pictured as shown in Figure 45(a) and (b).

Heat treatment, carried out on a continuous basis, will affect the transition zone in the following manner. As the specimen reaches the heat-treating temperature, diffusion of zinc will proceed from high-zinc regions (beta segments) to the low-zinc regions (alpha segments). The gradient of zinc concentration between the segments will decrease with time. With decreasing gradient, the rate of diffusion will decrease and eventually the microinhomogeneities will be removed. During this process, the composition between the lines AB and CD in Figure 45(a) will average to a zinc concentration intermediate to that of the alpha single crystal and the polycrystalline beta. The situation at this stage is indicated in Figure 45(c). It will be shown later that the transition zone will initially decrease in size owing to concentration gradients across the interfaces AB and CD. There is no guarantee, however, that the process will continue further. Such a continuous diffusion will reduce the gradients across AB and CD, and will finally come to a stable condition. This will be explained further in 4.1.3.2. In short, continuous diffusion will help to achieve the goal of minimizing the microscopic gradients, but will not give a sharp macroscopic gradient.

According to the principles of phase transformations in the copper-zinc system, a sharp macroscopic gradient can be created in the following manner. The region between AB and CD in Figure 45(a) transforms to beta during the heat treatment. By quenching from this

Fig. 45. (a) Schematic of the Widmanstätten plates which are parallel to the specimen length present in the transition zone. Lines AB and CD indicate the fictitious boundaries of this zone.
(b) Schematic of the change in the zinc concentration (on a microscale) in the transition zone along the length and width of the specimen.
(c) Transition zone between AB and CD becomes beta at high temperatures and assumes an average zinc concentration C_3 . . . . . .

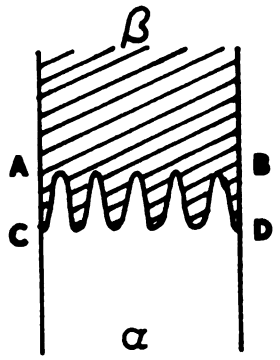

(a)

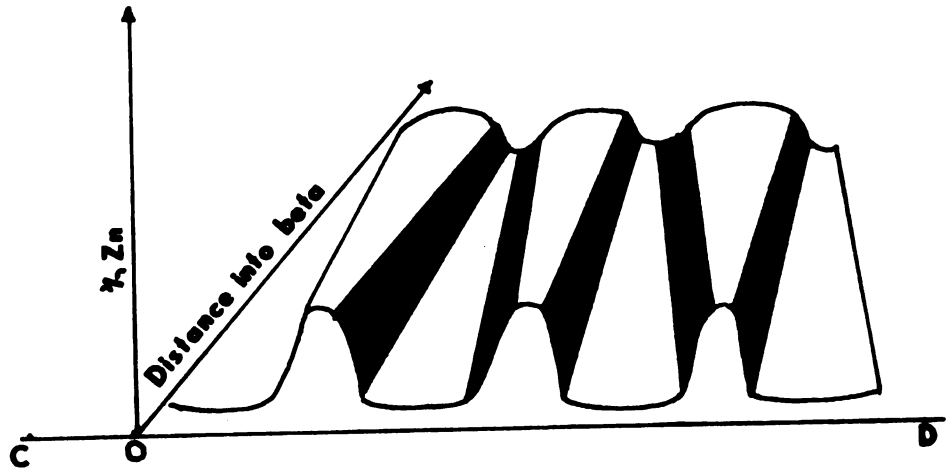

(b)

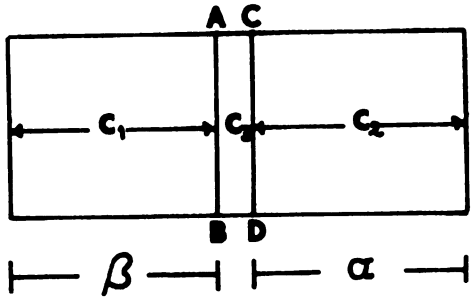

(c)

FIG. 45

temperature, the structure of the region between AB and CD can be retained as metastable beta. The objections to this procedure are the following:

(1) A part of the alpha single crystal immediately in contact with the transition zone gets heated during the heat-treatment. Sudden cooling causes excess vacancies to be trapped in this part of the crystal.

(2) The 'quenched-in' beta structure is unstable, and alpha will precipitate from this structure upon aging.

(3) Microscale composition gradients can still persist.

A satisfactory specimen, then, cannot be obtained by either diffusion or phase transformation operating alone. The heat treatment selected should combine both processes, and eliminate the drawbacks caused by their individual operation.

4.1.3.2 Unified Approach

The two heat treatments for obtaining a sharp boundary operate at such a temperature that the two-phase transition region transforms to single-phase beta. The temperature distributions for these treatments are given in Figure 46. This beta is not homogeneous in its composition. The inhomogeneities on the microscale are inherited from the room-temperature microstructure prior to the beginning of heat treatment.

On the macroscale, the diffusion phenomena work as stated below. The region between AB and CD in Figure 45 transforms to beta during the soaking parts of the heat treatments. This transformation of the two-phase structure to beta may be considered to occur without an incubation period, according to the work of Aaron and Kotler[75]. To determine whether the transition zone transformed into single-phase beta at

Fig. 46. (a) The schematic of the zinc concentration (on a macro-scale) near the transition zone.
(b) The temperature profiles in the specimens for the two heat-treatments.

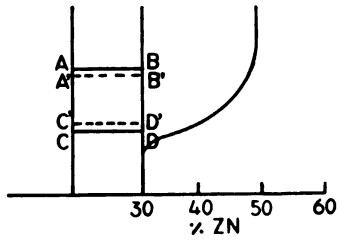

% ZN	TEMP.	D CM^2/SEC.
28	780°	1×10^{-8}
49	750°	$1{\cdot}2 - 1{\cdot}7 \times 10^{-6}$

(a)

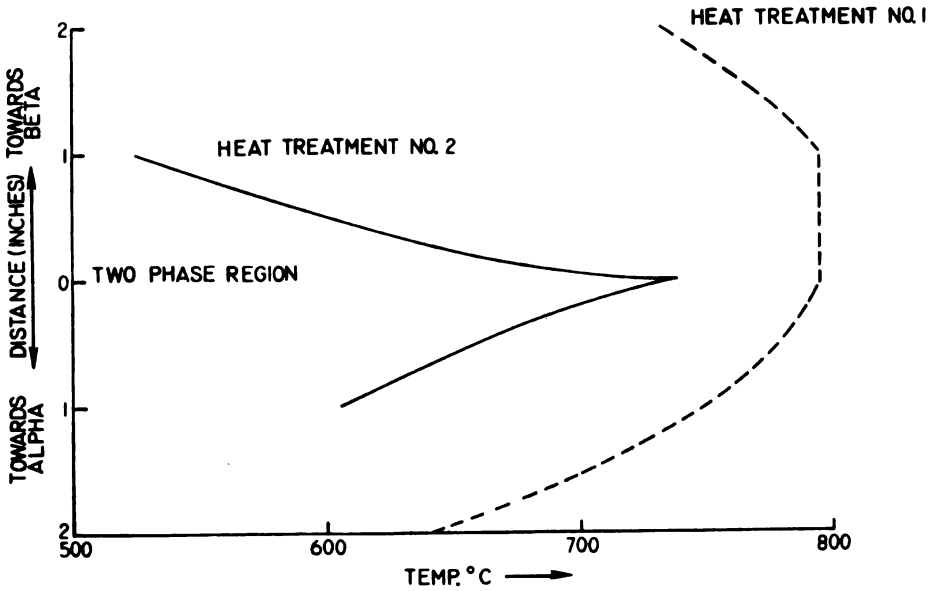

(b)

FIG. 46

the temperatures used, specimens were heated to 780°C for one hour and rapidly quenched in iced brine. The structure of these quenched specimens showed that the original two-phase zone transformed to metastable beta above the transformation temperature.

At the heat-treating temperature, the diffusion coefficient of zinc in beta (49 w/o zinc) is 1.2-1.7 $cm^2/sec \times 10^{-6}$ [76], and that in alpha (28 w/o zinc) is 1.0 $cm^2/sec \times 10^{-9}$ [77]. As a result of this difference in the magnitudes of the diffusion coefficients, the diffusion of zinc across CD becomes a predominant feature. Since alpha originally had only 30 w/o zinc, it can accommodate 7 to 8 percent more zinc and still remain alpha at room temperature. The line CD shifts to C'D' owing to this diffusion of zinc into alpha. A similar but much less severe concentration gradient also exists across AB. Above AB, the beta phase contains 49 w/o zinc, and just below AB, the beta phase contains 40-45 w/o zinc at the temperatures concerned. Diffusion of zinc in this region will shift the boundary AB to A'B' in the room-temperature microstructure.

The two-phase zone is originally an array of alpha-precipitate plates in a finite beta matrix. The composition variations depend on the distribution of the alpha plates. Heckel and coworkers[78] have considered the process of homogeneization in such arrays. It involves the movement of the phase interfaces and the diffusion in each of the two phases. Arrays consisting of precipitates having planar, cylindrical, and spherical geometries have been analyzed. The salient assumptions in these analyses of precipitate arrays are that the precipitates have equal radii (or thickness) and are uniformly spaced in the matrix. For modeling purposes, the matrix is divided into identical symmetrical cells, each having a precipitate particle at its center. Since the

symmetry requires that the normal component of the solute gradient at the cell walls be zero, it is further assumed that each particle is at the center of the cell, which has a symmetry identical to that of the particles and a volume equivalent to that of the cubic cell.

The arrays of Widmanstätten plates in the present case can be approximated by a combination of a tapering cylinder and a planar interface. The following analysis due to Heckel et al.[78] cannot be applied directly, but it does state the required equations for solving the homogenization problem mathematically. The planar and cylindrical geometries are shown in Figure 47, and the concentration-distance profiles at various stages of the homogenization are illustrated in Figure 48.

The time required for the homogenization process can be obtained by solving the following equations:

(i) Fick's second law in both the alpha and beta phases,

$$\frac{\partial c}{\partial t} = \frac{1}{x^m}\frac{\partial}{\partial x} D\left(x^m \frac{\partial c}{\partial x}\right) \quad , \tag{7}$$

where $m = 0,1,2$ for planar, cylindrical, and spherical geometries, respectively, x is the distance parameter, and D is the coefficient of diffusion, which is assumed to be independent of concentration;

(ii) the interface mass balance,

$$[C\beta\alpha - C\alpha\beta]\frac{d(\xi/2)}{dt} = D^{\alpha}\left(\frac{\partial c}{\partial x}\right)^{\alpha}_{x=\frac{\xi}{2}^{+}} - D^{\beta}\left(\frac{\partial c}{\partial x}\right)^{\beta}_{x=\frac{\xi}{2}^{-}} \tag{8}$$

where D^{α} and D^{β} are the diffusion coefficients of alpha and beta phases respectively, C^{α} is the average composition of the alpha phase,

Fig. 47. Geometric models showing symmetry elements for planar and cylindrical interfaces (Heckel et al[78]) . . . .

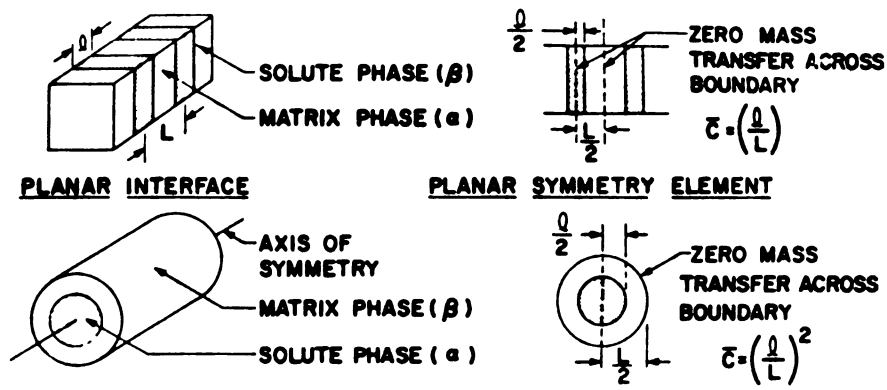
Q
L
SOLUTE PHASE (β)
MATRIX PHASE (α)
PLANAR INTERFACE
Q/2
L/2
ZERO MASS TRANSFER ACROSS BOUNDARY
C̄ = (Q/L)
PLANAR SYMMETRY ELEMENT
AXIS OF SYMMETRY
MATRIX PHASE (β)
SOLUTE PHASE (α)
Q/2
L/2
ZERO MASS TRANSFER ACROSS BOUNDARY
C̄ = (Q/L)²

FIG · 47

Fig. 48. Schematic concentration-distance profiles illustrating the stages of homogenization for a two-phase composite. Initially, the alpha-beta interface may move in either direction (cases 1 and 3) or remain stationary (case 2) depending on the relative values of the fluxes J at the interface (Heckel et al[78]) . . .

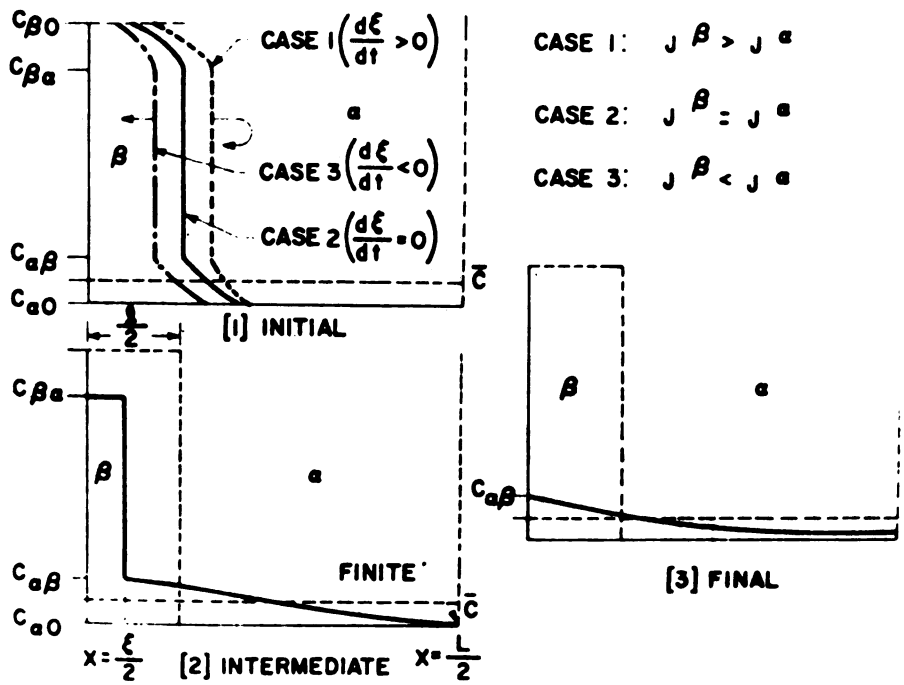
$C_{\beta 0}$
$C_{\beta\alpha}$
$C_{\alpha\beta}$
$C_{\alpha 0}$
CASE 1 $\left(\frac{d\xi}{dt} > 0\right)$
CASE 3 $\left(\frac{d\xi}{dt} < 0\right)$
CASE 2 $\left(\frac{d\xi}{dt} = 0\right)$
β
α
$\bar{C}$
$\frac{\xi}{2}$
[1] INITIAL
FINITE
$X = \frac{\xi}{2}$
[2] INTERMEDIATE
$X = \frac{L}{2}$
CASE 1: $J^{\beta} > J^{\alpha}$
CASE 2: $J^{\beta} = J^{\alpha}$
CASE 3: $J^{\beta} < J^{\alpha}$
[3] FINAL

FIG. 48

ξ is the size parameter of the precipitate, and $C^{\beta\alpha}$ and $C^{\alpha\beta}$ are the upper and lower composition limits of the two-phase alpha-beta field.

With the continuous heat treatment, $\partial c/\partial x$ decreases and thus decreases $\partial c/\partial t$. In the heat tretaments in this work, cooling to room temperature follows every cycle of the heat treatment. Owing to the cooling to room temperature, beta in the transition zone transforms to alpha and beta, creating a new set of alpha-precipitate plates. This transformation helps to reestablish the concentration gradients between alpha and beta, and to increase the rate of diffusion on reheating the specimen above the transformation temperature to form metastable beta in the transition zone. The dependence of the diffusion coefficients on the percentage of zinc present results in diffusion of zinc from regions of high zinc concentration (beta in room-temperature structure) to those of low zinc concentration (alpha in room-temperature structure). In addition, the low-zinc regions act as channels for carrying the zinc farther into the alpha single crystal. The microprobe analyses of individual alpha plates show a drop in composition towards the alpha single crystal, and thus confirm the above statements. The drop in composition from 37% to 30% zinc was observed to occur over a distance of 100 microns.

4.1.4 Study of Mechanisms

So far, the effects of heat treatments have been explained on the basis of concentration variations on macroscopic and microscopic scales. The effect of phase transformation on diffusion has been briefly stated.

During the course of this work, many specimens were examined with an optical microscope following heat-treating cycles. The morphological features of the shrinking transition zone were photographed, in order to

aid in understanding the roles of phase transformations and grain growth due to the heat treatments employed. Mechanisms for the development of various microstructures observed, and the effects of such mechanisms on the overall processes, are described in this section. For convenience the mechanisms are titled according to the microstructural observations.

4.1.4.1 Grain-Boundary Migration, Grain Growth, and Platelet Reorientation

The transition zone in the as-joined condition has several grains of beta in contact with the single crystal of alpha as shown in Figure 18(a). At the heat-treating temperatures, the two-phase alpha-beta transition zone transforms to a single phase beta. The grain boundaries in beta migrate to low-energy positions, thus causing grain growth. The repetition of this process during every heat-treating cycle causes only one or two grains of beta to remain in contact with the alpha-brass single crystal after prolonged heat treatment. If the heat-treatment temperature is such that no phase transformation can take place, such extensive grain growth of beta would not be possible. For, in the persisting two-phase microstructure, alpha precipitates will be present along the grain boundaries and inside the grains, hindering grain-boundary migration by pinning and dragging the boundaries.

A secondary effect of the grain growth is observed in the platelet reorientation. In the beta matrix there grow alpha Widmanstätten plates satisfying the following crystallographic orientation relationship:

$$\{111\}_\alpha \parallel \{110\}_\beta \qquad \langle 1\bar{1}0\rangle_\alpha \parallel \langle \bar{1}11\rangle_\beta \quad .$$

As seen in Figure 18, the plates change their orientation in order to conform with the crystallographic relationship in the growing grain.

In some specimens, it was observed, however, that the platelet growth is guided both by the crystallographic considerations and by the variations in zinc concentration. This mechanism can be explained with the help of Figure 19, and the mode of its occurrence can be visualized by the schematic shown in Figure 49. Consider the grain boundary between the grain A and B migrating to the right at high temperatures. The new position acquired by the grain boundary is shown by the dotted line in Figure 49b. When plates in the grain A try to grow in the newly acquired region 'C', they will try to grow as guided by the crystallographic relationships. Consider a plate originating at M. This plate will follow the crystallographic rules up to the point 'N'. At 'N' it meets a region where a portion of the plate RS existed in the consumed portion of grain B. During the heat treatment -- even though diffusion took place -- not all the concentration gradients were wiped out. A region containing low zinc remained in the direction RS, and the plate MN changed its direction to conform with this low-zinc region. This plate cannot continue growing along RS, since the crystallographic considerations tend to reorient it towards O. A similar process occurs at O and P. Thus the direction of a growing Widmanstätten plate seems to be governed both by crystallographic rules and concentration variations.

4.1.4.2 Diffusion-Controlled Growth

The following description of the diffusion-controlled growth process follows Christian[79].

In any transformation involving long-range transport, the diffusion equation

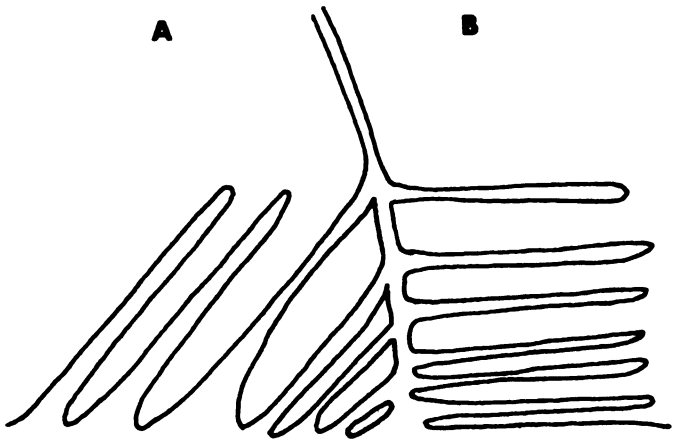

(a)

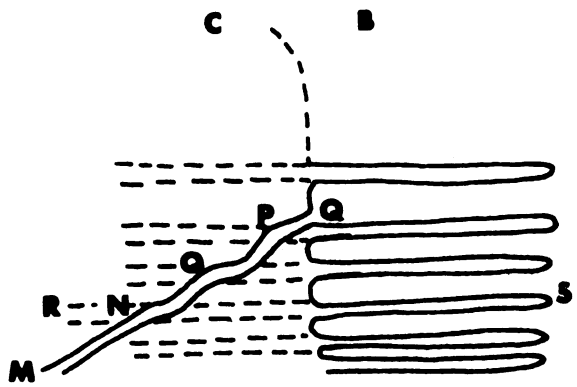

(b)

FIG. 49

$$\frac{\partial c}{\partial t} = D\nabla^2 c \qquad (9)$$

must be satisfied in all parts of the metastable phase under consideration. Here the concentration c is a function of position, and of time t. The diffusion coefficient D can usually be assumed to be independent of position, time, and concentration. Let the concentration of the initial beta phase be C^m and let this be the only phase present at $t = 0$; then the initial condition is

$$C(x,0) = C^m \quad . \qquad (10)$$

Consider a reaction in which alpha precipitates of composition C^α form from the beta phase. If the reaction rate is limited by diffusion, an appropriate boundary condition for the diffusion equation is that

$$C = C^\beta \qquad (11)$$

immediately adjacent to the interface where C^β does not differ appreciably from the equilibrium beta concentration. Away from the interface, the concentration changes to the average matrix composition. The other extreme occurs when the concentration in the beta phase near and away from the interface is almost uniform.

Consider now the growth of an isolated precipitate particle in an infinite matrix. Let r be a coordinate normal to the growing interface, whose position is specified by $r = p$. The boundary conditions are then

$$C(p,t) = C^\beta \quad , \quad C(\infty,t) = C^m \quad . \qquad (12)$$

The diffusion flux across a unit area at the boundary in time δt is $D[\partial c/\partial r]_{r=p}\delta t$. If the interface advances a distance δr during this

time, the extra number of solute atoms in the volume δr will be $(C^{\beta} - C^{\alpha})\delta r$. Equating the two expressions gives

$$D[\frac{\partial c}{\partial r}]_{r=p} \delta t = (C^{\beta} - C^{\alpha})\delta r \quad ; \tag{13}$$

$$\therefore \frac{\delta r}{\delta t} = \frac{D}{(C^{\beta} - C^{\alpha})} (\frac{\partial c}{\partial r})_{p} \quad . \tag{14}$$

It is convenient to express the concentration gradient in this expression as a ratio $\Delta c/y^{D}$, where $\Delta C = C^{\beta} - C^{m}$ is the difference in solute concentration near to and remote from the interface, and y^{D} is the effective diffusion distance.

Thus, the velocity of the interface, Y, is given by

$$Y = \frac{dr}{dt} = (\frac{D}{y^{D}}) (\frac{\Delta C}{C^{\beta} - C^{\alpha}}) \quad . \tag{15}$$

For a planar boundary, y^{D} must continually increase as the solute is added to the region ahead of the interface, and the growth rate decreases.

A theory for edgewise growth of a plate without thickening, given by Zener[80] and extended by Hillert, is often known as the Zener-Hillert[81] model. If the radius of curvature at the tip of a growing plate or a needle is constant, a linear growth rate will be obtained according to equation (15). When the radius of curvature is small, however, the change in the equilibrium concentration of solute at the interface due to the Gibbs-Thomson effect becomes appreciable.

Consider the tip of a Widmanstätten plate characterized by a constant radius of curvature r. This curvature causes a pressure difference between the growing phase and the matrix which changes the local equilibrium concentration in the matrix phase according to

$$C^{\beta}_{r=\infty} - C^{\beta}_{r=r_1} = \frac{\sigma}{RT\,Kr} \quad , \tag{16}$$

where $C^{\beta}_{r=\infty}$ is the local equilibrium concentration for an infinite radius of curvature, $C^{\beta}_{r=r_1}$ is the local equilibrium concentration corresponding to the radius r_1, σ is the surface tension, and K is a thermodynamic parameter of the order of unity. Zener assumed that curvature of the growing interface changes the concentration difference between the growing interface and a point in the bulk matrix from $C^{\beta}_{r=\infty} - C^{m}$ to $(C^{\beta}_{r=\infty} - C^{m})[1 - r_c/r]$, where r_c is a critical radius at which growth ceases. The equilibrium concentration of solute at the interface is c^{m} when $r = r_c$. If the diffusion distance ahead of the advancing front is proportional to the radius of curvature ($y^{D} = ar$ where $a \simeq 1$), then the lateral diffusion flux, J, per unit length of plate becomes

$$J = \frac{2rD(C^{\beta} - C^{m})[1 - (\frac{r_c}{r})]}{ar} \quad . \tag{17}$$

This allows the new phase to form with a velocity Y such that

$$J = 2rY(C^{\beta} - C^{\alpha}) \quad ; \tag{18}$$

$$\therefore \; Y = \frac{D(C^{\beta} - C^{m})}{(C^{\beta} - C^{\alpha})ar}[1 - (\frac{r_c}{r})] \quad . \tag{19}$$

Repas and Heheman[82] found, however, that the needles of alpha formed in beta brass have lengthening rates up to about three orders of magnitude higher than those calculated on this model. The higher discrepancies were found at the lower reaction temperature.

Aaronson et al.[82] have provided an explanation for such higher growth rates. The alpha precipitates may be viewed as cylinders with hemispherical caps. The concentration of the beta matrix at the tip of the Widmanstätten plate and around the cylindrical surface will differ from each other. Zinc will be able to diffuse along this concentration gradient, through the alpha-beta boundary at the tip of the precipitate, assumed to have a disordered structure, with a diffusivity $D_{\beta\alpha}$. It has been proved by Aaronson et al.[82] that this concept alone does not explain the fast lengthening. Accordingly they propose that the dislocation structure at the precipitate plate tip must probably be taken into consideration.

Purdy[83] has explained the high growth rates of the precipitates on the basis of non-ideality of the solution. The equation for Y (Equation 19) previously derived is well suited to dilute solutions. He has shown that for the rich solutions like alpha and beta brass, the diffusion coefficient is not independent of concentration, but the critical radius r_c for a given supersaturation decreases. Both these effects will increase the value of Y.

4.1.4.3 Dissolution of the Precipitate

Aaron and Kotler[75] have extensively reviewed the dependence of the dissolution on the prior growth process. This dependence is a consequence of the fact that the concentration profile ahead of a growing precipitate is a function of the diffusion path. A precipitate which grew by volume diffusion of the solute directly to, or from the growing precipitate, will generally dissolve faster than a precipitate which grew by interfacial diffusion. Just like the growth problem, the dissolution is concerned with the solution of the diffusion equation 9.

With the same symbols as in the previous section, a factor K is defined as follows:

$$K = \frac{2(C^{\beta} - C^{m})}{(C^{\alpha} - C^{m})} \quad . \tag{20}$$

For small values of K, the analysis is based on the invariant-size approximation, in which it is assumed that the interface is stationary. Although this assumption appears paradoxical, the solution is obtained for the growth conditions easily. The solution is

$$\frac{dr}{dt} = -K\left[\frac{D}{r} + \sqrt{\frac{D}{\pi t}}\right] \tag{21}$$

From this equation, it can be seen that for a smaller size of the precipitate (i.e., for small r), the dissolution velocity increases.

The principles of growth and dissolution in the previous sections apply for isothermal conditions. In the present work, the precipitation of alpha plates occurred during continuous cooling to room temperature. From Flewitt and Towner's[15] time-temperature-transformation (TTT) diagrams, it can be concluded that no bainitic product forms during this experiment. Conclusions of Aaron[75,84] regarding the solution process cannot be directly applied, since the exact growth process of the Widmanstätten plates of alpha phase is a combination of both diffusion and interface motion[82]. The only principle which will directly hold true in the present case is the dependence of the dissolution rate on the precipitate radius. The discussion below, therefore, does not attempt to solve the evolution of morphologies quantitatively.

The progressive decrease in the size of the two-phase transition zone occurred by two distinct modes. In the first, the alpha plates dissolve and reprecipitate as split islands, as shown in Figure 17.

In the second, the alpha plates become progressively thinner at the tip and thicker at the base, as shown in Figure 18.

The first mode, namely, alpha plates splitting into islands, can be explained with the help of the schematic diagram in Figure 50. A Widmanstätten plate can be visualized as a perturbation at the boundary CD. During the annealing process, the precipitate plate dissolves in the surrounding matrix. The rate of dissolution will be maximum at the tip, since the small radius of curvature at the tip increases the rate of diffusion of zinc. The scanning electron micrograph shown in Figure 20 shows the original sharp tip of a Widmanstätten plate. If Aaronson's[82] mechanism of boundary ledge coupled with diffusion aids the tip advance during growth, it should also aid the tip dissolution. At the end of the annealing cycle, the original plate can be visualized as a perturbation of much smaller amplitude. A region with low percentage of zinc compared with that of the matrix will exist in front of this perturbation. This region may exist as beta at the annealing temperature, but may give rise to several alpha nuclei during cooling. Growth of alpha around all these nuclei will increase the surface energy by increasing the area of the alpha-beta phase boundaries. During cooling, therefore, the initial perturbation dominates the nucleation and growth, and the plate grows at a fast rate, raising the zinc concentration ahead of itself. The length of the plate will depend on the ability of zinc to diffuse away from the advancing tip. There are two effects opposing such diffusion:

(1) Away from CD (shown in Figure 50), inside the transition zone, the average zinc concentration goes on increasing. Lines parallel to CD can be regarded as isoconcentration lines.

Fig. 50. Schematic of the process of alpha-island formation from a Widmanstätten platelet. (a) Original Widmanstätten platelet. (b) At high temperature, the plate exists only as a small perturbation. (c) On cooling, the plate can grow to a shorter length with islands forming at the tip . . . . . .

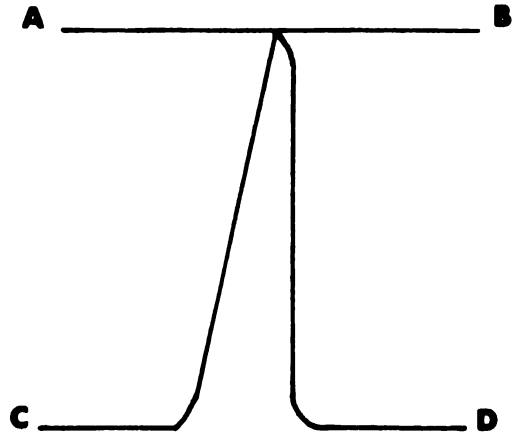

(a)

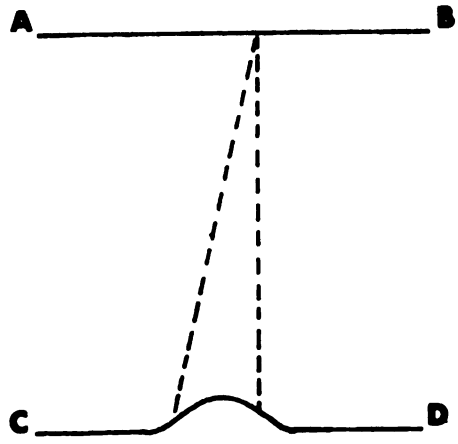

(b)

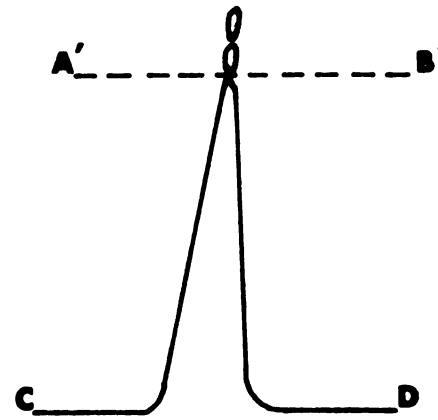

(c)

FIG. 50

Assume that the plate grew to the line AB originally. The effect of macroscale diffusion will be to move this line closer to the alpha single crystal with every annealing cycle.

(2) Any nucleus of alpha growing in the region between the dotted lines will give out the excess zinc. Such excessive zinc concentration will prevent the growth of the original plate.

The second mode, namely, plates thinning at the tip, can be attributed to the effect (1) just mentioned. The widening of the plate bases can be explained as follows. The spacing between the bases of alpha plates depends on the thickness of the beta regions between them. Just as the alpha plates have tips towards the beta, these beta regions have tips towards the alpha single crystal. In other words, the transition zone may be considered to be made up of interpenetrating plate-like regions of alpha and beta. Owing to the sharp radius of curvature at the tips of beta regions, zinc will diffuse into alpha at a faster rate. As the beta regions are depleted of zinc, their size decreases, and the size of the base of the alpha plates increases.

4.1.4.4 Mechanism for the Growth of Two-Phase Bicrystals of Alpha-Beta Brass

Various mechanisms considered in the previous sections on an individual basis are combined in this section to explain the process involved in growing two-phase bicrystals of alpha-beta brass.

A two-phase transition region develops between the single-crystal alpha and the polycrystalline beta during the joining operation. This development can be attributed to the extensive diffusion of zinc from the beta phase into the alpha phase of nonequilibrium composition. The two heat treatments narrow the two-phase region to yield a sharp

boundary. The temperature for both the heat treatments was selected so that the two-phase transition region transforms into a single-phase beta. Under these conditions, zinc diffuses locally to minimize the concentration variations, and grain growth takes place. On cooling from this temperature, alpha precipitates in the form of Widmanstätten plates. Thus the basic mechanisms operating during the heat treatments are (a) diffusion and (b) phase transformation. The heat treatments were chosen specifically so that these two mechanisms would complement each other in the two-phase region. Diffusion in regions away from the interface is minimal.

In attempts to melt and solidify beta brass on the alpha-brass substrates without the thin foil, wide transition regions developed. This development is due to the presence of large concentration differences between alpha brass containing 30 w/o zinc, and beta brass containing 49 w/o zinc. With the foil, which is of intermediate composition, the massive diffusion between single-crystal alpha and beta is reduced during the joining operation.

Both the concentration gradient and the temperature are known to affect the diffusion phenomena[85]. The entire specimen in the as-joined condition has different concentrations of zinc along its length. In both the heat treatments, definite temperature gradients are imposed on the specimens. The macroscopic concentration and the temperature along the length of the specimen are illustrated in Figure 46(a) and (b). The diffusion coefficients of zinc at two different compositions and temperatures, obtained from the published results[11,12], are included in Figure 46. The region ABCD in Figure 46(a) is the two-phase transition zone. During soaking, the region between AB and CD transforms to beta.

The conversion of the two-phase structure to beta may be considered to occur without an incubation period, according to Aaron and Kotler's work[75].

In both heat treatments, the differences in the interdiffusion fluxes become important. The diffusion coefficient of zinc in beta is several orders of magnitude greater than in alpha. Hence the diffusion of zinc across CD becomes a predominant feature. Since alpha originally had only 30 w/o zinc, it can accommodate a few percent more of zinc and still remain alpha at room temperature. The line CD shifts to C'D' owing to this diffusion of zinc into alpha. A similar but much less severe concentration gradient also exists across AB. Above AB, the beta phase contains 49 w/o zinc, and just below AB, the beta phase contains 40-43 w/o zinc at the temperatures concerned. Diffusion of zinc in this region will shift the boundary AB to A'B' in the room-temperature microstructure.

Another significant feature resulting from the heat treatment is the grain growth of the beta phase. Most of the beta grains in the two-phase zone immediately in contact with the alpha single crystal will satisfy the following relationship[74]:

$$\{111\}_\alpha \;||\; \{110\}_\beta \qquad \langle 1\bar{1}0\rangle_\alpha \;||\; \langle \bar{1}11\rangle_\beta$$

Since the heat treatments are carried out above 760°C, the alpha-precipitate plates dissolve. The grain boundaries in this high-temperature beta migrate, and grain growth takes place in beta, as seen in Figure 18. As a result, only one or two grains of beta tend to be connected to single-crystal alpha. On cooling from the heat-treatment temperature, beta transforms back to alpha and beta phases. The plate

morphology is, however, drastically different from the one in the as-joined condition. The most important effect of lowering in the first heat treatment is to cause the primary Widmanstätten alpha plates to grow in continuation of single-crystal alpha. It must be emphasized that the first heat treatment is not necessary when the as-joined structure consists of the primary Widmanstätten plates. The second heat treatment is more important in reducing the two-phase transition zone. Extensive grain growth takes place in beta during cyclic local annealing. As a result, usually one large grain of beta is in contact with the transition zone, and most of the Widmanstätten plates in the transition zone are parallel to each other. The plates display a regularity in size and spacing, and a group morphology. Nearly all the degenerate forms are eliminated. The plates now grow in such a way that their tips define an approximately planar front.

During the cyclic local annealing, the Widmanstätten plates tend to get thin near the tip and wide near the base, as seen in Figure 18. This phenomenon can be explained on the basis that the diffusion takes place on a microscopic scale. The phase transformation introduced by heating and cooling promotes this diffusion by creating sharp concentration gradients when the whole transition zone is heated to the beta region.

When the transition zone becomes beta on heating, inhomogeneities in zinc concentration exist on the microscale as a result of the low-temperature two-phase structure. Such inhomogeneities will promote the diffusion of zinc from high-concentration to low-concentration regions, which can proceed further into the alpha single-crystal regions. Since the original alpha single crystal contained only 30 w/o zinc, it can

accommodate a few percent of zinc and still remain as alpha. The beta regions (as shown in Region X of Figure 18) near the alpha single crystal separate out and ultimately dissolve in the alpha phase.

In the transition region near the beta part of the specimen, however, the zinc diffusion tends to change the two-phase structure into a single-phase beta structure. As a result, the alpha plates formed during cooling are thinner and ultimately break into islands as shown in region Y of Figure 17(b) and (c). Repeated cyclic annealing converts these islands into beta.

The phase transformations induced by heating and cooling are essential for making the diffusion process effective. During continuous heat treatment above the transformation range, the variation in zinc concentration present in the beta phase will promote zinc diffusion, but this process will not be effective over long periods of time. A sharp gradient in zinc concentration exists on heating above the transformation temperature, but it diffuses out fairly rapidly. As a result, the diffusion process becomes extremely slow. On cooling the specimen, the alpha and beta regions separate out with distinct zinc concentrations. On reheating, the metastable beta phase formed will once again have sharp concentration gradients.

Unless the alpha plates are connected to the alpha single crystal, the reduction of the transition zone progresses extremely slowly. In specimens which contained a continuous beta layer between the alpha plates and the alpha single crystal, it became impossible to eliminate the transition zone even after 100 hours of cyclic annealing. Zinc that is diffused into alpha in the transition region is carried further into the single-crystal alpha regions. When such a process is blocked,

further reduction of the transition zone thickness by cyclic local annealing becomes extremely slow.

4.2 Deformation of Alpha-Beta Brass Duplex Crystals

4.2.1 General Comments

At low stress levels, all the three regions, namely, alpha, alpha-beta, and beta of the duplex-crystal specimen behave elastically. The deformation of alpha-brass single crystals in the neighborhood of the duplex region is restricted owing to the higher strength of the duplex region as compared with that of the alpha single crystal. As a result of this, slip in alpha always starts at a point away from the duplex region. As long as slip does not reach the duplex region, that region and beta act as a grip in the tensile tests for practical purposes. When slip in the alpha finally reaches the duplex region, it is accommodated in the alpha segments, since the alpha segments are in continuation with the alpha single crystal.

The alpha-beta phase boundary acts as a barrier for the propagation of slip in the early stages. Dislocation pile-ups have been commonly observed in alpha brass[47,54,86]. These pile-ups are expected to be present in the alpha segments as a result of the resistance caused by the phase boundary. Stresses due to the pile-ups in alpha can be relieved by cross-slip in alpha, initiation of slip in beta, or both. The model required for analyzing the interactions at the phase boundary is discussed in section 4.2.3.

Beta brass is a B-2 type superlattice. The generation and motion of dislocations of type $\frac{1}{2}$ a<111> will create a trail of anti-phase boundaries behind them. Hence either superlattice dislocations of a<111> type or coupled pairs of $\frac{1}{2}$ a<111> type must be activated[61].

4.2.2 Crystallographic Considerations

The duplex-crystal region consists of alpha segments connected with the single crystal of alpha brass, and the beta segments connected with the beta grain in its immediate neighborhood. As discussed previously in the sections on the growth of duplex crystals and two-phase bicrystals, the alpha segments are in the form of Widmanstätten precipitates of alpha in the matrix of beta brass. These are known to satisfy the following Kurdjmov-Sachs orientation relationship:

$$\{111\}_{\alpha} \;||\; \{110\}_{\beta} \qquad \langle 1\bar{1}0\rangle \;||\; \langle \bar{1}11\rangle_{\beta} \quad .$$

It has been found, moveover, that this relationship holds between alpha and beta in the copper-zinc system regardless of whether the new phase is formed by diffusion[87], by precipitation[88], or by peritectic reaction[74]. Hsun and Smith[89] have observed the same relationship in their study of low-energy interfaces during the grain growth of alpha-beta brass.

In particular, the crystallographic relationship just given shows that the close-packed planes in alpha and beta segments of the duplex crystal are parallel; the close-packed directions in both these phases are also parallel. For alpha and beta phases, these are also the primary slip planes and slip directions, respectively. Hence for a slip plane in alpha that meets the phase boundary, there is a corresponding slip plane on the beta side. As a result of this, the phase boundary cannot act as an effective barrier. This point is further illustrated by Figure 51. In part (a) of this figure, the slip planes in grains A and B are exactly coincident and parallel. In (b), they coincide only and are not parallel, whereas in (c) there is no coincidence between the

Fig. 51. Meeting of slip planes at a grain boundary in a bicrystal: (a) Slip planes coincident and parallel, (b) Slip planes coincident only, (c) Slip planes neither coincident nor parallel. The cross-hatched region represents the boundary. (D. McLean[90]) . . . . . .

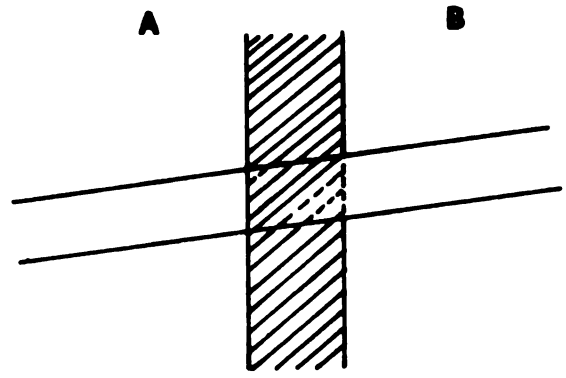

(a)

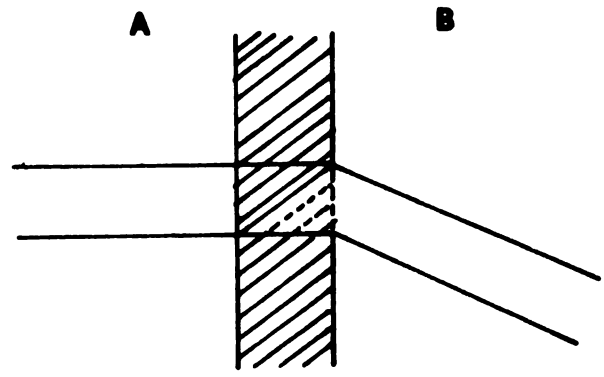

(b)

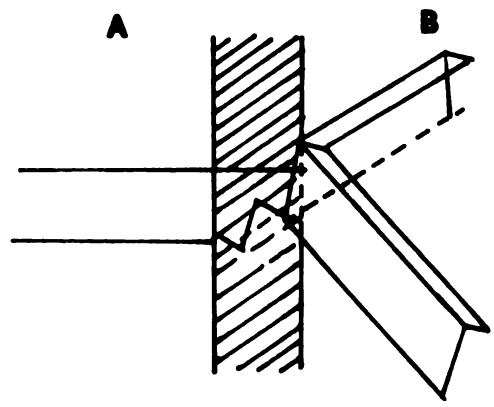

(c)

FIG. 51

slip planes. McLean[90] has pointed out that the effectiveness of a boundary as a barrier arises from the fact that the slip planes do not continue from one grain to another. As shown in (b) and (c) of Figure 51, the dislocations moving on a slip plane in grain A have to cross-slip onto the planes when they coincide, or zig-zag frequently when they do not. In case (a), however, there is no effective hindrance at the boundary. Effects of differences of shear moduli of alpha and beta phases in the present work and the difference in their Burgers vector are considered later.

During the course of this work, slip was observed to continue from segments of alpha to those of beta. In the polycrystalline two-phase materials, similar observations on the continuation of slip from one phase to another have been made by Honeycombe and Boas[34] for polycrystalline alpha-beta brass. Greenfield and Margolin[91] have studied the formation and growth of voids in a two-phase alpha-beta titanium alloy. Microstructures were classified as (i) those containing equiaxed alpha precipitates, and (ii) those containing Widmanstätten and grain-boundary alpha precipitates. Void nucleation was observed at all kinds of phase boundaries except where the alpha and beta were at Widmanstätten orientation. For such a structure, slip was observed to continue from alpha to beta phase.

A model based on dislocation pile-ups is not directly applicable because of the blunting of the pile-ups caused by the cross-slip and secondary slip in the alpha phase. The model adopted here is similar to that for explaining the continuation of yield across the grain boundary in a polycrystalline material. On deforming a polycrystal, a favorably-oriented grain deforms first by the occurrence of slip. The

slip band in this grain impinges on the grain boundary. Consider a grain A with a slip band in it and a region of dimensions 'r' in a neighboring grain, as shown in Figure 52. Following Johnston and Feltner[92], the effect of the slip band produced in grain A can be explained in dynamical terms. Let ρ_A be the density of mobile dislocations in the band, $\bar{v}_A$ be their average velocity determined by the resolved shear stress, $\bar{b}$ the Burgers vector, and ℓ_A the average mean free path. Then the rate of displacement imposed on the grain boundary by the formation of the slip band in A is given by

$$\dot{D} = \rho_A \, b \, \bar{v}_A \, \ell_A \quad . \tag{22}$$

The total plastic relaxation rate $\dot{R}$ in the region bounded by r is then given by the sum of the individual rates on each of the slip systems required to satisfy the local strain compatibility requirements,

$$\dot{R} = (r/\bar{m}) \sum_j M \rho_B \, b \, \bar{v}_B \qquad j = 1,2,3 \quad , \tag{23}$$

where ρ_B is the density of mobile dislocations in grain B, b is the Burgers vector, $\bar{v}_B$ is their average velocity, and M is a dislocation multiplication factor. Subscripts 1,2,3 refer to the individual operative slip systems, and $\bar{m}$ is the average orientation factor, which increases with plastic anisotropy. The ability of the grain boundary to act as an effective barrier depends on the relative values of $\dot{D}$ and $\dot{R}$. The difference between the rate of displacement imposed and the rate of relaxation causes an additional stress $\Delta\tau$ to act on the region bounded by r. If $\dot{R}$ continuously increases with $\dot{D}$, no additional stress is imposed on this region and as a result the grain boundary will not be an effective barrier.

Fig. 52. Stress concentration near a grain boundary during deformation. Slip band in grain A imposes a shear displacement upon a region of dimension r in grain B.

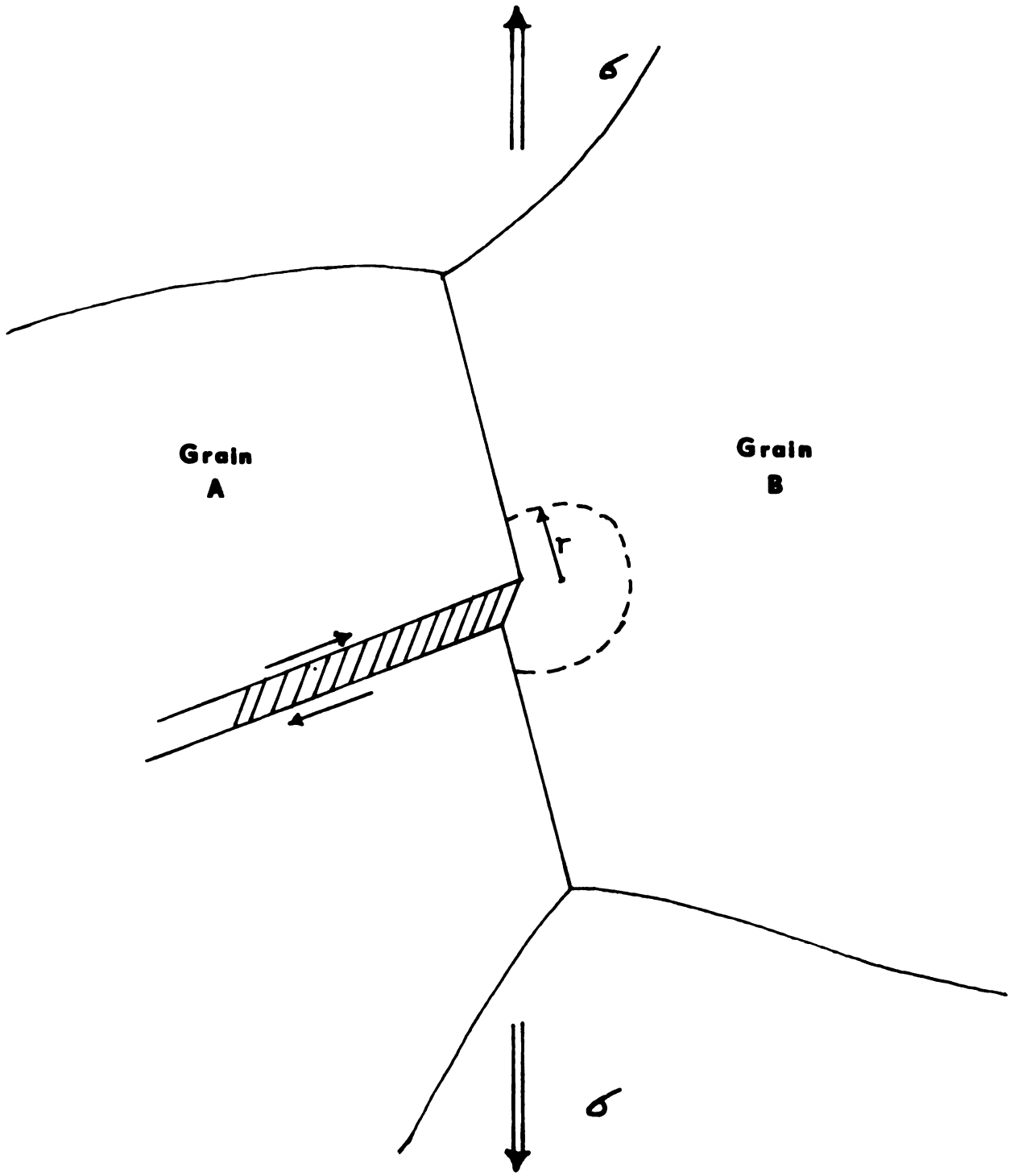

FIG 52

For a given applied strain and displacement rate $\dot{D}$, the rate of relaxation increases for (a) a smaller value of $\bar{m}$, (b) a higher rate of dislocation multiplication by cross slip, and (c) the ability to deform on two or more systems.

The average orientation factor $\bar{m}$ needs further explanation. For a single crystal under an applied tensile stress σ, the shear stress τ on the most favorably oriented slip system is given by

$$\tau = \sigma/\bar{m} \quad , \tag{24}$$

where $\bar{m}$ is the average orientation factor. In the literature, the reciprocal of $\bar{m}$ has been called the 'Schmidt factor,' designated by m. Then the equation for τ is

$$\tau = \sigma m \tag{25}$$

The Schmidt factor m can take a maximum value of 0.5, corresponding to an average orientation factor $\bar{m}$ of minimum value of 2.0.

For the case of duplex crystals of alpha-beta brass, slip originally occurs only in the alpha segments. The dislocations active in these segments impose a rate of displacement on the phase boundaries. The rate of shear displacement $\dot{D}$ due to the single slip in alpha may be written as

$$\dot{D} = \rho_{\alpha_1} b \bar{v}_{\alpha_1} \ell \quad , \tag{26}$$

where ρ_α, b, and $\bar{v}_\alpha$ are respectively the density, the Burgers vector, and the velocity of the mobile dislocations in the alpha phase. The subscript '1' refers to the initially active slip system, and 'ℓ' represents the width of the alpha segments. As observed in Figures 32 and 33, at every phase boundary between alpha and beta segments, cross-slip first occurs in alpha and then slip continues in the beta segments.

Slipping in both segments helps to relax the rate of shear displacement imposed on the boundary.

Equation 23, for the rate of relaxation in single-phase polycrystalline materials as given by Johnston and Feltner, can be modified for the present case. The main consideration is the cross-slip in alpha segments and the different Burgers vector for the beta phase. The rate of relaxation in the alpha phase itself can be written as

$$\dot{R} = \sum_i \rho_{\alpha_i} b \bar{v}_{\alpha_i} \ell \quad , \tag{27}$$

where the subscript $i = 2,3$ refers to the other slip planes that have become active in the alpha region near the boundary. With increasing strain, slip in beta is activated, since the rate of deformation can no longer be balanced by the relaxation rate in the alpha near the phase boundary. The equation for the total relaxation rate becomes

$$\dot{R} = \sum_i \rho_{\alpha_i} b \bar{v}_{\alpha_i} \ell + \frac{r}{\bar{m}} \sum_j M \rho_{\beta_j} b_\beta \bar{v}_{\beta_j} \quad , \quad \begin{matrix} i = 2,3,... \\ j = 1,2,3.. \end{matrix} \tag{28}$$

In the equation above, r represents the width of the beta segment, and $\bar{m}$ is the average orientation factor dependent on the orientation relationship between alpha and beta; ρ_{β_j}, b_β and $\bar{v}_{\beta_j}$ are the density, Burgers vector, and the velocity of the mobile dislocations in the beta phase, respectively.

The equation above only qualitatively explains the interaction of dislocations at the alpha-beta phase boundaries in duplex crystals. In view of the uncertainties arising in the measurement of dislocation densities and velocities, no attempt was made to measure these parameters during the course of this work.

4.3 Deformation Behavior of Two-Phase Bicrystals

4.3.1 General Comments

The deformation of the two-phase bicrystals can be discussed on the basis of the slip-line arrangement and the corresponding behavior of dislocations on the slip planes.

As shown in Section 3.3, three important features prevail during the deformation of these specimens.

(1) As shown in Figure 37, the slip lines approaching the phase boundary decrease in their intensity and depth. This observation is explained on the basis of the resistance caused by the phase boundary in Section 4.3.2.

(2) On further deformation, the slip was observed to take place on slip systems other than the primary, as illustrated in Figures 38 and 39. The reason for this cross-slip and secondary slip, and their effect on the dislocations moving in the primary slip planes, are discussed in Section 4.3.3.

(3) The slip in alpha could continue on the parallel slip planes in beta, as shown in Figures 39 to 42. This feature depends on the relative crystallographic orientation of the alpha and beta phases present in the specimens. For specimens T_1, T_3 and T_5, slip was observed to continue into beta. When the orientation relationship is such that the slip planes and slip directions are not parallel to each other, viz. in specimens T_2 and T_4, heavy slip was observed to take place at a stress lower than the yield stress of the multicrystal. The explanation for the initiation of slip in beta is provided in Section 4.3.4.

4.3.2 Resistance Caused by the Phase Boundary

Slip lines present in the alpha were seen to decrease in their depth and intensity as they approach the phase boundary, as illustrated in Figure 37. This decrease is due to the resistance for deformation caused by the boundary. The motion of the dislocation is influenced by changes in the shear moduli of the phases present in the specimen. A dislocation near a phase boundary has its strain field extending into both the phases. The strain energy in the phase with a higher shear modulus is larger per unit displacement than in the phase with a lower shear modulus. Hence, a dislocation in a medium with a lower value of shear modulus is repelled in order to reduce the energy of the system.

If an edge dislocation in a medium of shear modulus μ_1 is at a distance r from a region where the modulus abruptly becomes μ_2 across a phase boundary, the dislocation experiences a repulsive stress τ_μ given as

$$\tau_\mu = \frac{\mu_1(\mu_2 - \mu_1)\sin\theta\, b_1}{4\pi(1 - \nu_1)(\mu_1 + \mu_2)r} \qquad (29)$$

where ν_1 is Poisson's ratio of medium 1, and θ is the angle that the Burgers vector makes with the phase boundary. With the values of $\mu_1 = \mu_\alpha = 0.72 \times 10^{12}$, $\mu_2 = \mu_\beta = 0.822 \times 10^{12}$ dynes/cm^2, $\nu_1 = 0.33$, and $r = (10b)$, the repulsive stress is

$$\tau_\mu \simeq \frac{\mu_\alpha \sin\theta}{1000} \quad .$$

For a screw dislocation, this stress will be of the order of $(\mu_\alpha \sin\theta)/1400$. Since this stress is inversely proportional to the distance from the boundary, it will increase rapidly as the dislocation approaches the phase boundary.

As a result of the repulsive stresses, secondary slip and cross-slip are promoted and this provides more forest-type barriers for the motion of dislocations present in the primary-slip system.

A change of crystallographic orientation across a grain boundary in single-phase materials causes the resolved shear stresses (or Schmid factors) to differ for the slip systems most favored for the given applied stress in the two neighboring crystals.

Although the resolved shear stress may exceed the critical value for yielding in one grain, it may not cause plastic deformation in an adjacent grain, because of its lower Schmid factor. This phenomenon causes a constraint for deformation at the boundary. In addition, in the case of two-phase bicrystals, the critical resolved shear stresses of the individual phases will be different. When the Schmid factors in the two phases are equal (i.e., the active slip-planes in two-phases are parallel to each other and the active slip directions in these planes are parallel to each other), the constraint for deformation is caused by the difference in the critical resolved shear stresses.

The difference of Burgers vectors of slip dislocations present on both sides of the boundary causes further resistance through the 'micro-incompatibility.' If a set of dislocations in alpha is assumed to cross the boundary and enter beta where it will have a different Burgers vector, a grain boundary dislocation has to be left behind for each penetrating dislocation.

In the case of the two-phase bicrystals of alpha-beta brass, the lattice parameter changes from $3.6792A^{o}$ for face-centered cubic brass to $2.949A^{o}$ for the ordered beta brass. The corresponding Burgers vectors are along [110] and [111] in alpha and beta respectively. The magnitude

of the Burgers vector $\bar{b}_\alpha = (a/2)[110]$ in alpha is $2.6A^o$. Since beta is a superlattice, the dislocations move as pairs of dislocations with Burgers vector $\bar{b}_\beta = (a/2)[111]$. The magnitude of the Burgers vector for these pairs is $5.10A^o$.

Across a phase boundary between alpha and beta, the Burgers vector thus changes from $\bar{b}_\alpha$ to $\bar{b}_\beta$. Hence there is a reduction of $(\bar{b}_\alpha - \bar{b}_\beta)$ as the dislocation in alpha crosses into beta. An interface dislocation of this slip vector $\Delta\bar{b}$ is then retained at the boundary. If an interface dislocation is present at the phase boundary, it causes a repulsive stress τ_b on the dislocation approaching from the alpha side. This stress is given by

$$\tau_b = \frac{\mu_\alpha \, \Delta b}{2\pi(1 - \nu_1)r} \tag{30}$$

for an edge dislocation, where μ_α is the shear modulus of alpha, ν_1 is the Poisson's ratio, and r is the distance of the approaching dislocation from the phase boundary.

For the values of $\bar{b}_\alpha$ and $\bar{b}_\beta$ given above, when an edge dislocation in alpha is at a distance $r = 10(\bar{b})$ from the phase boundary, it experiences a repulsive stress of $\sim \mu_\alpha/1700$. For a screw dislocation, this stress is $\sim \mu_\alpha/2500$.

All these repulsive stresses make slip in the primary slip plane difficult and cause secondary slip and cross-slip at and near the boundary. Creation of such barriers and their effect is detailed further in the following section.

4.3.3 Dislocation Pile-ups

Hall[93] originally proposed a mechanism for yielding in polycrystalline materials with the aid of a model of pile-up against the grain boundaries. The external stress and the stress from dislocation pile-up can provide the stress required to initiate yielding across the boundary. Petch[94] proposed that this stress concentration is at the boundary region, which can activate grain-boundary dislocation sources[21]. On the other hand, Cottrell[95] suggested that the stress concentration at the boundary unpins a source near the grain boundary in the neighboring grain.

The large stress concentration created at the head of such a pile-up can be obtained by the principle of virtual work[45]. Consider a set of n dislocations in a given slip plane, where each of the dislocations is subjected to an applied stress τ_a and is moving along a slip plane. If the leading dislocation encounters some obstruction in its path, a dislocation pile-up can be created. Owing to increase in stress, if the leading dislocation moves further by a distance d, each of the n dislocations in the pile-up will move by the same distance, and the work done by the external stress will be $nb\tau_a d$. The work done by the leading dislocation against the internal stress τ_1 due to the presence of the obstruction is $\tau_1 bd$. At equilibrium, therefore,

$$\tau_1 bd = nb\tau_a d \quad , \tag{31}$$

$$\therefore \tau_1 = n\tau_a \quad . \tag{32}$$

The number of dislocations 'n' that can be piled up in a length L of the slip plane is[96]

$$n = \left(\frac{\pi K}{\mu b}\right) L\tau_a \quad , \tag{33}$$

where $K = (1-\nu)$ for an edge dislocation and unity for a screw dislocation, μ is the shear modulus, τ_a is the resolved shear stress on the slip plane due to the applied stress, and b is the magnitude of the Burgers vector of the dislocation. The distance between the leading dislocation and its nearest neighbor is

$$x_1 = (1.84)\frac{\mu b}{2\pi n K \tau_a} \quad . \tag{34}$$

The stresses in the neighborhood of the leading dislocation are as follows[96]:

(a) Near the leading dislocation, for distances $r \ll x_1$, the piled-up group exerts a shear stress in its glide plane given by

$$\tau_1 \approx n\,\tau_a \quad . \tag{35}$$

(b) At large distance, $r = L$, the piled-up group exerts the same stress as a single dislocation of Burgers vector nb located at its center of gravity; this stress is

$$\tau_3 \approx \left(\frac{L}{2r}\right)\tau_a \quad . \tag{36}$$

(c) At intermediate distance $(x_1/15 \ll r \ll L)$ the stress is

$$\tau_2 = \left[1 + \left(\frac{L}{r}\right)^{\frac{1}{2}}\right]\tau_a \quad . \tag{37}$$

Chou[97] considered linear dislocation arrays in materials composed of soft and hard phases. He showed that for the same applied stress and the span of distribution, the number of dislocations in a piled-up array is less for a material containing hard particles than for the pure matrix material. The number of dislocations n in a length L is given by

$$n = 2L\tau_a K/\mu b \tag{38}$$

where $K = (1-\nu)$ for an edge dislocation and unity for a screw dislocation, μ is the shear modulus, τ_a is the applied shear stress on the slip plane, and b is the magnitude of the Burgers vector of the dislocation. The stress at the head of an array of n dislocations piled up at a phase boundary is $n\tau_a$, the same as in the case of a homogeneous material.

In the present case, as the applied stress increases, slip starts approaching the phase boundary. The dislocations experience repulsive forces attributable to the presence of (i) another phase across the boundary and (ii) barriers on the primary slip planes. Small pile-ups from these two barriers cause enough stress concentration for secondary slip to begin at the head of these pile-ups. Such secondary slip relieves the stress concentration by the pile-ups. On the other hand, secondary and cross-slip builds up a set of Lomer-Cottrell[45] barriers. Further pile-ups are necessary to overcome these.

Consider dislocations moving on a slip plane at 45^{o} to the alpha-beta phase boundary. From equation 29, the repulsive stress at a distance $r = 10(b)$ stemming from the difference in the shear moduli is given by

$$\tau_{\mu} = \frac{\mu_{\alpha} \sin \theta}{1000} \approx \frac{\mu_{\alpha}}{1400} \approx 6.65 \text{ kg/mm}^2 \quad .$$

This stress will rapidly rise, however, to as much as 35 kg/mm^2 when the dislocations move closer to the boundary. To overcome this repulsive stress, about 10-15 dislocations are required to pile up at an applied stress level of 1.4-1.6 kg/mm^2. The stress concentration immediately ahead of the pile-ups will be such that the slip can initiate in the secondary systems and in the cross-slip systems. This can explain the observed cross-slip in alpha before slip reached the phase boundary.

Such an initiation of secondary slip systems and cross-slip systems will cause the Lomer-Cottrell locks to form as mentioned earlier. Further pile-ups are essential to break these barriers.

4.3.4 Slip in Beta

One or more of the following three processes, in general, can be considered to be acting when a beta grain immediately in contact with the boundary starts deforming plastically.

(1) Dislocations in alpha continue into beta on a slip plane which is parallel to the active slip plane in alpha.

(2) Dislocation sources at the phase boundary are activated.

(3) Dislocation sources within the beta grain are activated.

Nabarro[45,98] has pointed out that a dislocation would not pass from one grain to another when the slip directions in the two grains are different. If it were to continue in the next grain without changing its Burgers vector b, the dislocation would be trailed behind by a fault in which the atoms are badly distorted. This requires a stress $\tau = \epsilon/b$, where ϵ is the energy of a large-angle boundary, and therefore τ is of the order of the theoretical shear strength of the material. Of the specimens tested, in only two specimens, T_2 and T_4, the slip systems in alpha were not parallel to those in beta, and as a result Nabarro's analysis cannot be applied.

In specimens T_1, T_3, and T_5 the slip systems in alpha and beta are parallel. In spite of such a paralleleity, the movement of dislocations through the boundary will be difficult. A single dislocation crossing the phase boundary will leave in its wake a residual dislocation of Burgers vector Δb, and this will cause a repulsive stress of the order of $\mu_\alpha/1100$ as explained before. If 100 dislocations in alpha

were to cross the phase boundary, the stress that must be overcome by the following dislocations will be of the order of the theoretical shear strength.

If a piled-up group of 15 dislocations is considered at a phase boundary, the resolved shear stress of 2.5 kg/mm^2 will cause a stress of 37.5 kg/mm^2 immediately ahead of the pile-up. This stress is at least two orders of magnitude lower than the theoretical shear strength. Hence, crossing the boundary by the dislocation cannot be a process which will cause slip in beta.

The two other possibilities open are (i) activation of sources at the boundary and (ii) activation of sources within the beta grain. The possible Burgers vectors of the phase-boundary dislocations are not clearly understood at present. In the case of coherent boundaries that exist between the Widmanstätten alpha precipitates and the beta matrix, in a copper-37.8% zinc alloy, Hawbolt[99] found that a dislocation-type structure appears at the cylindrical face of the needles. He could not identify the Burgers vectors and attributed it to the large elastic anisotropy in beta brass. Kinsman and Aaronson[100] have provided another explanation. The habit planes of the alpha precipitates in beta are typically irrational, having large indigits of Miller indices.

As shown in Figure 53, reasonably good fit over about 25% of the area of the interface can be obtained through enlarging the proportion of the total interfacial area occupied by small local areas of good fit. These areas are produced by $\{11\bar{1}\}$ alpha parallel to $\{110\}_\beta$ planes by introducing monatomic steps in the interface at the appropriate positions. The resulting plane of irrational indices thus contains, as a reasonable fraction of its area, regions which are of good atomic fit.

Fig. 53. (a) Superimposed plot of the atomic configuration of the {111} fcc and {110} bcc planes.
(b) Corresponding superlattice of 'good fit' as in (a). The dashed lines show similar regions in adjacent atomic planes (K. R. Kinsman and H. I. Aaronson[100]) . . . . . .

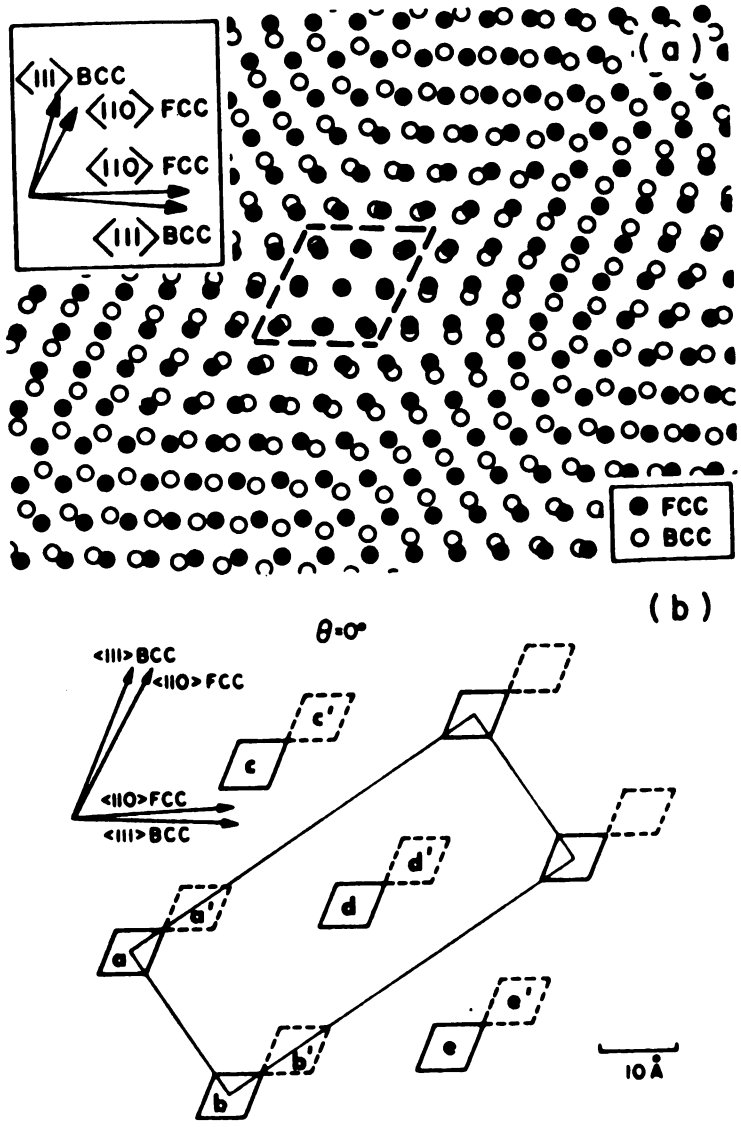
<111>BCC
<110>FCC
<110>FCC
<111>BCC
(a)
FCC
BCC
(b)
θ=0°
<111>BCC
<110>FCC
<110>FCC
<111>BCC
c'
c
d'
d
a'
a
b'
b
e'
e
10 Å

FIG.53

Accumulated bands of bad fit remain, however, in a direction normal to the broad faces of the steps which can be described as dislocations. Since these dislocations lie at interface planes of irrational indices separating two lattices of different symmetry, their strain field will be different from that observed in the interior of either crystal. The dislocations, therefore, either have markedly changed character at the interphase boundary, or else they have Burgers vectors unique to the boundary. They are called "interphase-boundary dislocations."

When the sources within beta grains are initiated, the dislocations produced from the source must be either perfect dislocations of Burgers vector $a[111]$ or coupled pairs of dislocations of Burgers vector $a/2[111]$. This condition is necessary to maintain the ordered structure in the wake of the moving dislocations.

The effect of the stress concentration from the pile-up of the slip dislocations in the neighboring grain depends on the relative orientation of the grains. The following analysis of the effect of relative crystallographic orientation is based on the work of Chyung and Wei[101].

Let $[\hat{n}]$ be the unit vector normal of the slip plane and $[\hat{s}]$ the unit vector in the slip direction. If $\tau_{n_1 s_1}$ is the applied shear stress on the slip system $(\hat{n}_1, \hat{s}_1)$ of alpha, the resolved shear stress on system $(\hat{n}_2, \hat{s}_2)$ in beta is

$$[a_{11}a_{22} + a_{12}a_{21}]\tau_{n_1 s_1}$$

where

$$a_{11} = \cos(\measuredangle[\hat{s}_1] \text{ and } [\hat{s}_2])$$

$$a_{22} = \cos(\measuredangle[\hat{n}_1] \text{ and } [\hat{n}_2])$$

$$a_{12} = \cos(\measuredangle[\hat{n}_1] \text{ and } [\hat{s}_2])$$

$$a_{21} = \cos(\measuredangle[\hat{n}_2] \text{ and } [\hat{s}_1])$$

The geometry is shown in Figure 54. The total shear stress acting on the system $[\hat{n}_2,\hat{s}_2]$ in beta is

$$\tau_{total} = \tau_{n_2s_2} + M[a_{11}a_{22} + a_{12}a_{21}]\tau_{n_1s_1} \quad , \tag{39}$$

where $\tau_{n_2s_2}$ is the applied resolved shear stress on $[\hat{n}_2,\hat{s}_2]$ system in beta, and M is the stress-concentration factor resulting from the piled-up group of dislocations in alpha.

When the orientation relationship is such that the slip planes and the slip directions in alpha are parallel to those in beta,

$$\tau_{n_2s_2} = \tau_{n_1s_1} \quad .$$

In this situation the total shear stress acting on the system $[\hat{n}_2,\hat{s}_2]$ in beta is

$$\tau_{Total} = \tau_{n_1s_1}[1 + M] \quad . \tag{40}$$

Consider the case of specimen T_1 when it shows slip in the beta grain at a resolved shear stress of 2.4 kg/mm^2. If the distance between the tip of the pile-up and the source within beta is assumed to be of the order of L, the length of the pile-up, then by equation 36, the stress-concentration factor M is 1/2. Therefore,

$$\therefore \tau_{Total} = \frac{3}{2}\tau_{n_1s_1} = 3.6 \text{ kg/mm}^2$$

Although the specimens tested in this work had single-crystal regions of beta in contact with the alpha single crystal, their yield was restricted by the grain boundaries of other beta grains above. The yield strength of a coarse-grained beta specimen used in this work was found to be 7-8 kg/mm^2. If there exists a most favorably oriented slip system for

Fig. 54. Schematic of the two-phase bicrystal with a slip system $[n_1 s_1]$ in alpha and $[n_2 s_2]$ in beta phases. . . . . .

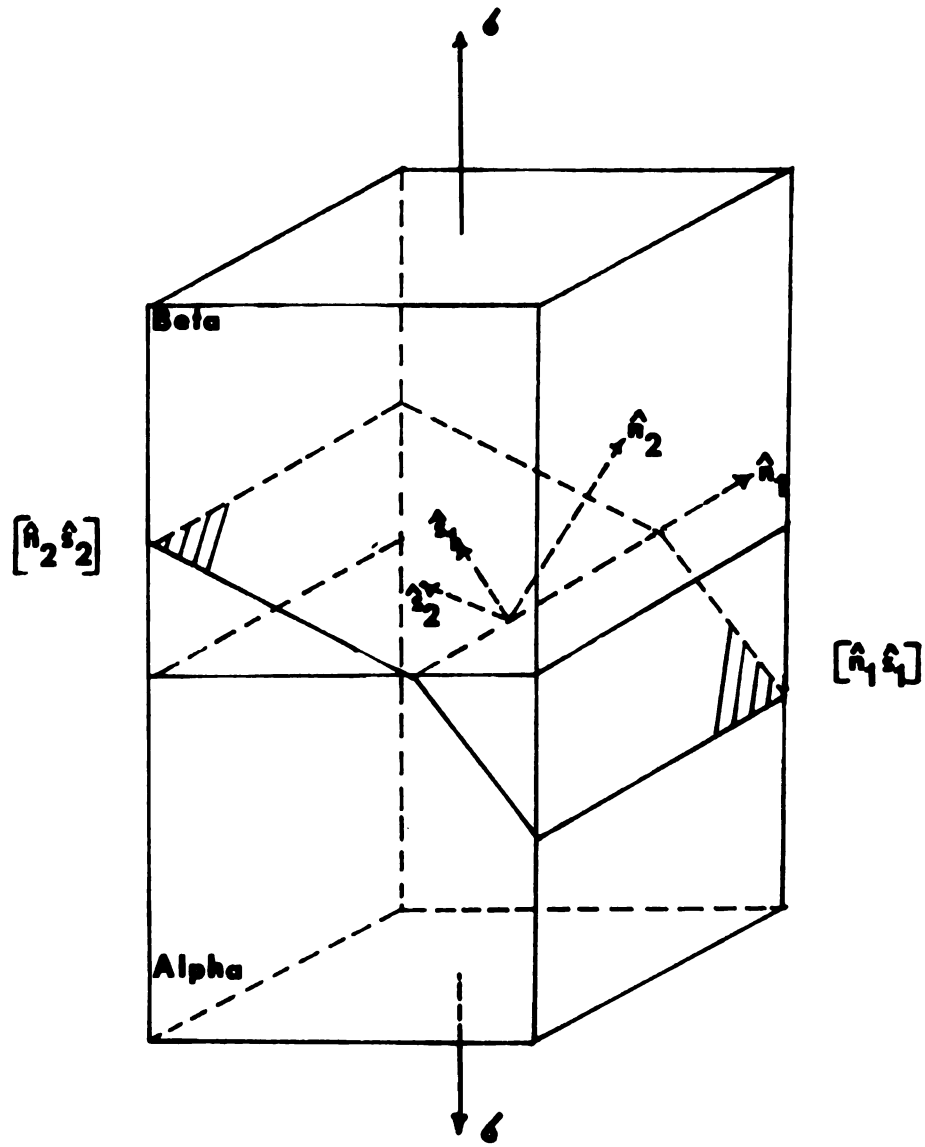
6
Beta
$\hat{n}_2$
$\hat{n}_1$
$[\hat{n}_2 \hat{s}_2]$
$\hat{s}_1$
$\hat{s}_2$
$[\hat{n}_1 \hat{s}_1]$
Alpha
6

FIG. 54

which the maximum Schmidt factor will be 1/2, the resolved shear stress is 3.5-6 kg/mm^2.

As can be seen by the example above, the yielding in beta is observed at a lower resolved shear stress of 2.4 kg/mm^2. This may be attributed to the stress concentration caused by the piled-up dislocations. Thus the piled-up group of dislocations in alpha helps the beta to yield.

In conclusion, the deformation of the two-phase bicrystals of alpha-beta brass results from the repulsive stress imposed by the phase boundary on the oncoming dislocations, and the overcoming of this repulsive stress by the pile-up of dislocations. The stress concentration from the pile-up helps the initiation of slip inside beta.

4.4 Duplex Crystals and Two-Phase Bicrystals: A Comparison

Duplex-crystal specimens had the segments of alpha and beta phases oriented in such a way that the relationships

$$\{111\}_\alpha \;||\; \{110\}_\beta \quad \text{and} \quad \langle 1\bar{1}0\rangle_\alpha \;||\; \langle \bar{1}11\rangle_\beta$$

were always satisfied. In the case of two-phase bicrystals, the growth process consisted of eliminating the transition zone; and, during this growth process, a sharp two-phase boundary resulted. It can be expected that the phase boundary will occupy the low-energy position. For the alpha-beta phase boundary, the orientation relationship mentioned above gives a lowest-energy configuration. However, only in three bicrystal specimens, T_1, T_3, and T_5, was this orientation relationship observed.

Whenever the crystallographic relationship stated above is satisfied, the slip planes and slip directions in alpha and beta are parallel to each other. Hence slip initiation inside beta is easy. Slip was always

observed on the corresponding slip planes in beta in the case of duplex crystals. In the case of two-phase bicrystals, slip was seen to take place in beta only for the three specimens T_1, T_3 and T_5.

In both kinds of specimens, a phase boundary initially acts as a barrier to slip. This resistance is experienced on a very large scale in the two-phase bicrystals. When the stress was high enough to cross the barriers imposed, slip in beta segments in the duplex crystals occurred on fine scale. The slip in beta in two-phase bicrystals was seen as fine slip lines or as a general rumpled surface. Many times a depression was observed inside beta where several slip lines in alpha met the phase boundary. This phenomenon may be due to the microincompatibility effects stemming from the difference in Burgers vectors. These depressed areas in beta are expected to have a high density of dislocations[20].

When the crystallographic orientation relationship was not satisfied, as in the case of the specimens T_2 and T_4, no slip could be observed in beta regions near the phase boundary up to high stresses. However, beta regions ultimately deformed and showed slip markings.

No void formation was observed at the phase boundary in any of the specimens tested.

V. CONCLUSIONS

1. Two-phase bicrystals of alpha-beta brass can be prepared by melting beta brass over substrates of single crystals of alpha brass. The two-phase transition zone produced in such a joining process can be eliminated by scheduling special heat treatments. Cyclic local annealing is very effective in transforming the two-phase transition zone into a sharp phase boundary.
2. The phenomena of diffusion, phase transformations, and grain growth play major roles in such a growth process.
3. In the initial stages of deformation, the alpha-beta phase boundary poses a barrier to slip propagation. This can be partly attributed to the image stresses and to the difference in shear moduli and Burgers vectors of the phases present on either side of the phase boundary. The dislocations present at the boundary, however, are the most effective barriers for slip propagation.
4. At high stress levels the effectiveness of this boundary as a barrier for slip propagation depends on the relative crystallographic orientation of the two phases.
5. In duplex crystals and in bicrystals having the slip planes and the slip directions parallel in alpha and beta phases, slip cannot be effectively stopped from crossing the boundary.
6. In bicrystals that did not have specific orientation relationship between alpha and beta phases, slip propagation across the boundary

is more difficult. However, even in such cases. slip is initiated ultimately in beta.

7. Irrespective of whether crystallographic relations are satisfied or not, void formation is not necessary at these phase boundaries during plastic deformation of alpha-beta brass.
8. Slip cannot continue in the beta grains immediately in contact with the single-crystal alpha by dislocations merely crossing the phase boundary. Slip initiation in beta was proposed to be caused by the activation of dislocation sources present at the phase boundary and/or within the beta grains.

LIST OF REFERENCES

LIST OF REFERENCES

1. C. S. Smith, Met. Rev. 9 (1954) 1.

2. J. W. Rutter and B. Chalmers, Can. J. Phys. 31 (1953) 15.

3. W. A. Tiller, K. A. Jackson, J. W. Rutter and B. Chalmers, Acta Met. 1 (1953) 428.

4. B. Chalmers, Can. J. Phys. 31 (1953) 132.

5. E. M. Savitskii and N. I. Novokhatskaya, 'Producing Single Crystals of Copper, Alpha Brass and Beta Brass' in 'Growth and Imperfections of Metallic Crystals' (Consultants Bureau, N. Y. 1968) p. 114.

6. R. Maddin, Trans. A. I. M. E. 175 (1948) 86.

7. K. T. Aust, 'Crystal Growth from the Solid State' in 'Techniques of Metals Research' v. 1, Ed. R. F. Bunshah, (J. Wiley, N. Y. 1968) p. 991.

8. J. D. Livingston, Mater. Sci. Eng. 7 (1971) 61.

9. H. Sang and W. A. Miller, J. Crystal Growth 6 (1970) 303.

10. Yu. D. Chistyakov, A. I. Pekarev and M. V. Gartman, Soviet Phys. Cryst. 4 (1968) 597.

11. C. Lemercier and J. M. Thuillier, Mater. Res. Bull. 1 (1966) 109.

12. R. D. Sisson and M. A. Dayananda, Met. Trans. 3 (1972) 647.

13. P. G. Shewmon, Transformations in Metals (McGraw Hill, N. Y. 1969) p. 253.

14. M. Hansen and K. Anderko, 'Constitution of Binary Alloys' (McGraw Hill, N. Y. 1958) p. 650.

15. P. E. J. Flewitt and J. M. Towner, J. Inst. Metals, 95 (1967) 273.

16. H. Warlimont, Iron and Steel Inst. London, Spec. Rept. No 93 (1965) 58.

17. A. B. Greninger and V. J. Mooradian, Trans. A. I. M. M. E. 128 (1938) 337.

18. J. E. Reynolds, Jr. and M. B. Bever, Trans. A. I. M. E. 194 (1952) 1065.

19. D. Hull and R. D. Garwood, 'The Diffusionless Transformations of Metastable β-Brass,' in 'The Mechanism of Phase Transformations in Metals,' (Inst. of Metals, London, 1956) p. 219.

20. J. P. Hirth, Met. Trans. 3 (1972) 3047.

21. J. C. M. Li, Trans. A. I. M. E. 227 (1963) 239.

22. J. D. Livingston and B. Chalmers, Acta Met. 5 (1957) 322.

23. R. L. Fleischer and B. Chalmers, Trans. A. I. M. E. 212 (1958) 265.

24. J. J. Hauser and B. Chalmers, Acta Met. 9 (1961) 802.

25. R. E. Hook and J. P. Hirth, Acta Met. 15 (1967) 1099.

26. U. F. Kocks, Acta Met. 6 (1958) 85.

27. J. H. van der Merwe, 'Interfacial Misfit and Bonding Between Oriented Films and Their Substrates,' in 'Single-Crystal Films' Eds. M. Francombe and H. Sato, (Pergamon Press, N. Y. 1964) p. 139.

28. J. D. Eshelby, Phil. Trans. A.244 (1951) 87.

29. A. K. Head, Phil. Mag. 44 (1953) 92.

30. G. H. Conners, Int. J. Engng. Sci. 5 (1967) 25.

31. E. H. Yoffe, Phil. Mag. 6 (1961) 1147.

32. M. F. Ashby, Phil. Mag. 21 (1970) 399.

33. H. Unckel, J. Inst. Metals 61 (1937) 171.

34. R. W. K. Honeycombe and W. Boas, Australian J. Sci. Research, A-1 (1948) 70.

35. L. M. Clareborough, Australian J. Sci. Research A-3 (1950) 72.

36. L. M. Clareborough and G. R. Perger, Australian J. Sci. Research A-5 (1952) 114.

37. W. M. Baldwin and B. I. Edelson, Trans. A. S. M. 55 (1962) 230.

38. I. G. Palmer, G. C. Smith and R. D. Warda, 'Some Aspects of Ductile Fracture in Metals' in 'Physical Basis of Yield and Fracture, Conference Proceedings' Ed. A. C. Strickland (Inst. of Physics and Physical Society, London, 1966) p. 53.

39. K. Honda and J. Arima, Proc. of the Eighth Japan Congress of Testing Mats. (1965) 7.

40. J. Arima, N. Hosokawa and K. Honda, J. Soc. Mats, Sci. Japan, 19 (1970) 1042.

41. F. Bolenrath, V. Hauk, W. Ohly and H. Preut, Z. Metallkunde 60 (1969) 288.

42. I. L. Mogford, Met. Rev. 12 (1967) 49.

43. F. von Göler and G. Sachs, Z. Physik 55 (1929) 581.

44. J. C. Fisher, Acta Met. 2 (1954) 9.

45. A. H. Cottrell, 'Dislocations and Plastic Flow in Crystals' (Clarendon Press, Oxford, 1953).

46. H. Suzuki, 'The Yield Strength of Binary Alloys' in 'Dislocations and Mechanical Properties of Crystals, Eds. J. Fisher et al, (J. Wiley, N. Y. 1957) p. 361.

47. J. D. Meakin and H. G. F. Wilsdorf, Trans. A. I. M. E. 218 (1960) 737, 745.

48. R. Maddin, Trans. A. I. M. E. 194 (1952) 270.

49. T. E. Mitchell and P. R. Thornton, Phil. Mag. 10 (1964) 315.

50. W. Pfeiffer and A. Seeger, Phys. Stat. Sol. 2 (1968) 668.

51. J. Garstone and R. W. K. Honeycombe, 'The Deformation of Alloy Single Crystals' in 'Dislocations and Mechanical Properties of Crystals' Eds. J. Fiser et al, (J. Wiley, N. Y. 1957) p. 391.

52. J. P. Hirth and J. Lothe, 'Theory of Dislocations' (McGraw Hill, N. Y. 1968) p. 764.

53. P. R. Thornton, T. E. Mitchell and P. B. Hirsch, Phil. Mag. 7 (1962) 1349.

54. J. T. Fourie, Acta Met. 8 (1960) 88.

55. D. Kuhlmann Wilsdorf and H. Wilsdorf, Acta Met. 1 (1953) 394.

56. J. E. Burke and C. S. Barrett, Trans. A. I. M. E. 175 (1948) 106.

57. D. McLean, J. Inst. of Metals 74 (1947-48) 95.

58. H. Wilsdorf and J. T. Fourie, Acta Met. 4 (1956) 271.

59. J. S. Koehler and F. Seitz, J. Appl. Mech. 14 (1947) A-217.

60. N. Brown, Phil. Mag. 4 (1959) 693.

61. A. H. Cottrell, 'Interactions of Dislocations and Solute Atoms,' in 'Relation of Properties to Microstructure' (ASM, 1954) 131.

62. W. A. Rachinger and A. H. Cottrell, Acta Met. 4 (1956) 109.

63. A. K. Head, M. H. Loretto and P. Humble, Physica Stat. Solidi 20 (1967) 521.

64. G. W. Ardley, Acta Met. 3 (1955) 525.

65. J. H. Westbrook, 'Mechanical Properties of Intermetallic Compounds - A Review of the Literature' in ' Mechanical Properties of Intermetallic Compounds,' (J. Wiley, N. Y. 1960) p. 1.

66. C. S. Smith, Trans. A. I. M. M. E. 152 (1943) 144.

67. N. Brown, Acta Met. 7 (1959) 210.

68. N. Brown, 'The Interaction between Dislocations and the Superlattice,' in 'Mechanical Properties of Intermetallic Compounds' Ed. J. H. Westbrook, (J. Wiley, N. Y. 1960) p. 177.

69. H. Green and N. Brown, Trans. A. I. M. E. 197 (1953) 1240.

70. A. B. Greninger, Trans. A. I. M. M. E. 128 (1938) 369.

71. C. S. Barrett, Trans. A. I. M. E. 200 (1954) 1003.

72. G. Bassi and J. P. Hugo, J. Inst. Metals 87 (1958-59) 155.

73. B. J. Brindley, D. J. H. Corderoy and R. W. K. Honeycombe, Acta Met. 10 (1962) 1043.

74. A. B. Greninger, Trans. A. I. M. M. E. 124 (1937) 379.

75. H. B. Aaron and G. R. Kotler, Met. Trans. 2 (1971) 393.

76. G. T. Horne and R. F. Mehl, Trans. A. I. M. E. 203 (1955) 88.

77. U. S. Landergren, C. E. Birchenall and R. F. Mehl, Trans. A. I. M. E. 206 (1956) 73.

78. R. W. Heckel, R. D. Lenam and R. A. Tanzilli, 'Techniques for the Study of Homogenization in Compacts of Blended Powders' in 'Perspectives in Powder Metallurgy,' Ed. J. S. Hirschhorn and K. H. Roll, (Plenum Press, N. Y. 1970), vol. 5 p. 139.

79. J. W. Christian, 'The Theory of Transformations in Metals and Alloys,' (Pergamon Press, Oxford, 1965), p. 440.

80. C. Zener, Trans. A. I. M. E. 167 (1946) 550.

81. J. S. Kirkaldy, 'Theory of Diffusional Growth in Solid-Solid Transformations' in 'Decomposition of Austenite by Diffusional Processes,' Eds. V. F. Zackay and H. I. Aaronson, (Interscience, N . Y. 1962) p. 39.

82. H. I. Aaronson, C. Laird and K. R. Kinsman, in 'Phase Transformations' (ASM, Metals Park, Ohio, 1971) p. 313.

83. G. R. Purdy, Metal. Sci. J. 5 (1971) 81.

84. H. B. Aaron, Acta Met. 17 (1969) 407.

85. P. G. Shewmon, 'Diffusion in Solids,' (McGraw Hill, New York, 1963)

86. P. A. Jaquet, Acta Met. 2 (1942) 752, 770.

87. S. Woo, C. S. Barrett and R. F. Mehl, Trans. A. I. M. M. E. 156 (1944) 100.

88. O. T. Marzke, Trans. A. I. M. M. E. 104 (1933) 64.

89. Hsun Hu and C. S. Smith, Acta Met. 4 (1956) 638.

90. D. McLean, 'Grain Boundaries in Metals' (Clarendon Press, Oxford, 1957).

91. M. A. Greenfield and H. Margolin, Met. Trans. 3 (1972) 2649.

92. T. L. Johnston and C. E. Feltner, Met. Trans. 1 (1970) 1161.

93. E. O. Hall, Proc. Phys. Soc. London, B 64 (1951) 747.

94. N. J. Petch, J. I. S. I. 174 (1953) 25.

95. A. H. Cottrell, Trans. A. I. M. E. 212 (1958) 192.

96. J. Friedel, 'Dislocations' (Pergamon Press, London,1964) p. 262.

97. Y. T. Chou, Acta Met. 13 (1965) 779.

98. F. R. N. Nabarro, 'Some Recent Developments in Rheology,' (British Rheologist's Club, London, 1950), p.38.

99. B. Hawbolt, Univ. of British Columbia, Unpublished Research (1970).

100. K. R. Kinsman and H. I. Aaronson, 'Structure of Crystalline Interfaces,' Ford Scientific Research Staff, Publication Preprint, June 12, 1972.

101. C. K. Chyung and C. T. Wei, Phil. Mag. 15 (1967) 161.